

OPPORTUNITIES FOR TECHNOLOGICAL ADVANCES IN THE CONVERSION
OF NATURAL GAS TO LIQUID FUELS AND CHEMICALS.

Imre Puskas
Research Services
939 Brighton Drive
Wheaton, IL. 60187

KEYWORDS: Natural gas, synthesis gas, methanol, syncrude.

INTRODUCTION.

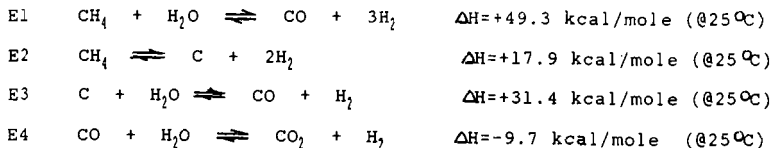
Natural gas is a premium fuel because of its high heating value (210.8 kcal/g-mole methane) and clean burning characteristics. However, transportation costs from source to market may prevent its fuel use. Alternative uses of natural gas are conversions to chemicals and liquid fuels. Natural gas is the favored starting material for ammonia and methanol. Natural gas can also be converted to easily transportable liquid fuels. However, conversions to alternative fuels with lower heating values (~156-167 kcal/carbon atom for hydrocarbons; 170.9 kcal/g-mole for methanol) can be rational and economical only under special circumstances.

Excellent reviews are available by Rostrup-Nielsen (1), Fox (2), Mills (3), Fierro (4), Lunsford (5), Kuo et al. (6), and by many others on the research and development status of the natural gas conversion technologies. By comparing salient chemical, technological, historical and economic features of the major conversion technologies, this study is an attempt to define the best opportunities for further technological advances.

SYNTHESIS GAS FROM NATURAL GAS.

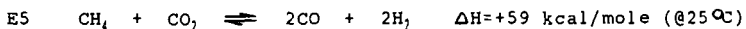
Synthesis gas is a common intermediate in the syntheses of ammonia, methanol and synthetic crude. Natural gas can be converted to synthesis gas by three different reactions: 1./ Steam reforming. 2./ Reforming by carbon dioxide. 3./ Partial oxidations.

Steam reforming. The overall reaction is shown by Equation 1 (E1). This reaction takes place in two steps. First methane is decomposed to carbon and hydrogen (E2), which is followed by a carbon-steam reaction (E3). All three reactions are endothermic equilibrium reactions and require high temperatures for favorable equilibria. During steam reforming, the water gas shift reaction (E4) is an inevitable side reaction. This latter is exothermic; its equilibrium is shifted to its reversal (i.e. to the left) by increasing temperature. Steam reforming requires a catalyst. Nickel on alumina is used most widely. The temperature of most of the reformers is in the 730-860 °C range. Steam is used in large excess (2-5 fold) for faster rates and to prevent carbon build-up on the catalyst.



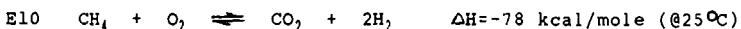
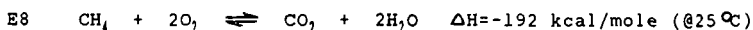
Review articles (7-10) provide details on the chemistry and technology of methane steam reforming. Some aspects are highlighted here. Kinetic evidence suggests that the reaction rate is controlled by diffusion. Steam reforming is carried out in furnaces which contain parallel catalyst tubes made of HK-40 alloy (25% Cr, 20% Ni, 0.35-0.45% C). The tubes are designed for a minimum life of 10 years. Inside the tubes is the catalyst. The tubes are heated from the outside by burners. Reforming pressure on the tube side can be as high as 500 psi. Since natural gas is usually available under high pressure, reforming under pressure can result in substantial savings in downstream compression costs if compressed synthesis gas is needed. Due to improved heat recovery and efficient energy management, current steam reformers operate with good thermal efficiency (11-12).

Carbon dioxide reforming. This reaction has much resemblance to steam reforming. The overall reaction is illustrated by E5. It is



highly endothermic. It occurs in two separate steps, the first step being methane decomposition (E2). In a subsequent step, the carbon is gasified by carbon dioxide (E6). The reverse reaction of E6 is the Boudouard reaction, which can be a source of carbon deposition. Carbon dioxide reforming, as indicated by E5, cannot be practiced commercially because the carbon gasification by E6 is not fast enough to prevent carbon accumulation. Steam addition to the feed is required for successful operations. Commercial interest in carbon dioxide reforming originates from the need for synthesis gas compositions with low H₂ to CO ratios. Haldor-Topsoe (13,14) and Calorific GmbH (15) reported on process developments. The Midrex-Process for the reduction of iron ores generates syngas essentially by carbon dioxide reforming with low steam usage (16).

Partial oxidation. Controlled reaction of methane with oxygen can give good yield of synthesis gas. The desired reaction is shown by E7. However, early studies (17) have already revealed, that even if a 2:1 molar mixture of methane and oxygen is reacted, the initial reaction is complete burning (E8) and incomplete burning (E9 and E10). These are very fast reactions, requiring only milliseconds. Following the initial fast reactions, the unreacted methane reacts with steam and carbon dioxide generated by the reactions E8-E10. However, these reforming reactions are slower



by more than an order of magnitude. The reaction temperature depends on the preheat temperature of the reagents. Mixing occurs in a burner. A flame is spontaneously produced with adequate preheat, even though at room temperature the composition would be non-flammable. Outside the flame, the temperature quickly falls due to the endothermic reforming reactions. The reactor is a refractory-lined vessel. The first commercial installation of a non-catalytic partial oxidation unit using 95% pure oxygen was in the Brownsville synthetic fuel plant in 1950, operating at 425 psi (18). The new syngas plant in Malaysia designed by Shell International Gas Ltd. uses a similar process (19).

Partial oxidation can be conducted catalytically. The catalyst maintains the reaction without a flame, and accelerates the slower reforming reactions to establish thermodynamic equilibria. However, truly catalytic partial oxidations have been restricted mostly to laboratory studies (20). Most of the commercial "catalytic partial oxidation" processes consist of a sequence of non-catalytic partial oxidation and catalytic reforming. Synthesis gas generation for copper smelters may involve truly catalytic partial oxidation (21).

The oxidant in the partial oxidation processes can be air or pure oxygen. In case of air use, the nitrogen appears in the synthesis gas as a diluent.

Combined reforming. Steam reforming, carbon dioxide reforming and partial oxidation supply synthesis gas with greatly differing composition. The H₂/CO ratios from the three processes are >3, <1 and <2, respectively. Combination of the various processes can lead to the desired synthesis gas compositions. Furthermore, combination of steam reforming and partial oxidation also led to the development of more energy-efficient reactors and processes. These advances came from BASF (22), Haldor-Topsoe (23), Lurgi (24), ICI (25) and Uhde GmbH (26), etc. A recent review by Orphanides (27) gives more detail on the progress. Some of the advances will be illustrated by specific examples:

For ammonia synthesis, hydrogen is required rather than synthesis gas. The CO content of the synthesis gas is converted to hydrogen and carbon dioxide by the water gas shift reaction (E4). In newer ammonia plants, the steam reforming furnaces have been replaced by two reactors (Figure 1). The first reactor is the "Gas Heated Reformer" (GHR) where about 75% of the methane is reformed to synthesis gas around 700°C and up to 600 psia. The heat for the reforming is supplied by the effluent gases of the second reactor. This latter one is an "autothermal reformer" which converts the residual methane of the first reactor effluent by partial catalytic air oxidation. This combination has the following benefits: 1./ It introduces the nitrogen required in the ammonia synthesis step. 2./ It generates heat in the second reactor which is very efficiently utilized in the first reactor and eliminates the need for the bulky steam reformer furnaces. Heat transfer in the GHR is much better than in the old furnaces because both sides of the exchanger tubes are under pressure. In some of the newer ammonia plants, a single reformer replaces the two reactors of Figure 1 (as in Figure 2).

Figure 1. Combined Reforming.

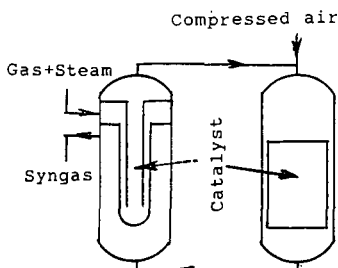
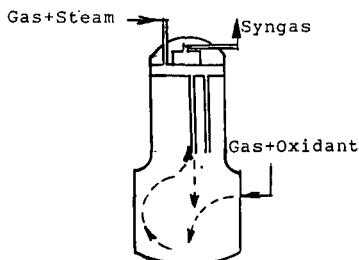


Figure 2. Schematic Showing of a Combined Autothermal Reformer.



The synthesis gas generated by the conventional steam reforming furnaces is acceptable for methanol synthesis even though the hydrogen content is too high. The combined reforming concept shown in Figure 1 is also applicable to methanol synthesis if pure oxygen is the oxidant in the second reformer. According to Lurgi (24), the process economics are more favorable for the combined reforming option because of improved methane to methanol conversion efficiency. The Combined Autothermal Reformer (CAR) (Figure 2) currently under development by Uhde GmbH (26) appears attractive for the next generation methanol plants.

If inexpensive carbon dioxide is available at the site of the methanol plant, a combination of steam reforming (E1) and carbon dioxide reforming (E5) results in more favorable synthesis gas composition and also in higher methane-based conversion efficiency to methanol. For these reasons, natural gas sources with 10-30% carbon dioxide content might be particularly favored for methanol synthesis. Indeed, good methanol yield was reported from the CO₂-containing gas fields of New Zealand (28-29).

AMMONIA SYNTHESIS.

Ammonia production from hydrogen and nitrogen was pioneered by Haber and Bosch in 1913. This led to the development of the giant ammonia industry which provides fertilizer to agriculture to feed the growing world population. Ammonia is one of the largest volume chemicals. World production is estimated at 110 MM tons per annum. About 84% of the production goes to fertilizers. Ammonia prices during the last fifteen years ranged from less than \$100/ton to \$350/ton due to variations in supply and demand.

Scheme 1. Ammonia Synthesis from Natural Gas and Air.

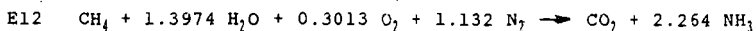
Natural gas purification	Combined reforming	Shift reaction	CO ₂ removal	Gas purifications	Compression	NH ₃ loop
--------------------------	--------------------	----------------	-------------------------	-------------------	-------------	----------------------

Scheme 1 illustrates the process steps involved in ammonia synthesis starting with natural gas (7). The ammonia synthesis step is shown by Ell. The reaction is exothermic and leads to equilibrium. The synthesis is conducted at 2000-5000 psi and



475-500°C over an alkalized, promoted magnetite catalyst. About 13-16% conversion is obtained in commercial recycle operations, with 100% selectivity to ammonia. The ammonia is recovered by condensation after refrigerating the gas stream. A small purge stream is taken from the synthesis loop to prevent inert buildup. Two kinds of converter designs are in commercial use: tubular and multiple bed. Recent developments in the synthesis loop include more efficient converter designs (30) and the introduction of magnetite-ruthenium catalyst combination for higher conversion (31). The largest ammonia plants have 1600 t/d capacity.

During the last two decades, the economics of ammonia production have substantially improved due extensive modernization programs. The progress is reflected by reduction of the energy requirements (i.e. the heating value of the feed including fuel use) per ton of ammonia from about 36 GJ to about 28 GJ. The overall process efficiency based on E12 is about 82%.



METHANOL SYNTHESIS.

Synthetic methanol has become available in 1923. Currently worldwide production is approaching 30 MM ton per annum. Nearly half goes for formaldehyde synthesis, which represents a declining market. Other uses include acetic acid synthesis, synthesis of methyl esters, solvent use and recently methyl t-butyl ether (MTBE) synthesis. This latter use is rapidly growing because MTBE is the most preferred octane booster for reformulated gasoline. In recent years, possible "clean fuel" use of methanol was also widely studied (32). The energy crises of the seventies motivated broad range of scientific research in methanol-related subjects as indicated by review articles (33-37). In the last two decades, large capacity plants were constructed near to inexpensive gas sources, exerting a downward trend on methanol prices. During the last decade prices ranged between \$0.35-0.75/gal until a recent escalation to above \$1/gal.



The synthesis gas from the reformer requires water removal and compression before methanol synthesis. The synthesis (E13) is an exothermic equilibrium reaction. The original catalyst was zinc-chromium oxide which required high temperatures and pressures. Since the late sixties, copper-zinc oxide catalysts have been adopted which function well at much lower temperature and pressure (230-270°C; 700-2000 psi). The reactors in commercial service are either of the "quench type" or exchanger type; slurry reactors have also been piloted. Synthesis gas conversion is about 15% per pass, but the methanol concentration is only 4-7 % because of accumulation of inerts and excess reagents in the recycle loop. After cooling, the methanol is condensed from the reactor effluent; the gases are recompressed and recycled. A purge stream is taken from the recycle loop which is rich in hydrogen if steam reforming is the source of synthesis gas. Methanol can be obtained in up to 98-99% selectivity. Ethers, aldehydes, ketones, esters, water, higher alcohols, methane and hydrocarbons are the by-products. The energy requirements for the various natural-gas based methanol processes are estimated at 32.4-35.3 GJ/ton methanol, corresponding to 78-85% carbon based efficiency.

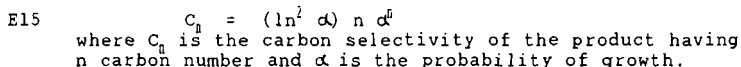
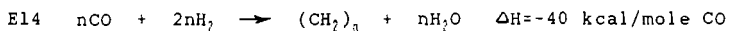
Recent research and development efforts on methanol appear to have two different directions: 1./ Finding improved catalysts (35, 38-39). 2./ Increasing conversions to methanol by shifting the equilibrium (40-44).

HYDROCARBONS VIA FISCHER-TROPSCH (FT). SYNTHESSES.

The FT synthesis dates back to 1923 with the discovery of a catalyst to convert synthesis gas to hydrocarbon mixtures. Based on this discovery, an industry was developed in Germany for the conversion of coal-based synthesis gas to synthetic fuels (45). The economic justification for this industry collapsed with the

end of World War II, when inexpensive oil became available. In the early fifties, a natural gas-based FT plant was built in Brownsville, Texas. Unfortunately, economic factors forced the shut down of the plant before sustained continuous operations could be achieved (18). At about the same time, new markets opened up for industrial and household use of natural gas by the construction of long distance pipelines, which eliminated the economic need for a FT conversion plant. However, the German and the American technological advances were utilized and further developed by South Africa where a giant coal-based synthetic fuels and chemicals industry was established (46-49). The rest of the world had very little interest in FT chemistry in the post war era until the energy crises of the seventies. These events rekindled research and development interests. Now the technology is approaching the status when natural gas conversion to liquid fuels and chemicals can be accomplished in commercially viable operations under specific circumstances. In 1993, Shell Intl. Gas Ltd has started up a large conversion plant in Malaysia, using their proprietary new technology (19). Also, since 1993, Moss gas in South Africa has been converting offshore gases to fuels using Sasol's fixed fluid bed technology (50).

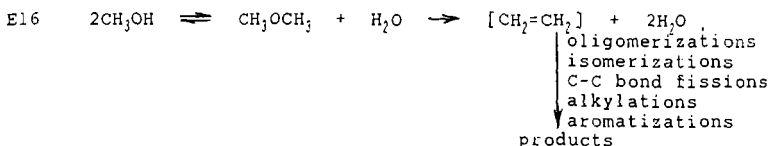
The FT chemistry and technology has numerous ramifications. Only some very basic concepts will be reviewed here. E14 illustrates the basic chemistry. The reaction can be considered as a polymerization reaction of C1 intermediates. A broad range of



products is obtained which are defined by a single parameter, the chain-growth probability or alpha according to the Anderson-Schulz-Flory (ASF) kinetic scheme (see E15). To-day a good qualitative understanding exists about the factors which can cause deviations from the ASF kinetics (51). In E14, the products are formulated as olefins. While the primary products are, indeed, predominantly olefins, the olefins may hydrogenate to paraffins in secondary reactions. A variety of oxygenated products also forms to some extent. Furthermore, the water gas shift reaction (E4) is also a side reaction. E14 is not limited by equilibrium. Ru, Ni, Fe, and Co catalyze the reaction; the latter two are the commercial choices. The Fe catalyst are usually unsupported, but they need alkali metal and other promoters and also require operations under pressure. They can be used in a wide temperature range (200-350°C). Co is more active than Fe. It also shows greater hydrogenation tendency for paraffin formation. The exothermic heat of the FT reaction is very high, requiring well controlled heat removal. With Fe catalyst, there is a wide choice for reactor and process design: fixed bed, circulating fluid bed, fixed fluid bed and slurry bed. For Co catalysts, to date only fixed bed operations were found satisfactory. Kinetic studies have amply demonstrated that the catalytic activity is limited by diffusion (51-53).

GASOLINE VIA METHANOL. THE METHANOL TO GASOLINE (MTG) PROCESS.

As an offshoot of the pioneering work on synthetic zeolites, it was discovered in Mobil Oil's laboratories, that methanol can be converted to a variety of hydrocarbon products over ZSM-5 zeolite (54,55). E16 illustrates the types of reactions occurring.



Ethylene is indicated as an intermediate, though this mechanistic assumption is debated. The products are mixtures of olefins, isolefins, isoparaffins and aromatics with less than 11 carbon per molecule. The product slate can be varied within certain

limits because the relative rates of the indicated reactions vary, aromatization being the slowest. Subsequently processes have been developed for high octane gasoline production from methanol. A fixed bed process version was commercialized in 1986 in New Zealand for the conversion of natural gas to premium grade gasoline (28,29).

COMPARATIVE ECONOMICS. OPPORTUNITIES FOR R&D.

Previous economic studies have clearly established that the large capital requirement is the major obstruction to the evolution of a natural gas-based synthetic fuel industry (19,56). Other important factors are the cost (i.e. the local value) of the natural gas, the quantities of fuel produced by the conversion (i.e. the process efficiency) and the market value of the fuel or chemicals produced. Table 1 compares salient economic features of the natural gas conversion technologies, assuming 100 MMscft/day natural gas usage. For the ammonia, methanol and syncrude technologies, it can be assumed that the capital cost requirements are approximately the same, hence the production volumes and the product heating values are directly related to the economics of these processes. The gasoline via methanol conversion has higher capital requirements because of the extra MTG process step.

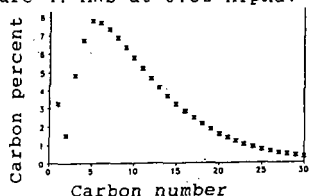
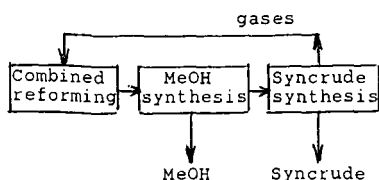
Technology	% Process efficiency	Daily production quantities	
		Weight (tons)	Heating Gkcal
Ammonia (old)	69	3357	-
Ammonia (new)	82	3985	-
Methanol	78	3154	16.8
via combined reforming	85	3437	18.4
Syncrude (Shell MDS)	80	1414	16.2
Syncrude (possible)	88	1557	17.8
Gasoline (via methanol)	76	1317	14-15

For syncrude synthesis, 80% methane-based process efficiency is estimated from the data reported by Shell. While this is a high value, with advances much higher efficiency is possible for the following reasons: All the gaseous products from the FT reactor can be recycled into synthesis gas generation and hence 100% liquid selectivity is possible. Furthermore, energy requirements (for compressors, etc.) in the FT process are less than in methanol synthesis while more energy is produced in the reaction. Hence higher process efficiencies and lower capital requirements may be possible in the FT process. Comparing methanol and syncrude, it is apparent that methanol is a much preferred product over syncrude because of its quantity. However, this statement is valid only if methanol can be marketed for chemical use. For the fuel market, methanol and syncrude product values are nearly equal on the basis of their heating values.

To make the syncrude process viable, the simplest possible process must be assembled, requiring the lowest amount of capital. Furthermore, search must go on to enhance the value of the syncrude fractions. It is already known, that syncrude commands a premium price, because it is practically free of S and N; its Diesel fraction has high cetane value and its wax fractions have high chemical values. In Figure 3 a process scheme is shown for staged coproduction of methanol and syncrude. This seems feasible because there is an overlap around 450-500 psi where syngas generation, methanol synthesis and syncrude synthesis all could be accomplished. With coproduction of methanol, the quantity and the value of the products are increased. Substantial reduction of the capital requirements of the syncrude process may be possible by making synthesis gas by an energy efficient combined reforming technology similar to that used in the ammonia industry, with air as the oxidant. In this case, the research challenge is the efficient and selective conversion of the nitrogen-diluted synthesis gas. It may be possible to control the probability of growth in the FT synthesis around 0.82, resulting in high selectivity to liquids (see Figure 4). This would eliminate the need for hydrocracking of the heavy paraffins which is the current practice. Yet another opportunity for capital reduction and improving the process efficiency could be the introduction of efficient plate exchangers for heat

exchange duties, including in the design of the reactors. Of course, FT catalyst selection and design need to pay special attention to minimize the diffusional limitations.

Figure 3. MeOH-Syncrude Process. Figure 4. MWD at 0.82 Alpha.²



²Co catalyst. See reference 57.

In conclusion, the natural gas conversion technology to synthetic fuels offers the best opportunities for advances. Some approaches to reduce the capital requirements and simultaneously improve the process efficiency and product values have been outlined. Development and demonstration of these opportunities may lead to commercially attractive natural gas conversion even at the current oil price environment, if natural gas is available at low cost.

REFERENCES.

- 1 J.R. Rostrup-Nielsen, *Catalysis Today*, 21, 257 (1994).
- 2 J.M. Fox, *Cat.Rev.-Sci.Eng.*, 35, 169 (1993).
- 3 G.A. Mills Paper C43, 13th North American Meeting of the Catalysis Society, May 2-7, 1993, Pittsburgh, PA. See also Idem, DOE, Nat. Renewable Energy Lab, HZ 1-11208-1 (1992).
- 4 J.L.G. Fierro, *Catal. Lett.*, 22, 67 (1993).
- 5 J.H. Lunsford, *Catalysis Today*, 6, 235 (1993).
- 6 J.C.W. Kuo, C.T. Kresge and R.C. Palermo, *Catalysis Today*, 4, 463 (1989).
- 7 T.A. Czuppon, S.A. Knez and J.M. Rovner in *Encyclopedia of Chemical Technology*, Fourth Ed. Vol.2, p.638. Wiley 1992.
- 8 J.R. Rostrup-Nielsen in *Catalysis Science and Technology*, J.R. Anderson and M. Boudart, Eds., Vol.5, p.1, Springer 1984.
- 9 J.P. Van Hook, *Catal.Rev.-Sci.Eng.* 21, 1 (1980).
- 10 F.E. Biasca, R.L. Dickenson, A.J. Moll, E.D. Oliver, D.R. Simbeck, *Synthesis Gas for Chemicals and Fuels. Technology, Economics and Market Outlook*. SFA, Inc. Final Report, October 1983.
- 11 J.D. Fleshman, *Chem.Eng.Progr.*, October 1993, p.20.
- 12 J.R. LeBlanc, *Energy Progress* 5 (1), 4 (1985).
- 13 J.R. Rostrup-Nielsen in *Catalyst Deactivation*, C.H. Bartholomew and J.B. Butt, Eds., Elsevier, 1991. See also Idem, *J.Catal.*, 85, 31 (1984).
- 14 N.R. Undergaard, J-H.B. Hansen, D.C. Hanson and J.A. Stal, *Oil&Gas J.*, March 9, 1992, p.62.
- 15 S. Teuner, *Hydr.Proc.*, May 1985, p. 106 and July 1987, p.52.
- 16 H-J. Toepfer, *GWG-Gas/Erdgas*, 117, 412 (1976).
- 17 Prettre, Ch. Eichner and M. Perrin, *Trans.Far.Soc.*, 42, 335 (1946).
- 18 Anonymous, *Chem.Eng.Progr.*, 53 (10), 1957, p.50.
- 19 P.J.A. Tijm, Preprint, Fuel Division, ACS, 39, 1146 (1994).
- 20 S.S. Bharadwaj and L.D. Schmidt, *J.Catal.*, 146, 11 (1994) and references cited therein.
- 21 J.B. Huttli, *Eng.& Mining J.*, 162 (7), 82 (1961).
- 22 H. Sachsse, *Chem.-Ing.-Technik*, 21 (1/2), 1 (1949).
- 23 Anonymous, *Chem.Eng.* July 9, 1962, p.88.
- 24 E. Supp, *Hydr.Proc.*, July 1984, p.43-C.
- 25 D. Kitchen and A. Pinto, *Ammonia Plant Safety*, 31, 219 (1991).
- 26 H-D. Marsch and N. Thiagarajan, *Ammonia Plant Safety*, 33, 108, (1993).
- 27 P. Orphanides, *Ammonia Plant Safety*, 34, 292 (1994).
- 28 J. Haggin, *C&EN*, June 22, 1987, p.22.
- 29 C.J. Maiden, *Chemtech*, January 1988, p.38.
- 30 N. Shannahan, *Hydr.Proc.*, January 1989, p.60.
- 31 S.A. Knez, D.O. Moore and R.V. Schneider, Kellogg Ammonia Club Meeting, San Diego, CA, August 1990.

- 32 M.D. Jackson and Carl B. Moyer in *Encyclopedia of Chemical Technology*, Fourth Ed., Vol.1, p.826, Wiley, 1991.
- 33 E. Supp, *How to Produce Methanol from Coal*. Springer, 1990.
- 34 K.C. Waugh, *Catalysis Today*, 15, 51 (1992).
- 35 G.C. Chinchin, J.P. Denny, J.R. Jennings, M.S. Spencer and K.C. Waugh, *Appl.Catal.*, 36, 1 (1988).
- 36 J.C.J. Bart and R.P.A. Sneed, *Catalysis Today*, 2, 1 (1987).
- 37 K. Klier in *Advances in Catalysis*, Eds. D.D. Eley, H. Pines and P.B. Weisz, Vol.31, p.243, Academic Press, 1982.
- 38 D.L. Trimm and M.S. Wainwright, *Catalysis Today*, 6, 261 (1990)
- 39 R.A. Koeppe, A. Baiker and A. Wokaun, *Appl.Catal.A:General*, 84, 77 (1992).
- 40 D.M. Brown, B.L. Bhatt, T.H. Hsiung, J.J. Lewnard and F.J. Waller. *Catalysis Today*, 8, 279 (1991).
- 41 J.M. Berty, C. Krishnan and J.R. Elliott, *Chemtech*, October 1990, p.624.
- 42 K.R. Westerterp, M. Kuczynski and C.M.M. Kamphuis, *Ind.Eng. Chem.Res.*, 28, 763 (1989).
- 43 J.B. Hansen and F. Joensen in *Proc. Nat. Gas Conversion Symposium*, Oslo, Aug.1990, p.457, Elsevier, 1991.
- 44 S.G. Neophytides and G.F. Froment, *Ind.Eng.Chem.Res.* 31, 1583 (1992).
- 45 H.H. Storch, N. Columbic and R.B. Anderson, *The Fischer-Tropsch and Related Syntheses*, Wiley, 1951.
- 46 M.E. Dry and H.B.deW. Erasmus, *Ann.Rev.Energy*, 12, 1 (1987).
- 47 M.E. Dry in *Catalysis Science and Technology*. Eds. J.R. Anderson and M. Boudart, Vol.1, p.159. Springer, 1981.
- 48 M.E. Dry, *Catalysis Today*, 6, 183 (1990).
- 49 B. Jager, M.E. Dry, T. Shingles and A.P. Steynberg, *Catal. Lett.* 7, 293 (1990)
- 50 Anonym, *Oil&Gas J.*, Jan.20, 1992, p.53.
- 51 R.S. Hurlbut, I. Puskas and D.J. Schumacher, *This Symposium*.
- 52 M.F.M. Post, A.C. van't Hoog, J.K. Minderhoud and S.T. Sie, *AIChE Journal*, 35, 1107 (1989).
- 53 R.E.Anderson, J.F. Shultz, L.J.E. Hofer and H.H. Storch, *Bulletin 580*, Bureau of Mines, US Govmnt. Printing Office, 1959.
- 54 S.L. Meisel, J.P. Mc Collough, C.H. Lechthaler and P.B. Weisz, *Chemtech*, February 1976, p.86.
- 55 C.D. Chang and A.J. Silvestri, *J.Catal.*, 47, 249 (1977).
- 56 D. Gray and G. Tomlinson, *Coal Liquefaction and Gas Conversion Contractor's Review Conference*, Sept, 7-8, 1994, Pittsburgh.
- 57 I. Puskas, R.S. Hurlbut, R.E. Pauls, *J.Catal.*, 139, 591 (1993)

NEW PROCESS DEVELOPMENT OF NATURAL GAS CONVERSION TECHNOLOGY TO LIQUID FUELS VIA OCM REACTION.

Tomoyoshi Sasaki, Shinichi Suzuki, Takashi Kojima
Japan National Oil Corporation
1-2-2 Hamada, Mihama-ku, Chiba-shi, 261 JAPAN

Masami Yamamura
Japan Petroleum Exploration Co.,Ltd
1-2-1 Hamada, Mihama-ku, Chiba-shi, 261 JAPAN

Tomohiro Yoshinari
Cosmo Research Institute Co.,Ltd
1134-2 Gongendo, Saitama-shi, Saitama-ken, 340-01 JAPAN

Keywords: Natural gas conversion, Oxidative coupling of methane, Circulating fluidized bed

Abstract

The conversion of methane via an OCM (Oxidative Coupling of Methane) to transportable liquid fuel has been investigated in order to utilize remote natural gas effectively. A conceptual view of this new process was developed for gasoline production based on reviews of other conventional processes and sensitivity analyses. The process developed, "ORIGINAL", is characterized by simplification of the total process and application of an advanced fluidized bed reactor to the OCM reaction. Full economic comparisons between the "ORIGINAL" and conventional OCM technologies were carried out. The results showed that the "ORIGINAL" process is substantially more economical when compared with existing technologies under the same conditions.

Introduction

Many natural gas fields have been discovered recently in Southeast Asia, which has become one of the main areas for oil and gas exploration. In many cases, however, the developments of the discovered gas fields have been obstructed by the demand for large investments in the transportation facilities (e.g., gas pipeline) and other related infrastructure.

Some liquefaction methods of natural gas, which include liquefying natural gas at an extremely low temperature (LNG), and converting natural gas into liquid fuel through the synthetic gas, have already been put into industrial use. These methods, however, also require large investments in the facilities and are expensive to operate. Consequently, even the existing methods remain a significant obstacle in the development of natural gas fields, in particular marginal fields.

Thus, to exploit natural gas resources more widely, a new method is required which converts natural gas into liquid fuel more efficiently and economically than the existing methods. With this in mind, the purpose of this study is to research and to develop a new process which converts methane, the main component of natural gas, into liquid fuel (e.g., gasoline), rather directly than through synthetic gas.

Scope of work

First of all, we devoted our time largely to reviewing the current development trends overseas, and conducted a feasibility study. Among the various direct reaction processes in which methane is converted into a highly reactive intermediate product, the oxidative coupling of methane (OCM) reaction process, in which ethylene is the intermediate product, was chosen from the standpoint of economic efficiency and feasibility in practical use. Furthermore we conducted a sensitivity analysis on the existing OCM processes which we thought promising, to evaluate the impact of various process parameters on the economy of the process itself. A "conceptual view" of the newly integrated "ORIGINAL" process was developed on the basis of these findings and the process was evaluated from the standpoint of economy.

Description of the conventional technology

A sensitivity analysis was carried out on the conventional methane conversion technology[2] [3]. This liquid fuel synthesizing process is based on the OCM. Conceptual block flow diagrams of this process, which have been modified under our consideration to simplify the process, is shown in Figure 1.

This process called Co-feed mode is characterized by point that methane and oxygen are co-fed to the oxidative coupling reactor, therefore air separation unit is required. Pyrolysis of C2 + hydrocarbon is undergone at the upper side of the reactor which oxygen is relatively free. The pyrolysis approach leads to the removal of heat from the OCM reaction and the production of more olefins. Coupling products after separation of unconverted methane and byproducts are fed with oligomerization reactor. Higher hydrocarbon produced are refined to gasoline in a distillation unit. Unconverted methane, carbon oxide and hydrogen mixed with natural gas are fed to a decarbonator to remove carbon dioxide. In the following methanation reactor, carbon oxides are converted to methane by the hydrogen produced in the pyrolysis reactor in order to utilize natural gas effectively.

Sensitivity analysis of existing processes

In discovering factors relative to product costs, we conducted sensitivity tests on the parameters listed below regarding conventional technology. When each factor was analyzed to study the causative effect on economics, other parameters took respective basic values underlined to ignore an effect of themselves.

- (1) Plant scale (natural gas volume): 10,50,100 (* 10 thousand Nm³/D)
- (2) Methane conversion ratio : 10,15,20 (%)
- (3) C2+ selectivity : 70,80,90 (%)
- (4) Reaction pressure : 1,4,10 (Kg/cm²G)
- (5) GHSV : 5000,10000,20000 (hr-1)
- (6) C5+ yield rate : 60,70,80 (%)
- (7) Natural gas price : 0.5,1.0,2.0 (\$/MMBTU)

The impact of variable factors on the gasoline production cost is shown in Figure 2. Within the scope of the present evaluation, the reaction results of the oxidative coupling process had a much more significant impact than those of the polymerization process. In general, several sensitivity studies indicated that C2+ selectivity was more important economically to the OCM reaction than methane conversion ratio. This sensitivity analysis showed that the reaction results for the methane conversion ratio were found to have been subject to a much more significant impact within the various factors involved in the oxidative coupling reaction under these conditions. Among the factors other than the reaction result, plant size was the significant factor which had the most impact on gasoline production cost.

We also carried out the sensitivity analysis with respect to conventional Redox-mode process [1] and got the same tendency with Co-feed mode.

ORIGINAL process implication

A conceptual view of the basic original overall process "ORIGINAL" was developed for gasoline production on the basis of reviews of the conventional processes, sensitivity analysis and reaction results likely to be obtained in the oxidative coupling reaction and polymerization reaction. A general outline of the designed process can be seen on flowsheet (Figure 3).

This process incorporated the OCM and pyrolysis reaction is similar to the Co-feed mode OCM process. It also includes facilities for oligomerization, product separation and methanation. The following two points characterize the new process. In general, with conventional technology wholly recycled gas including unconverted methane is fed to the decarbonation unit to remove CO₂ and treated recycled gas enters the methanator with new additional CO₂ which corresponds with H₂ and CO in order to enhance the carbon utilization efficiency.

Firstly, the flowsheet shows recycled unconverted methane gas, hydrogen, CO₂ and CO are split in two and are fed to a decarbonator and a methanator respectively. Regarding reduction of scale of the decarbonation unit, it is effective to feed directly part of the recycled gas, including

CO₂ corresponding to methanation with the methanator, not through the decarbonator. The integrated process with the conceptual view is economically competitive compared with existing methods because of the reduced plant cost.

Secondly, the question which we must consider is what types of reactor to apply to the OCM reaction. The OCM reaction is very exothermic and operated in a relatively narrow temperature range, placing high demands on heat removal and temperature control. In general, application of the fixed bed for OCM reactions has several disadvantages, difficulty selecting cooling agents and a complicated reactor structure. As for the bubbling fluidized bed reactor, which has a high heat transfer coefficient, scaling-up is known to be an important problem.

This research activity has also led to the identification of new natural gas conversion concepts using a circulating fluidized bed design with a riser reactor. This reactor is used to combine the methane oxidative coupling step with the pyrolysis of ethane and higher alkane components present in natural gas, to provide an efficient method for total conversion of natural gas to liquid fuel. The circulating fluidized bed is schematically illustrated in Fig. 4. The OCM is carried out in the riser reactor as FCC technology and an important feature of the process is pyrolytic conversion within a bubbling fluidized bed, which is the disengaging section located at the top of the riser zone, using heat generated by the OCM reaction via catalyst particles. For the circulating fluidized bed, it is possible to recycle the catalyst continuously, and to replace it if deactivation occurs. The temperature inside both reaction phases can be easily controlled and scaling-up to a commercial size is relatively simple.

Economic evaluations

The concept of the ORIGINAL process was then evaluated from the standpoint of process efficiency. From the sensitivity analysis, we understood that the methane conversion ratio is more important than C₂₊ selectivity under our condition. Therefore we investigated process efficiency and plant costs in a high methane conversion region. A correlation between methane conversion and C₂₊ selectivity, which is derived from extrapolation of catalytic performances of the best catalysts known in literatures at present[4], used in our evaluations is shown in Table 1.

Under these conditions we calculated the investment cost on plant construction regarding ORIGINAL as shown in Figure 5 and found CASE-2 to be the more economical condition. Furthermore the economic evaluations of ORIGINAL and conventional technologies in the region of high methane conversion (25~30%) are summarized in Table 2. The results showed that ORIGINAL is more economically feasible compared with existing technologies.

Conclusion

We have analyzed the relationship and causative effects of several factors on plant and product costs to existing methods. It was noted that the rate of methane conversion was economically significant compared to C₂₊ selectivity under 30% methane conversion. On the basis of these results we have designed a new process with conceptualized the circulating fluidized bed reactor to OCM reaction and carried out the economical evaluations. The result showed that the correlation between about 30% of methane conversion and 77% of C₂₊ selectivity was the optimum condition for reducing plant costs for our process. Furthermore, this ORIGINAL process has shown to be more efficient and economically feasible than conventional technologies under the same conditions.

References

- 1) J.A.Sofranko et al., PACIFIC '89 Paper No.165
- 2) A.Robine et al., "NOVEL PRODUCTION METHODS FOR ETHYLENE, LIGHT HYDROCARBONS, AND AROMATICS" ,DEKKER, p.141 (1992)
- 3) J.H.Edwards et al FUEL., 71, 325, (1992)
- 4) J.W.M.H.Geerts et al, "NOVEL PRODUCTION METHODS FOR ETHYLENE, LIGHT HYDROCARBONS, AND AROMATICS" ,DEKKER p.207 (1992)

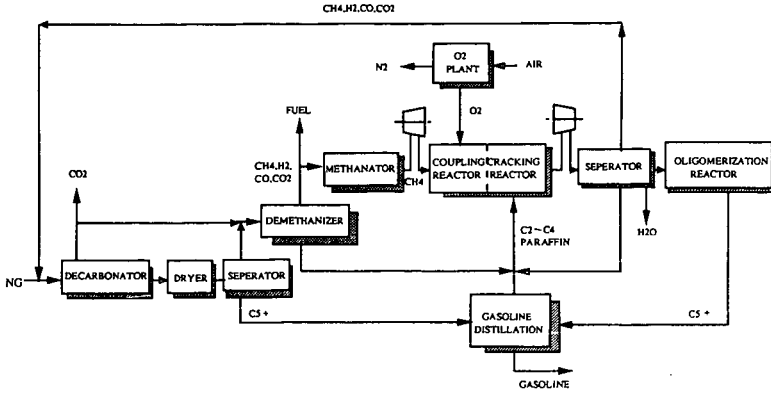


Figure 1. Block Flow Diagram of Conventional OCM Process

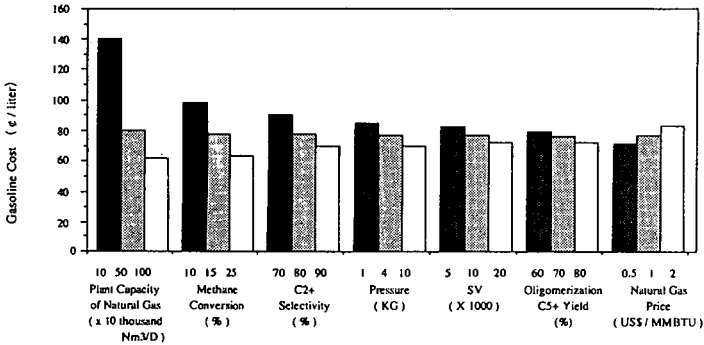


Figure 2. Effects of Various Factors on Gasoline Cost

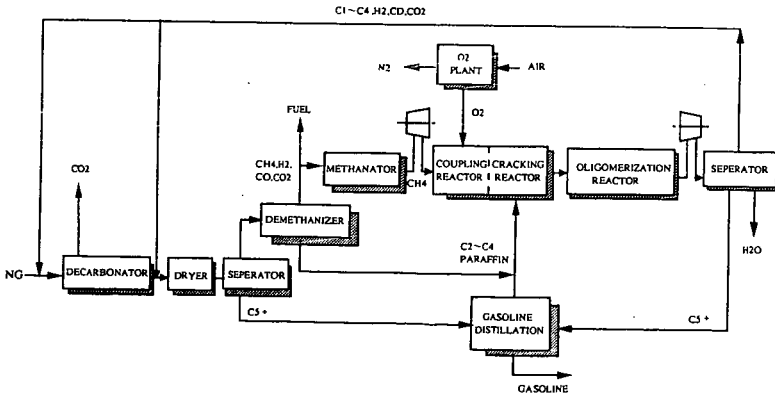


Figure 3. Block Flow Diagram of ORIGINAL Process

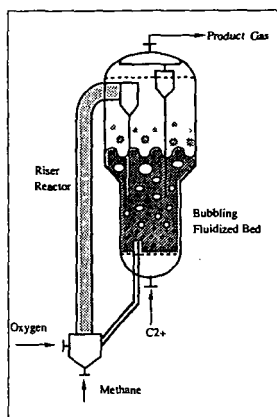


Figure 4. Circulating Fluidized Bed Reactor

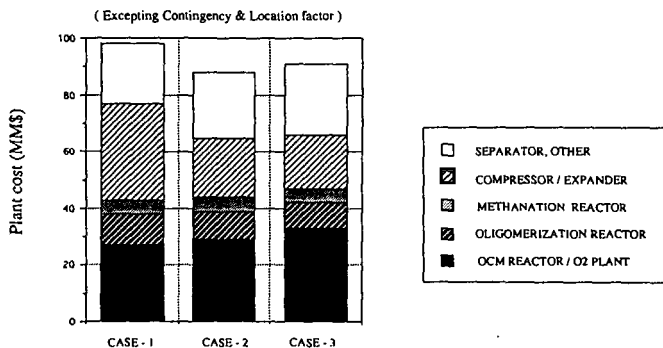


Figure 5. Constituent Proportion of Plant Costs regarding ORIGINAL processes (Plant Capacity : 2,100 BPSD)

Table 1. Estimated Correlation Between Methane Conversion and C₂₊ Selectivity

	CASE-1	CASE-2	CASE-3
METHANE CONVERSION (%)	20	30	40
C ₂₊ SELECTIVITY (%)	84	77	69

Table 2. Comparison of Process Efficiencies and Plant costs (Plant Capacity : 2,100 BPSD)

	ORIGINAL	OCM (REDOX MODE)		OCM (COFEED MODE)	
OCM REACTION CONDITION					
METHANE CONVERSION (%)	30	25	30	25	30
C ₂₊ SELECTIVITY (%)	77	80	77	80	77
PLANT COST (MM\$)	88	103	91	123	111
THERMAL EFFICIENCY (%)	57.8	57.1	55.0	60.8	58.5

PARTIAL OXIDATION OF METHANE TO SYNGAS IN DIFFERENT REACTOR TYPES.

Jacek A. Lapszewicz, Ian Campbell, Brian G. Charlton, Gary A. Foulds
CSIRO Division of Coal and Energy Technology, Lucas Heights, PMB 7, Menal 2234, Australia.
Ph. +61 2 710 6889, Fax. +61 2 710 6800

KEYWORDS: Methane, Partial Oxidation, Pressure

INTRODUCTION

Most of the reported work on catalytic partial oxidation (CPO) of methane to syngas has concentrated on catalyst development and testing in fixed bed reactors at atmospheric pressure (1). Very few workers have investigated CPO in fluidised bed reactors (2-4) or at elevated pressures (5,6). All results reported for high pressure experiments were obtained either with diluted (with excess steam or inert gas) or non-stoichiometric (low oxygen) feeds and are therefore not indicative of the performance under conditions required for a commercial plant. In this paper we report the results obtained in fixed and fluidised bed reactors at atmospheric and elevated pressures with a methane to oxygen ratio of 2. These results are discussed in the context of further development of the CPO process.

EXPERIMENTAL

The catalyst tested in this work was 0.25%Rh/5%ZnO/ γ -Al₂O₃. The experiments were carried out using three reactors made of silica: fixed bed and fluidised bed, the latter type configured either in the conventional way with porous distribution plate or as a spouted reactor (Fig 1). The design of the spouted reactor was such that methane and oxygen were mixed immediately before entering the catalyst bed. The spouted reactor was designed specifically for experiments at high pressures where short mixing times were important to limit the contribution of non-catalytic gas phase reactions between methane and oxygen.

Typical experimental procedure was as follows. Prior to each experiment the catalyst was reduced in flowing hydrogen (CIG, >99%, 500 mL/min) at 500°C for 3 hrs and cooled to ambient temperature. Flows of methane (Matheson, >99%) and oxygen (CIG, 99.99%) into the reactor were adjusted to the desired level using mass flow controllers (Brooks 5850TR), keeping CH₄/O₂ ratio = 2. The reactor temperature was raised slowly until the reaction was initiated (300 - 500°C) and then stabilised at constant level. After the reaction reached steady state, the products were analysed several times under each set of conditions.

RESULTS AND DISCUSSION

The performance of the rhodium catalyst at different space velocities in the fixed bed reactor is shown in Figure 1. At temperature of 900°C methane conversion and syngas selectivity are close to equilibrium and do not vary with contact time. At 800°C the departure from this pattern becomes noticeable and both the conversion and the selectivity increases with decreasing contact time. This trend becomes even more pronounced at 700°C. At gas flows above 300 L/h/g it was impossible to maintain the reaction temperature at 700°C even after removal of the external heater. In some cases temperature differences across the catalyst bed exceeded 150°C.

This example is a good illustration of the autothermal character of the partial oxidation reaction. It also points to the major disadvantage of the fixed bed reactor, namely the heat transfer limitation leading to the formation of the "hot spot" in the upper zone of the catalyst bed. Even at lowest gas flows used overheating of the top layers of catalyst was noticeable.

Entirely different behavior was observed in fluidised bed reactor. Even though the range of space velocities feasible in this type of reactor was restricted by the terminal velocity, some valid conclusions can be drawn from the comparison.

First, methane conversions are generally lower compared with fixed bed reactor. This is most likely the result of much better heat dissipation within the catalyst bed. The highest observed temperature differences between the top and the bottom of the reactor were 40°C and in most cases fell below 20°C despite the fact that the diameter of the fluidised bed reactor was almost three times larger than the fixed bed reactor.

Second, both methane conversions and carbon monoxide selectivities tend to decrease with increasing gas flows indicating the lack of autothermal effect. Similar pattern was observed for hydrogen selectivities, except that they tend to increase at space velocities below 30 L/h/g before declining at higher gas flows. This effect is probably caused by secondary reactions (*i.e.* combustion of hydrogen) at longer contact times.

The greater thermal stability of a fluidised bed reactor makes it more suitable for carrying out the partial oxidation reaction on a larger scale. It also seems that the activity of the catalyst is not an important factor within the temperature range >900°C needed to achieve high methane conversions required by commercial application, since equilibrium is reached easily under wide range of conditions. This is well illustrated by the results shown in Figure 4. They show that variation in catalyst loading from 12g to 3g has no significant effect on performance.

It appears that apart from efficient handling of heat transfer the greatest challenge in practical implementation of partial oxidation as an alternative technology for syngas production will be successful

and safe operation of the reactor at elevated pressures. The requirement for the use of high pressure is driven mostly by economic factors. Operation at high pressure allows the use of a smaller reactor and reduces demand for syngas compression for downstream processes.

There are two major problems that arise when the reactor pressure increases. First, as pressure exceeds about 0.2 MPa, the mixture of CH_4/O_2 at ratio of 2 becomes explosive. Second, the rates of non-catalytic homogeneous gas phase reactions between methane and oxygen leading to the formation of a wide range of products (methanol, formaldehyde, light hydrocarbons, carbon monoxide) increase quickly making it difficult to preheat the reactor feed.

One possible solution to these problems is to preheat methane and oxygen separately and to mix them immediately before introduction into the catalyst bed. To achieve this, a spouted reactor equipped with low residence time mixer (approx. 0.1 ms) was built (C, Figure 1). Ambient pressure tests have shown that its performance was identical to the conventional fluidised bed reactor. The results of high pressure operation of this reactor are presented in Figure 5. They show very minor drop in performance up to 0.6 MPa pressure. Several attempts to increase the pressure beyond 0.6 MPa were unsuccessful. They led to thermal instability indicated by temperature oscillations and resulted in damage to the reactor vessel in the region where methane and oxygen were mixed.

These results clearly indicate that further research aimed at development of a commercially viable partial oxidation process will have to concentrate on the reactor design to overcome problems associated with spontaneous ignition of the feed. Possible solutions may include multi-point oxygen injection, addition of steam to control the reaction exothermicity or the use of several reactors with heat recovery between stages.

CONCLUSIONS

The above results lead to the following conclusions :

1. Superior heat dissipation characteristics of fluidised bed reactors renders them most suitable for the partial oxidation reaction.
2. Further research should be aimed at overcoming problems associated with efficient heat removal from the reaction zone and elimination of autoignition of methane - oxygen mixtures.

ACKNOWLEDGMENT

Financial support for this project by the Energy Research and Development Corporation is gratefully acknowledged.

LITERATURE CITED

1. Foulds, G.A., Lapszewicz, J.A., (review)
2. Olsbye, U., Tangstad, E., Dahl, I.V., *Stud. Surf. Sci. Catal.*, **81**, 303 (1994)
3. Bharadwaj, S.S., Schmidt, L.D., *J. Catal.*, **148**, 11 (1994)
4. Goetsch, D.A., Say, G.R., US Patent 4,877,550 (1989)
5. Vernon, P.D.F., Green, M.L.H., Cheetham, A.K., Ashcroft, A.T., *Catal. Lett.*, **8**, 181 (1990)
6. Hochmuth, J.K., *Appl. Catal. B*, **1**, 89 (1992)

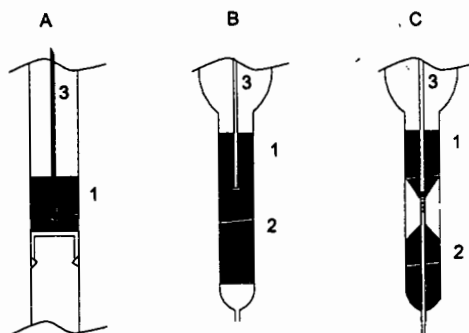


Figure 1. Design of the fixed bed (A, i.d. 10 mm), fluidised bed (B, i.d. 30 mm) and spouted (C, i.d. 30 mm) reactors. Catalyst (1), preheater (2), thermocouple well (3). All reactors made of silica.

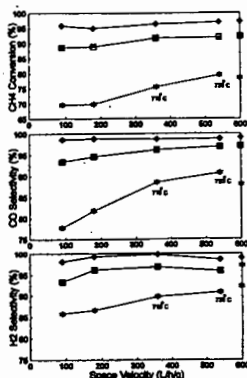


Figure 2. Space velocity vs. temperature profiles for the fixed bed reactor. (◆) 700°C, (■) 800°C, (*) 900°C. Catalyst loading 0.25g, particle size +125-250 μm . Symbols on right axis indicate thermodynamic equilibrium.

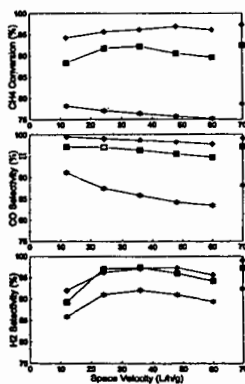


Figure 3. Space velocity vs. temperature profiles for the fluidised bed reactor. (◆) 700°C, (■) 800°C, (*) 900°C. Catalyst loading 3.0g, particle size +180-250 μm . Symbols on right axis indicate thermodynamic equilibrium.

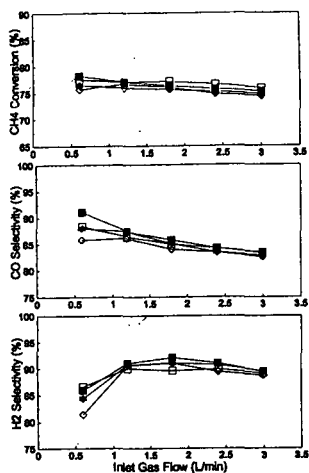


Figure 4. Effect of catalyst loading on performance in fluidised bed reactor at 700°C. (○) 1.5g, (■) 3.0g, (*) 6.0g, (□) 12.0g.

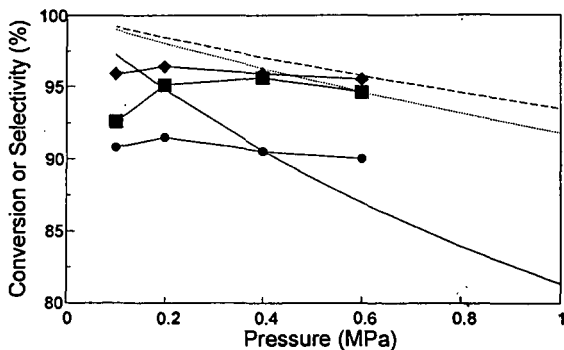


Figure 5. Performance of spouted reactor at high pressure at 900°C. Catalyst loading 3.0g, particle size +250-500 μm . (●) CH₄ conversion, (◆) CO and (■) H₂ selectivity observed. (—) CH₄ conversion, (---) CO and (.....) H₂ selectivity predicted at equilibrium.

HEMILABILE PHOSPHONATE-PHOSPHANE-RH-CATALYSTS FOR HOMOGENEOUS AND HETEROGENEOUS CARBONYLATION

S. Bischoff*, A. Weigt, H. Mießner, B. Lücke
 Institute for Applied Chemistry Berlin, Rudower Chaussee 5,
 124B9 Berlin-Adlershof, F.R.Germany

Keywords: methanol carbonylation, rhodium catalysts, hemilabile catalysts

Introduction

Mixed bidentate phosphane ligands such as ether-phosphanes [1-3], phosphane oxide-phosphanes [4], phosphanopyridines and amine-phosphanes [5] containing weak O- or N-donor groups and a strongly electron-donating phosphane group, are known to enhance activities or selectivities of Rh-catalyzed carbonylations. Also other transition metals form hemilabile O,P-chelated complexes, which have been extensively reviewed by Lindner [6]. A

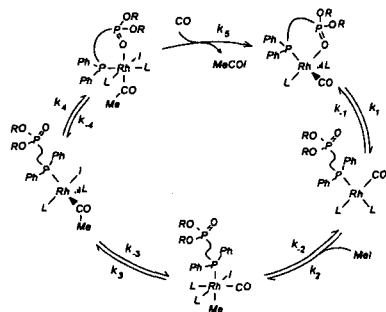
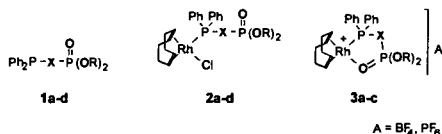


Fig. 1. Methanol carbonylation with hemilabile Rh complex catalysts

row of these complexes catalyzed not only carbonylations effectively but also hydrogenation [7], hydrosilylation [8], and ethylene polymerization [9]. The assumed function of the heterobidentate ligands in the rhodium catalyzed methanol carbonylation is illustrated in Fig. 1. It has been suggested that the oxygen-donating site of the bidentate ligand changes between a coordinated and an uncoordinated state during the catalytic cycle, thus forming chelate and open-chain metal complex structures [1,4]. The intramolecular generation and occupation of free coordination sites, stabilizing Rh-intermediates of different oxidation states and proceeding faster than according intermolecular processes, is assumed to accelerate rate-determining steps in the carbonylation route.

Rh-complexes with phosphonate-phosphanes [10] appeared as promising catalyst precursors because they form hemilabile complexes, which should enhance the necessary creation of free coordination sites in Rh^I-intermediates by ring-opening of chelate structures and ease the generation of the more oxophilic Rh^{III}-intermediates by O,P-chelate formation (Fig. 1). The concept of hemilabile catalysts with chelate structures involved in rate determining steps implies that the distance and structure between the phosphane and the phosphonate group should affect the carbonylation activity. Unlike the ether-, phosphane oxide-, amino- or pyridine-groups in previously described ligands [1-4], the phosphonate group should additionally facilitate a surface-anchoring of the transition metal complexes on oxidic materials such as silica or alumina, which is a necessary condition for stable slurry- and vapor-phase carbonylation catalysts. In this paper we wish to compare the new soluble Rh-complex catalysts 2a-d, derived from ligands 1a-d (Fig. 2), with known systems and report on the influence of the structure between strongly coordinated phosphane and weakly donating phosphonate moiety in homogeneous methanol carbonylation. Furthermore, we wish to report on supported hemilabile complexes and their properties in slurry- and vapor-phase methanol carbonylation.



	X	R
a	-CH ₂ -	ⁱ Pr
b	-CH ₂ CH ₂ -	Me, Et
c	-CH ₂ CH ₂ CH ₂ -	ⁱ Pr
d		ⁱ Pr

Fig. 2. Ligands and catalyst precursors

Experimental

The methylene bridged ligand 1a was accessible via reaction of LiCH₂P(O)(OⁱPr)₂ with bromodiphenylphosphane. Reaction of 2-chloro-ethyl-dimethylphosphonate or 3-bromo-propyl-diisopropylphosphonate with diphenylphosphane and potassium-tert.-butylate afforded the

phosphonate-phosphanes **1b** and **1c**. Reaction of the O,P-ligands with $[\text{ClRh}(\text{cod})]_2$ gave open-chain complexes, **2a - c** which could be easily converted with AgBF_4 or AgPF_6 into O,P-chelate structures **3a - c** (Fig. 2, Fig. 4). The structures of ligands and complexes were verified by MS, NMR and IR. A detailed report on preparation details and properties of the starting complexes will be given elsewhere [11].

Catalytic activities of the soluble Rh-catalysts were tested in a stirred 100 ml-autoclave made of stainless steel. During the catalytic runs, the autoclave-pressure was kept constant at 30 bar. To exclude air contact, the autoclave was filled using Schlenk-techniques with 100 mmol methanol, 6 - 48 mmol methyl iodide, 0.05 - 0.2 mmol rhodium complex and methyl acetate was used as solvent to reach a total volume of 25 ml. After pressurizing with CO (15 bar cold), the filled autoclave was heated up to reaction temperature between 120 and 195 °C and then the pressure was adjusted to 30 bar. The CO-consumption was calculated from the pressure decrease in a closed tank with a known volume which was connected to the autoclave via a pressure regulator. Carbonylation activity was calculated from the initial CO-conversion rate ($X_{\text{CO}} < 20\%$). A typical plot for the CO uptake vs. time is given in Fig. 3. The linearity of the plot clearly shows the zero-order of the substrate methanol and is in accord with the rate laws Eq. (1) and Eq. (2) below (p_{CO} , c_{Rh} , and $c_{\text{MeI}} = \text{constant}$). Second order rate constants k_i [$\text{l}\cdot\text{mol}^{-1}\cdot\text{s}^{-1}$] were related to the concentrations of Rh and MeI.

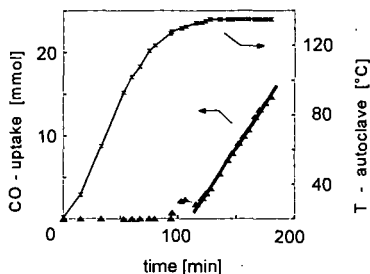


Fig. 3. Typical kinetic run

Results and discussion

The hemilabile character of phosphonate-phosphane-Rh complexes

The presumption for the catalytic concept has been preparatively confirmed for the phosphonate-phosphane-ligands. Both, cyclic and open-chain complexes were isolated after stoichiometric reactions (Fig. 4) at mild conditions. For instance, $(\text{cod})\text{RhCl}(\text{pepe})$ is smoothly converted with AgBF_4 into the halogene-free chelate complex at room-temperature and the ring-opening is easily achieved with CO at room-temperature under atmospheric pressure. Reversibility of the last process under reaction-like conditions is assumed from IR investigations of supported complexes. IR shifts in the stretching band of the phosphoryl group $\nu_{(\text{P}=\text{O})}$ to lower values in **3a - c** (KBr-wafer or solution), indicate the coordination of phosphoryl oxygen.

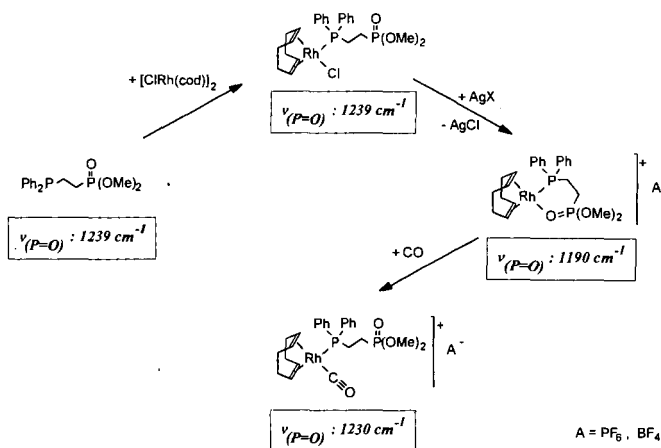


Fig. 4. Preparation and IR - data of catalyst precursors

^{31}P NMR data are depicted in Tab. 1. Not surprisingly, the shift in the ^{31}P NMR signal for the phosphane group ($\delta_{\text{phosphane}}$) shows that this group is coordinated in the open-chain complexes. The chelate structure of **3a - c** is confirmed by low field shifts of the phosphoryl-phosphorus signal ($\delta_{\text{P}=\text{O}}$, compared to **1a - c**, **2a - c**) and additionally by coupling with rhodium ($J_{\text{P}=\text{O}-\text{Rh}}$). Considering the IR spectra of **3a - c**, it is concluded that the P=O - groups and not the P-O-R' - groups act as oxygen donors.

Table 1. NMR data of ligands and Rh complexes

	$\delta_{P=O}$	J_{PORh}	J_{PP}	$\delta_{Phosphane}$	J_{PRh}
ligands					
1a	24.91 (d)	-	45.9	-25.32 (d)	-
1b	34.50 (d)	-	62.0	-12.10 (d)	-
1c	29.71 (d)	-	2.9	-17.37 (d)	-
open-chain complexes					
2a	21.33 (d)	-	16.9	21.51 (dd)	156.8
2b	32.80 (d)	-	63.0	26.80 (dd)	150.0
2c	29.28 (d)	-	4.9	26.60 (dd)	151.6
chelate complexes					
3a	48.85 (dd)	5.7	50.8	14.69 (dd)	149.6
3b	38.79 (dd)	2.9	13.1	21.21 (dd)	154.0
3c	40.13 (d)	8.1	-	23.74 (dd)	153.5

Catalytic properties of the hemilabile catalysts in homogeneous methanol carbonylation

The methanol carbonylation to acetic acid can roughly be formulated as a sequence of rate determining oxidative addition of the promoter MeI, methyl group migration to a CO-ligand and reductive elimination of acetyl iodide induced by CO-attack (Fig.1). The promoter is regenerated from methanol and HI, the last being liberated in the fast and irreversible proteolysis of acetyl iodide. Second order rate constants in a temperature range between 120 and 195 °C were obtained for various Rh-complexes in autoclave experiments monitoring the CO-consumption. The resulting activation parameters are summarized in Tab.2.

Table 2. Ligand effects on activation parameters of the Rh-catalyzed methanol carbonylation

	active carbon	cod	PPh ₃	dppe	1a	1b	1c	1d
ΔH^\ddagger [kJ/mol]	20.4	67.5	54.9	27.5	38.6	55.2	61.8	76.0
\pm	9.2	13.1	5.4	6.2	3.4	5.2	5.3	9.1
ΔS^\ddagger [J/mol/K]	-233	-112	-141	-211	-179	-141	-126	-90
\pm	22	32	13	15	8	12	12	22

cod - 1.5-cyclooctadiene, PPh₃ - triphenylphosphane, PPh₃:Rh = 2:1, dppe - bis(diphenylphosphano)ethane

The activation enthalpies in Tab.2 differ significantly over a wide range, but a general superiority of the hemilabile catalysts compared to known systems can not be postulated. With the data given here, one can choose certain temperatures to show the superiority of the hemilabile catalysts and the opposite can be done at another temperature, which may illustrate the sometimes questionable comparison of activities at one more or less arbitrary chosen temperature. It is interesting that activation enthalpies of hemilabile catalysts increased with growing distances between phosphonate- and phosphane-group. The highest activation enthalpy was obtained with the p-phenylene-bridged phosphonate-phosphane 1d, which can not form chelate complexes. This indicates that chelate structures are involved in one of the rate-limiting steps. The additionally to the oxidative MeI- addition emerging rate-limiting steps in P-ligand systems (see also Fig 5) can be the reductive elimination of acetyl iodide ($k_d \cdot k_g$) or methyl-group migration (k_g). With the given kinetic data, none of these alternatives can clearly be appointed to be more likely.

The hemilabile complex precursors showed generally higher activation entropies than the Rh-bisphosphane complex precursor. This is explained with the generation of open-chain structures of the phosphonate-phosphane complexes during the oxidative addition step, creating additional degrees of freedom for bond-rotation and vibrations. The apparently low activation enthalpy estimated (from only three points) for Rh supported on active carbon is probably caused by diffusion control. Observations in the vapor-phase methanol carbonylation confirmed this assumption.

It has to be stated here, that Tab. 2 shows apparent parameters, which do not merely reflect the rate determining oxidative addition of MeI as known for phosphane-free systems (e.g. cod as ligand), where a simple rate law (Eq. (7)) can be applied.

$$r = - \frac{dn_{CO}}{dt} = f(c_{MeI}) = k \cdot c_{MeI} \cdot c_{Rh} \quad (7)$$

The general case, considering additional rate-determining steps to the oxidative MeI addition, is a more complex function (Eq. (2)). This rate law has been derived from Fig. 1 applying network techniques [12] and covers also Eq. (1) as a special case (when $B \gg A \cdot c_{MeI}$).

$$\frac{1}{r} = A + B \cdot \frac{1}{c_{MeI}} \quad \text{with} \quad (2)$$

$$A = \frac{k_5 P_{CO} (k_3 k_4 + k_1 k_4 + k_1 k_3 + k_1 k_3) + k_1 (k_3 k_4 + k_3 k_4 + k_3 k_4)}{k_1 k_2 k_3 k_4 k_5 c_{Rh} P_{CO}} \quad \text{and}$$

$$B = \frac{k_5 P_{CO} (k_3 k_4 k_{-1} + k_1 k_4 k_{-2} + k_1 k_3 k_4 + k_4 k_1 k_{-2} + k_1 k_2 k_{-3} - k_1 k_{-2} k_{-3}) + k_2 k_3 k_4 (k_1 + k_{-1})}{k_1 k_2 k_3 k_4 k_5 c_{Rh} P_{CO}}$$

Indeed, Eq. (2) describes the influence of MeI concentration on the activity for both phosphane-containing and phosphane-free catalysts satisfactory, while the simple power law (Eq. (1)) failed, when phosphanes (e.g. **1a**) served as ligands (Fig.5). The changed reaction order of MeI is probably caused by the enhancement of MeI-addition due to phosphane ligands, consequently making other steps relatively slower and partly rate-limiting.

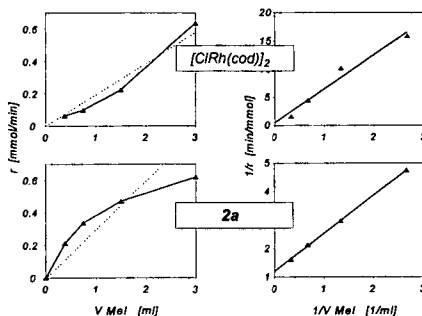


Fig. 5. Influence of MeI on the carbonylation rate; plots on the left side are derived from Eq. (1), on the right side from Eq. (2)

The new phosphonate - phosphane - complexes presented in this work were intended to be fixed on oxide surfaces via the phosphonate groups. While attempts of preparing stable complex-catalysts fixed on silica or alumina for slurry-phase reactions failed because of significant metal-leaching under carbonylation conditions, active carbon was found widely superior with respect to the leaching problem. In contrast to the results obtained for the homogeneous reaction, no significant ligand effects on the activation energies were observed, when the methanol carbonylation was conducted in the vapor-phase using active carbon supported complexes (Fig. 6). Normal diffusion of reactants begins to limit the activity of the supported Rh-complexes and leads to the observed uniform activation energies of about 30 kJ/mol.

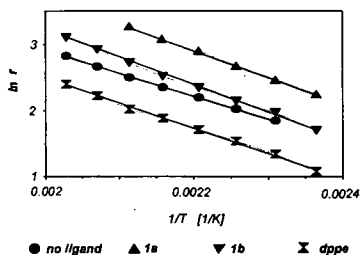


Fig. 6. Ligand effects on Arrhenius plots of active carbon-supported Rh-catalysts

IR-spectroscopic investigations of supported Rh-complex precursors revealed that the bisphosphane-ligand dppe hinders the formation of stable carbonyls (Fig. 7) and that the hemilabile ligands such as 2-(diphenyl-phosphano)ethyl dimethyl phosphonate (**2b**) form very stable monocarbonyl species, which are easily converted into dicarbonyl-species with increasing CO partial pressure even at elevated temperatures (Fig.8). The catalytic results in the vapor-phase suggest that phosphonate-phosphanes can also act as hemilabile ligands on supported catalysts.

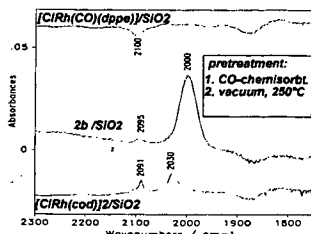


Fig. 7. FTIR spectra of supported Rh catalysts

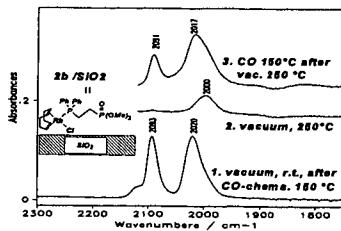


Fig. 8. Supported Rh-carbonyl species derived from 2b

Acknowledgements

The authors thank the Deutsche Forschungsgemeinschaft for financial support and Mrs. R. Dressel for the numerous catalytic measurements.

References

- [1] E. Lindner, H.A. Mayer, P. Wegner, *Chem. Ber.*, **119** (1986) 2616
- [2] E. Lindner, A. Sickinger, P. Wegener, *J. Organomet. Chem.*, **349** (1988) 75
- [3] E. Lindner, A. Bader, H. Bräunling, R. Jira, *J. Mol. Catal.*, **57** (1990) 291
- [4] R.W. Wegmann, A.G. Abatjoglou, A.M. Harrison, *J. Chem. Soc., Chem. Commun.*, **1987** 1891; R.W. Wegmann, A.G. Abatjoglou, *PCT Int. Appl. WO 8600888* (1986), C.A. **105** 174788
- [5] C. Abu-Gnim, I. Amer, *J. Mol. Catal.*, **85** (1993) L275, C. Abu Gnim, I. Amer, *J. Chem. Soc., Chem. Commun.*, **1994** 115
- [6] A. Bader, E. Lindner, *Coordination Chem. Rev.*, **108** (1991) 27-110
- [7] W.S. Knowles, *Acc. Chem. Res.*, **16** (1983) 106
- [8] Z. M. Michalska, *J. Mol. Catal.*, **19** (1983) 345
- [9] K.O. Starzewski, J. Witte, *Angew. Chem. Int. Ed. Engl.*, **24** (1985) 599
- [10] J. Freiberg, A. Weigt, H. Dilcher, *J. Prakt. Chem.*, **335** (1993) 337
- [11] A. Weigt, S. Bischoff, *Phosphorus, Sulfur, and Silicone*, in print
- [12] H.J. Bittrich, D. Haberland, G. Just: *Methoden chemisch-kinetischer Berechnungen*, VEB Deutscher Verlag für Grundstoffindustrie, Leipzig, 1979

FUEL OXYGENATES: ORGANIC CARBONATE SYNTHESIS

Ajit K. Bhattacharya
Texaco Inc., Texaco R&D
Beacon, NY 12508

Keywords: C₁ Chemistry & Catalysis, Oxygenates, Organic Carbonates

INTRODUCTION

Owing to the 1990 amendments to the Clean Air Act, two major programs, namely the oxygenated fuels program and the reformulated gasoline program have been mandated. Currently, ethers (MTBE, ETBE, and TAME) and alcohols (mainly ethanol) are employed as fuel oxygenates. However, several dialkyl carbonates exhibit attractive fuel properties and might emerge as future fuel oxygenates. This paper consists of an overview of related literature and highlight of some of our work on the synthesis of organic carbonates from C₁ feedstocks.

Dialkyl carbonates such as dimethyl carbonate (DMC), diethyl carbonate (DEC), and ethyl methyl carbonate (EMC) exhibit excellent gasoline blending properties such as high blending octane numbers and low blending Reid vapor pressures (RVP). Owing to their significantly higher oxygen content compared with alcohol (e.g., ethanol) and ether (e.g., MTBE, ETBE, and TAME) oxygenates, lower volume percent of the carbonate blending components will be needed to satisfy the 2.7 and 2.0 wt% oxygen requirements of the oxygenated and reformulated gasoline programs, respectively (1).

Dimethyl carbonate, for example, may be used as a fuel oxygenate, as a nontoxic and nonpolluting solvent, or as an environmentally harmless chemical in place of toxic and corrosive phosgene in the preparation of isocyanates, polycarbonates, synthetic lubricants, and various agricultural and pharmaceutical intermediates.

Dimethyl, diethyl, and dipropyl carbonates are manufactured, for use as specialty chemical or solvent, by the reaction of the corresponding alcohols with phosgene. Major producers of dialkyl carbonates by the conventional phosgene route are Van de Mark (USA), SNPE (France), BASF and Bayer (Germany). However, tremendous amount of research and development work has been going on worldwide for over thirty years to develop environmentally compatible and economically viable nonphosgene routes for the large scale production of these dialkyl carbonates.

BACKGROUND

Among the nonphosgene routes for the preparation of dialkyl carbonates, direct oxidative carbonylation of alcohols in the presence of various metal complex catalysts has been most widely investigated. A concise description of significant patents and publications in this area during 1963 to 1983 is given below.

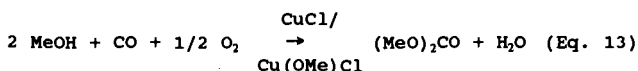
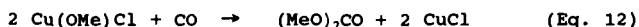
Mador et al(2) disclosed the preparation of aliphatic carbonates from alcohols and CO in the presence of costly platinum or palladium salts and usually large excess of an oxidizing metal salt such as copper (II) chloride. The need to use oxygen or air as an additional oxidizing agent was not mentioned. Alkyl halides, ethers, and CO₂ were obtained as undesired side products. The use of toxic mercuric salts in an organic solvent was described by D. M. Fenton (3).

The carbonylation of copper salts such as copper (II) dimethoxide or copper (II) methoxychloride was reported by Saegusa et al (4). In the presence of pyridine, the reaction proceeded even at room temperature. The reaction of copper (II) methoxychloride with CO was studied in great detail by Romano et al (5-7). Perotti et al (8,9) claimed the employment of copper complexes of pyridine and other amines, nitriles, and alkyl or aryl phosphines. However, Rivetti et al (10) showed that the reaction of methanol with CO to give dimethyl oxalate (DMO) and dimethyl carbonate (DMC) in the presence of palladium (II) acetate was inhibited almost completely by a trialkyl or an arylalkyl phosphine. Triaryl phosphines led to the formation of mostly DMO, whereas the yield of DMC was poor (1-6%). Gaenzler et al (11) patented the use of a catalyst system containing a copper salt and a phosphine oxide, phosphite, phosphate or a phosphonate.

routes. EniChem (Italy) has been successfully operating a stirred-tank DMC process involving the direct oxidative carbonylation method since 1983. At present, EniChem's DMC capacity at its plant in Ravenna is about 12,000 metric tons per year. EniChem has also licensed its DMC technology to GE and its joint venture partners Mitsui Sekka and Nagase & Co. for a 25,000 metric ton per year of polycarbonate plant in Japan. In 1993, Ube Industries (Japan) began operation of a semicommercial 3,000 metric ton per year DMC plant based on its proprietary vapor phase process via methyl nitrite which employs multimetallic (Pd-Cu-Mo-K) halides supported on activated carbon as a fixed bed catalyst (32). Furthermore, Ube is contemplating a 40,000 metric ton unit.

OXIDATIVE CARBONYLATION OF METHANOL

Preparation of dimethyl carbonate (DMC) by the reaction of methanol with carbon monoxide and oxygen in the presence of copper(I) chloride/copper(II) methoxychloride may be carried out in a stirred tank reactor by either a two-step batch process (Eq. 11 and 12) or a one-step catalytic process (Eq. 13), as follows.



Production of DMC by the oxidative carbonylation of methanol is exothermic and occurs with the coproduction of an equimolar amount of water. The produced water should be continuously removed from the reactor for several reasons. The catalyst activity as well as selectivity to DMC may be reduced at higher water concentration. Direct oxidation of carbon monoxide to carbon dioxide is likely to increase due to formation of water soluble catalytic species. At high water concentration, the possibility of DMC decomposition due to hydrolysis is also higher.

However, continuous removal of water from the reactor, separation of the catalyst system from reactants and products, and separation of DMC from methanol and water are challenging problems. To develop an improved and continuous DMC process, one should satisfy the following conditions:

- (i) the rate of DMC formation should be augmented,
- (ii) the heat of reaction should be dissipated, and
- (iii) the desired activity/stability of the catalyst system should be maintained while removing DMC and water from the reaction mixture.

It is noteworthy that DMC/water cannot be removed by an evaporative procedure without increasing the water concentration in the reaction mixture containing a methanolic slurry of Cu(I)Cl/Cu(II) (OMe)Cl as catalyst.

We have found that on the average, the rate of DMC formation may be enhanced by about eight times in the presence of N-methyl-2-pyrrolidone (NMP) as a high boiling point cosolvent which also helps in dissipating the heat of reaction (23). NMP can also serve as a catalyst carrier during the removal of DMC/H₂O by any flash procedure. Thus, a hot reaction mixture may be flashed to remove volatiles including DMC and water while the catalyst system, dissolved/suspended in NMP, may be recycled back to the reactor.

Low rates of DMC formation with copper(I) chloride/ copper(II) methoxychloride are partly due to low solubilities of these salts in methanol. Higher reaction rates can be attained with a solubilizing metal halide promoter such as calcium chloride (24), a phase-transfer agent such as benzyltriethylammonium chloride (25) or a polar cosolvent such as HMPA (26) or 2-pyrrolidone (23). The ability of copper to bind and activate carbon monoxide can be augmented with a nitrogenous ligand such as pyridine (27), imidazole (28), or a suitable cosolvent such as NMP or urea (29). For example, high rates of DMC formation can be achieved with copper(II) methoxychloride or imidazole-copper(II) methoxychloride in methanol-NMP.

CONCLUSIONS

A new and improved copper based homogeneous or slurry phase DMC process involving direct oxidative carbonylation of methanol can be successfully carried out in the presence of various ligands, promoters and organic cosolvents. A suitable high boiling point cosolvent (i.e., NMP) enhances the reaction-rate, helps in maintaining uniform temperature by dissipating the heat of reaction and serves as a catalyst carrier during the separation of methanol, DMC and water from the reaction mixture by a flash technique.

REFERENCES

1. A. K. Bhattacharya and E. M. Boulanger, "Organic Carbonates As Potential Components of Oxygenated Gasoline", Preprints of the Division of Environmental Chemistry, 471-473, the 208th ACS National Meeting, Washington, D.C., August 21-25, 1994.
2. I. L. Mador and A. U. Blackham, U.S. Patent 3,114,762 (1963).
3. D. M. Fenton, U.S. Patent 3,227,740 (1966).
4. T. Saegusa, T. Tsuda, and K. Isayama, J. Org. Chem., 35, 2976-2978 (1970).
5. U. Romano, R. Tesei, M. M. Mauri and P. Rebora, Ind. Eng. Chem. Prod. Res. Dev., 19, 396-403 (1980).
6. U. Romano, R. Tesei, G. Cipriani, and L. Micucci, U.S. Patent 4,218,391 (1980).
7. U. Romano, F. Rivetti, and N. Di Muzio, U.S. Patent 4,318,862 (1982).
8. E. Perrotti and G. Cipriani, U.S. Patent 3,846,468 (1974).
9. G. Cipriani and E. Perrotti, U.S. Patent 3,980,690 (1976).
10. F. Rivetti and U. Romano, J. Organomet. Chem., 174(2), 221-226 (1979); Chem. Abstr., 91, 174405e (1979).
11. W. Gaenzler, G. Schroeder, and K. Kabs, U.S. Patent 3,952,045 (1976).
12. J. E. Hallgren and G. M. Lucas, U.S. Patent 4,360,477 (1982).
13. Y.-P. Yang and A. L. Lapidus, Izv. Akad. Nauk SSSR, Ser. Khim., No. 2,363-365 (1977); Chem. Abstr., 86, 171868u (1977).
14. A. L. Lapidus and Y.-P. Yang, Izv. Akad. Nauk SSSR, Ser. Khim., No. 5,1180-1182 (1980); Chem. Abstr., 93, 72338j (1980).
15. H. Itatani and S. Danno, Jpn. Kokai Tokkyo Koho 79, 24, 827 (1979); Chem. Abstr., 91, 74204v (1979).
16. G. Stammann, R. Becker, J. Grolig, and H. Waldmann, U.S. Patent 4,370,275 (1983).
17. D. Cipris and I. L. Mador, U.S. Patent 4,131,521 (1978).
18. W. Gaenzler, K. Kabs, and G. Schroeder, U.S. Patent 4,113,762 (1978).
19. J. E. Hallgren, U.S. Patent 4,361,519 (1982).
20. E. Drent, European Patent 0,071,286 (1983).
21. F. Rivetti, U. Romano, and D. Delledonne, "Dimethyl Carbonate And Its Production Technology", Preprints of the Division of Environmental Chemistry, 332-335, the 208th ACS National Meeting, Washington, D.C., August 21-25, 1994.
22. F. Ancillotti and E. Pescarollo, European Patent 512,593 A1 (1992).
23. A. K. Bhattacharya and J. T. Nolan, U.S. Patent 4,636,576 (1987).
24. A. K. Bhattacharya, U.S. Patent 4,785,130 (1988).
25. A. K. Bhattacharya, U.S. Patent 4,879,266 (1989).
26. A. K. Bhattacharya, U.S. Patent 4,638,076 (1987).
27. A. K. Bhattacharya, U.S. Patent 4,761,467 (1988).
28. A. K. Bhattacharya and J. T. Nolan, European Patent 217,651 A2(1987).
29. A. K. Bhattacharya, U.S. Patent 5,001,252 (1991).
30. S. Yokota, H. Koyama, and H. Kojima, U.S. Patent 5,089,650 (1992).
31. European Patent 259,788 A2 (1988).
32. T. Matuzaki, T. Simamura, S. Fujitsu and Y. Toriyahara, U.S. Patent 5,214,184 (1993).
33. J. F. Knifton and R. G. Duranleau, J. Molecular Catal., 67, 389-399 (1991).
34. Y. Okada, T. Kondo, and S. Asaoka, "Dimethyl Carbonate for Fuel Additives", Fuel Chemistry Division, 359-364, the 207th ACS National Meeting, San Diego, CA, March 13-17, 1994.
35. G. E. Morris, International Patent W084/02339 (June 21, 1984).

A NEW CATALYST FOR HIGHER ALCOHOL SYNTHESIS. J. Skrzypek, K. Krupa, M. Lachowska and H. Moroz, Institute of Chemical Engineering, Polish Academy of Sciences, PI-44-100 Gliwice, ul. Baltycka 5, Poland.

Higher alcohols C_1-C_9 are of current interest as blending stocks for motor gasoline. Furthermore, they can be a real alternative for MTBE since they are entirely based on natural gas and are good octane boosters and combustion improves.

A catalyst containing CuO (50-60 wt.%), ZnO (25-30 wt.%), ZrO_2 (7-14 wt.%), Fe_2O_3 (1-4 wt.%), MoO_3 (7-15 wt.%), ThO_2 (1-3 wt.%), and Cs_2O (0.5-1.5 wt.%) has been developed. The catalyst was prepared by an original method of decomposition of organic complexes containing metallic components of catalyst, e.g., thermal decomposition of citrates. This catalyst yielded up to 150 g/kg_{cat}·h liquid product containing 30-40 wt.% of the most valuable alcohols C_{2+} .

The effect of temperature, pressure, contact time and synthesis gas composition were determined. The best results were obtained for temperature $T = 630-650$ K, pressure $P = 10$ MPa, GHSV = 6000-8000 hr⁻¹ and $H_2/CO = 1.0-1.3$ [mol/mol].

COMMERCIAL-SCALE DEMONSTRATION OF A LIQUID-PHASE METHANOL PROCESS

Steven L. Cook
Eastman Chemical Company
Eastman Road
Kingsport, TN 37662

Keywords: Liquid-Phase-Methanol Process, Demonstration-Scale, Synthesis Gas

ABSTRACT

The Eastman Chemical Company operates a coal gasification complex in Kingsport, Tennessee. The primary output of this plant is carbonylation-derived acetic anhydride. The required methyl acetate is made from methanol and acetic acid. Methanol is currently produced from syngas by a gas-phase process, which must receive stoichiometric quantities of carbon monoxide and hydrogen to avoid overheating the catalyst. Control of this CO/H₂ ratio is accomplished with a shift reactor. A liquid-phase methanol process (LPMEOH™) has been developed by Air Products. Efficient heat removal permits the direct use of syngas without the need for the shift reactor. An Air Products/Eastman joint venture, with partial funding from the Department of Energy under the Clean Coal Technology Program, has been formed to build a demonstration-scale liquid-phase methanol plant. This talk will focus on the unique features of this plant and how it will be integrated into the existing facilities.

INTRODUCTION

Eastman Chemical Company has practiced the carbonylation of methyl acetate to acetic anhydride for many years.^{1,2} In an array of integrated plants, coal is gasified and the resulting synthesis gas purified to a high degree. This gas, which consists chiefly of carbon monoxide and hydrogen, is used to feed the chemical plants. Methanol is produced in one plant by the Lurgi low-pressure gas-phase process. The methanol is combined with returned acetic acid to produce methyl acetate. Acetic anhydride is produced by the reaction of this methyl acetate with carbon monoxide.

The syngas needed for these plants is produced by two high-pressure gasifiers. High-sulfur coal is ground and fed to these gasifiers as a water slurry with pure oxygen. The hot gas is scrubbed with water to reduce the temperature and remove ash. A portion of the crude syngas is routed to a water-gas shift reactor to enrich the stream in hydrogen so that the stoichiometry required for methanol synthesis can be attained. Hydrogen sulfide is then scrubbed from the gas streams and converted to elemental sulfur. After final purification in a cryogenic "cold box" the syngas is pure enough to serve as feed to the methanol and acetic anhydride processes. Key changes to the gas stream as a result of these manipulations are illustrated in Figure 1.

DISCUSSION

In a methanol plant, the reaction between carbon monoxide, carbon dioxide, and hydrogen is exothermic and, because of the fixed bed reactor design, heat control and removal is of prime concern. If too much carbon dioxide or carbon monoxide is present, the reactor can overheat and damage the catalyst. Catalyst sensitivity to overheating is a chief reason that a more forgiving reaction system has been sought for syngas-based methanol production.

For a given catalyst, a liquid-phase reactor is preferable for numerous reasons. The basic characteristics of a liquid-phase reactor allow it to be cooled internally. This is a significant advantage for removing the rather large net heat of reaction encountered during methanol synthesis. By removing this heat with an internal heat exchanger, steam can be co-generated and employed for various process uses. In the liquid-phase reactor, an inert oil is used to slurry the methanol catalyst and to carry away the heat of reaction. Because of the efficient heat removal offered by the oil component, isothermal operation is possible, and per pass conversion is not as limited in comparison to a gas-phase reactor. While the latter reactor must rely upon dilution with recycle gas to control the reaction and carry away the heat, the inert oil in the liquid-phase reactor serves as a heat sink, thereby protecting the active sites of the catalyst from overheating. Added benefits resulting from this configuration are that the H₂/CO/CO₂ stoichiometry need not be controlled as closely (CO-rich mixtures are permissible) and carbon dioxide can be present in high concentrations. The net result of this last feature is that the expense and added complexity of a shift reactor can be eliminated because, in most cases, syngas can be used directly.

The liquid-phase methanol process (LPMEOH™)³, developed by Air Products and Chemicals, Incorporated, offers a sound way to take advantage of the benefits of internal heat removal. As shown in Figure 2, this process allows purified but otherwise unaltered synthesis gas to be fed directly to the reactor. The copper/zinc oxide-based methanol catalyst is suspended in an inert oil, which serves as the heat transfer medium. Internal heat exchangers remove the heat generated by the highly exothermic reaction and provide process steam for appropriate uses. The gross effluent is separated from the oil in a cyclone separator and then cooled to condense traces of oil. The vapor

is then chilled to remove the methanol, and the off-gas is warmed and compressed for recycle or sent to downstream uses.

An Air Products/Eastman joint venture, with partial funding from the Department of Energy under the Clean Coal Technology Program, has been formed to build a demonstration-scale version of liquid-phase methanol plant. The gasification complex in Kingsport, Tennessee provides an ideal source of synthesis gas to test this plant. In addition to providing methanol for the carbonylation process, the demonstration unit will be tested under a large variety of operating conditions. This is possible because smooth operation of the integrated plants will not be completely dependent on the output of the liquid-phase methanol plant. It will therefore be possible to ramp the output up and down, co-produce dimethyl ether (DME), and produce fuel-grade methanol for testing in on- and off-site applications, such as power plant boilers, buses, and vans.

To illustrate how the new methanol process will affect the overall configuration of the coal gas facility, two schematic diagrams of the entire complex are provided below. The conventional, gas-phase methanol process is included in the first schematic (Figure 3), while changes resulting from incorporation of the liquid-phase process are summarized in Figure 4.

A brief description of the overall operation of this complex is offered: Coal is systematically unloaded from rail cars and continuously fed to grinding mills by a highly automated Coal Handling system. In the Coal Slurry section, coal is mixed with water during the grinding process to provide a mobile slurry that can be pumped to the gasifiers. Oxygen is provided by an Air Products separation plant. Use of pure oxygen allows the gasifiers to operate at over 1000°C, which eliminates the coproduction of environmentally undesirable byproducts. Within the Gasification Plant the coal slurry and oxygen combine in Texaco-designed gasifiers in a sustained reaction to produce a CO-rich product. The high-temperature exhaust is then quenched with water to cool the gas and remove ash particles. The crude gas is then passed through a water-gas shift reactor to increase the hydrogen content. Before exiting the gasification plant, the product gas is cooled by water-fed heat exchangers that produce low-pressure process steam for use elsewhere in the complex. Within the Gas Purification section hydrogen sulfide and carbon dioxide are removed by the Linde AG-developed Rectisol process. This is accomplished by selectively absorbing the gases in cold methanol. The hydrogen sulfide/carbon dioxide stream is sent to the Sulfur Recovery plant where a Claus unit, coupled with a Shell off-gas treating unit, converts it to elemental sulfur. This sulfur is clean enough to be sold as a pure byproduct. The final off-gas consists mainly of carbon dioxide, which is converted to the solid form for various commercial uses. As the syngas exits the purification section, a portion of it is passed to CO-Hydrogen Separation, essentially a cryogenic "cold box" (also developed by Linde) which permits separation of carbon monoxide and hydrogen by low-temperature distillation. The hydrogen from this unit is combined with CO/H₂ from the Gas Purification section to serve as feed for the Methanol Plant. The methanol product is fed to an Eastman-developed Methyl Acetate Plant, which uses a novel reactor-distillation column⁴ to continuously convert methanol and acetic acid to methyl acetate in essential one piece of equipment. Carbon monoxide from the cryogenic unit, along with methyl acetate, is sent to the Acetic Anhydride Plant, also developed by Eastman, where carbonylation produces acetic anhydride. If methanol is also fed to this plant, a portion of the acetic anhydride is converted to acetic acid and methyl acetate.

Although the changes appear minor from the level of detail provided in this diagram, many process details are simplified when the CO/CO₂/H₂ mix is not critical:

- * Need for shift reactor eliminated
- * Low sensitivity to flow variations
- * Higher per-pass conversion requires less off-gas recycle
- * Less waste CO₂ because more can be utilized in methanol production
- * Less complex and expensive catalyst replacement requirements

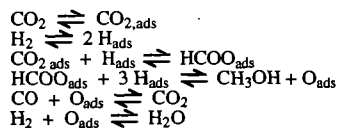
A shift reactor is normally needed to increase the hydrogen/CO ratio of raw synthesis gas so that enough hydrogen is available to satisfy the required stoichiometry for conversion to methanol. If the methanol reactor could operate properly with syngas that is lean in hydrogen, this processing equipment could be eliminated. Moreover, processes downstream of the methanol plant that need CO containing little or no hydrogen, such as that required by the methyl acetate carbonylation process, would also benefit because the methanol plant serves to reduce the hydrogen content from the off-gas so that further processing is either not needed or requires smaller separation equipment. Because of the large heat sink provided by the internal heat exchanger of the LPMEOH™ process, excess CO/CO₂ does not damage the catalyst by inadvertent overheating.

Another way to damage the catalyst in a gas-phase reactor is by transient variations in the syngas flow rate. Here, excess reactant feed rates rather than stoichiometry are the concern. The result of

this condition is similar, however, in that the increased evolution of heat without an accompanying way to remove it can overheat the pellets.

Having an effective way to remove heat also permits the reactors to be operated at higher conversion rates. This benefits the space-time yield of the reactor and significantly reduces the off-gas recycle rate. It also serves to deplete the off-gas of hydrogen, which, as described above, is beneficial to downstream processes needing CO that is low in hydrogen content.

It is well known that the presence of CO₂ is essential to optimal operation of copper/zinc oxide-based methanol reactors. It is critical for conditioning and preventing damage to the catalyst.⁵ Isotopic labeling studies have shown⁶ that essentially all methanol is produced from the reaction of CO₂ with hydrogen. An internal water-gas shift reaction between the resulting water with CO generates more CO₂ for methanol production. The proposed mechanism is provided below for convenience:



Again, because of the heat management capabilities of the LPMEOH™ process, the amount of carbon dioxide normally present in raw syngas can be used without concern for overheating the catalyst. This results in a much more efficient use of carbon in the syngas. Indeed, a substantial amount of waste carbon dioxide is generated by the water-gas shift reactor needed for gas balance in the gas-phase methanol process.⁷

One final benefit of the LPMEOH™ process is that catalyst replacement is less complex and can be done on an on-going basis. Even though the catalyst in a gas-phase methanol reactor can typically operate for about two years before replacement is needed, the actual mechanics of replacement are a challenge. The catalyst itself is difficult to handle in the large quantities involved, and the reactor must be shut down, isolated and opened up to carry out the task. This can result in significant downtime resulting in inconvenience at the least to lost product sales as a major negative consequence. In the case of the liquid-phase process, the catalyst can be intermittently replaced as needed in substantially smaller amounts. Some of the benefits described above have also been discussed in a recent review.⁷

CONCLUSION

The construction and successful operation of the LPMEOH™ plant will be a landmark in development of synthesis gas technology. Given the importance of methanol not only as a chemical feedstock but as a fuel, demonstration of this technology on a commercial scale could have far-reaching importance. We at Eastman are pleased to be a part of this effort.

ACKNOWLEDGMENTS

Eastman Chemical Company gratefully acknowledges Air Products and Chemicals, Incorporated and the Department of Energy for their technological and financial support.

REFERENCES CITED

- (1) V. H. Agreda, *Chemtech*, 18, 250 (1988).
- (2) S. L. Cook, *Acetic Acid and Its Derivatives* (V. H. Agreda and J. R. Zoeller, ed.), Marcel Dekker, Inc. New York, 1993, Chapter 9.
- (3) W. R. Brown, "Flexible Electric Power Generation, The Integrated Gasification/Liquid Phase Methanol (LPMEOH™) Demonstration Project", Third Annual Clean Coal Technology Conference, Chicago, IL, September 6-8, 1994.
- (4) V. H. Agreda and R. L. Partin, U.S. Patent 4,435,595, 1984.
- (5) S. Lee, B. G. Lee, and V. R. Perameswaran, Fundamentals of Methanol Synthesis, Electric Power Research Institute, Proceedings, Thirteenth Annual EPRI Contractor's Conference on Clean Liquid and Solid Fuels, Palo Alto, January 1989.
- (6) G. C. Chinchin, K. Mansfield, and M. S. Spencer, *Chemtech*, 20, 692 (1990).
- (7) A. Cybulski, *Catal. Rev. - Sci. Eng.*, 36, 557 (1994).

Figure 1.

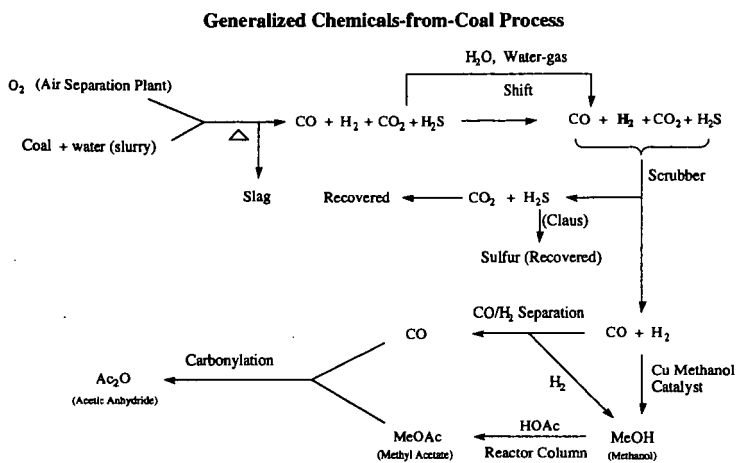


Figure 2. Air Products LPMEOH™ Process.

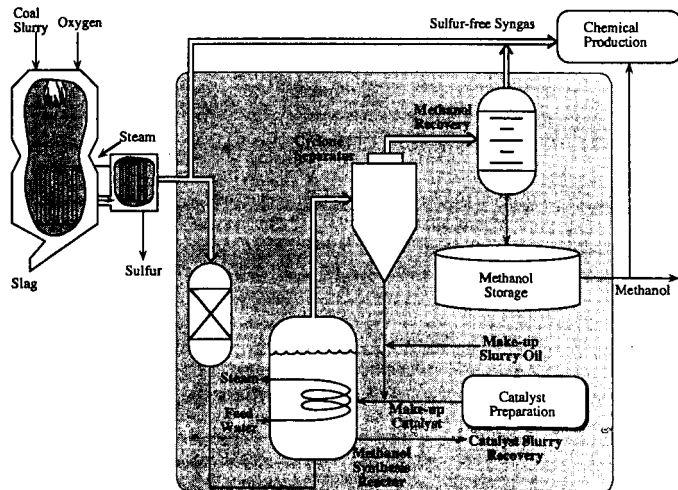


Figure 3: Configuration of Coal-Gasification/Acetic Anhydride Plant with Gas-Phase Methanol

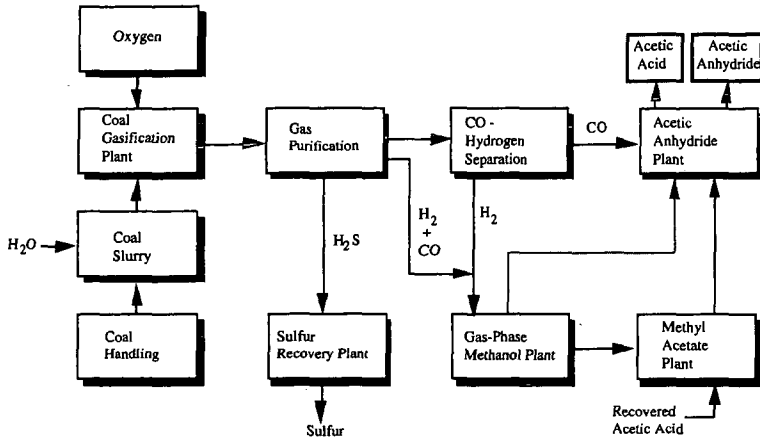
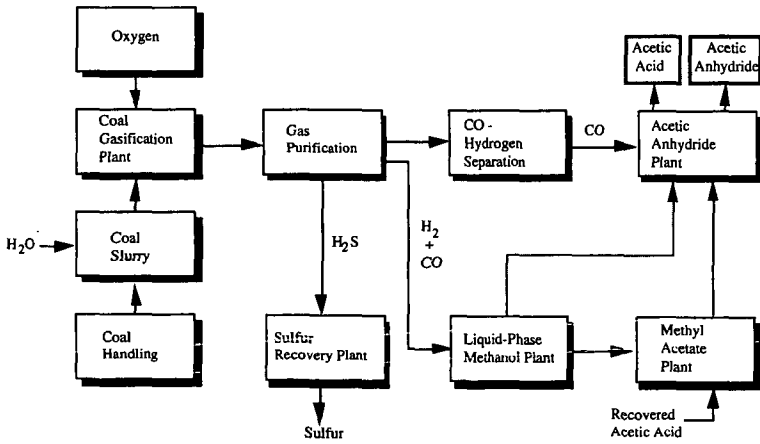


Figure 4: Configuration of Coal-Gasification/Acetic Anhydride Plant with Liquid-Phase Methanol



Kinetics and Dynamics of Heterogeneous Hydroformylation Rh Catalyst

Mark A. Brundage, Steven S. C. Chuang, and Michael W. Balakos
Department of Chemical Engineering,
The University of Akron,
Akron, OH 44325-3906, U.S.A.

Keywords: CO insertion, Oxygenates, Reaction pathway, Langmuir-Hinshelwood Kinetics.

Heterogeneous CO/H₂/C₂H₄ reaction of 4 wt% Rh/SiO₂ catalyst was studied using steady-state pulse transient method coupled with *in situ* infrared spectroscopy. The dynamic responses measured at various partial pressures of reactants show that the CO/H₂/C₂H₄ reaction can accurately be described by a Langmuir-Hinshelwood-Hougen-Watson (LHHW) model with the hydrogenation of adsorbed C₂H₃CO as the rate-determining step for propionaldehyde formation and the hydrogenation of adsorbed C₂H₅ as the rate-determining step for ethane formation. The kinetic model also accurately describes the adsorption isotherm of acyl intermediates measured by the pulse isotopic transient and adsorption isotherm of CO measured by IR spectroscopy. This study also demonstrates that the measurement of coverage of adsorbates by isotopic tracer pulsing and *in situ* infrared spectroscopy provides direct experimental evidence to confirm a postulated mechanism and rate law.

INTRODUCTION

The determination of reliable rate expressions is paramount in the design and modeling of heterogeneously catalyzed processes. Langmuir-Hinshelwood-Hougen-Watson (LHHW) kinetics of heterogeneous catalytic reactions has been studied for many years (1-7). However, the formalism has been the subject of much discussion and criticism. Most of the criticisms in the LHHW formalism are results of the inability to measure the coverage of adsorbates and reaction intermediates as a function of partial pressure of reactants and to identify the rate-determining step during the reaction (8,9). The objectives of this paper are to combine isotopic transient and *in situ* IR methods to study heterogeneous CO/H₂/C₂H₄ reaction and to test a LHHW model that can describe the overall kinetics for its ability to describe the adsorption isotherms of surface intermediates. Kinetic equations were derived from LHHW formalism with the postulation of a rate-determining step for both propionaldehyde and ethane formation. *In situ* IR coupled with transient isotopic tracing was used to observe the coverage of adsorbed species during the reaction and compared to the coverage predicted by the LHHW model.

EXPERIMENTAL

A 4 wt% Rh/SiO₂ catalyst was prepared from RhCl₃·3H₂O solution by the incipient wetness impregnation method. After impregnation, the catalyst was dried overnight in air at 300 K and then reduced in flowing hydrogen at 673 K for 16 hr. The exposed metal atoms was determined to be 122 μmol/g by H₂ pulse chemisorption at 303 K assuming an adsorption stoichiometry of H_{ads}/Rh = 1.

The apparatus used in this study is similar to that previously reported (10). Four independent quantities, including the rates of propionaldehyde and ethane formation and the surface converges of adsorbed CO and adsorbed acyl species, were measured as a function of partial pressure of reactants during steady-state condition. The coverage of intermediates during ethylene hydroformylation was determined from the dynamic response of C₂H₅¹³CHO to a ¹³CO pulse input. The coverage of adsorbed CO was measured by *in situ* IR spectroscopy.

RESULTS

Steady-State Measurements

The steady-state rate of formation of ethane and propionaldehyde during heterogeneous hydroformylation (CO/H₂/C₂H₄ reaction) on 4 wt% Rh/SiO₂ was measured by a gas chromatograph at 0.1 MPa. The main products in the reaction are ethane and propionaldehyde. Other minor hydrocarbon products include methane, propylene, butene, and butane. To determine the dependence of the reaction rates on the partial pressures of reactants, the rates were measured as the partial pressures of reactant at a total pressure of 0.1 MPa and 513 K. The flow rate of He was varied to maintain a constant total flowrate of 120 cm³/min. Both ethane and propionaldehyde formation rates are negative order in CO partial pressure while positive order in both hydrogen and ethylene.

The *in situ* IR spectra during the experiments of varying partial pressures are shown in Figure 1. The top spectra in Figure 1 show the variation of the spectra with CO partial pressure. The spectra at partial pressure of 0.083 MPa exhibit a linear CO band at 2037 cm⁻¹; a small bridged CO band at 1885 cm⁻¹; propionaldehyde band at 1740 cm⁻¹; and gaseous ethylene and ethane bands between 1900 and 3300 cm⁻¹ (11,12). The intensity and the wavenumber of adsorbed CO show stronger dependence on P_{CO} than P_{H₂} and P_{C₂H₄}.

Dynamic Measurements

The transient response of C₂H₅¹³CHO and the IR spectra to 10 cm³ pulse of ¹³CO into the ¹²CO feed to the reactor was recorded during the steady-state experimental runs. Figure 2 is the transient response of Ar, ¹³CO, and C₂H₅CHO measured by mass spectrometry under the conditions of 0.1 MPa, 513 K and CO/H₂/C₂H₄/He = 1/1/1.

Infrared spectra taken during the pulse of ^{13}CO in the CO feed show that the gas phase CO and adsorbed CO exchange with their isotopic counterparts at a rate much faster than the scanning rate of the IR. No other feature in the IR spectra changed during the course of the experiment, including those attributed to gaseous ethylene.

From the transient response, the average residence time of ^{13}CO adsorbed on the catalyst surface can be obtained by (10,13)

$$\tau_{^{13}\text{CO}} = \int_0^{\infty} t E_{^{13}\text{CO}}(t) dt \quad (1)$$

Since the gaseous CO and adsorbed CO exchange rapidly, the gaseous ^{13}CO response measured by mass spectrometry can be used as the response for the adsorbed ^{13}CO . The average residence time of all intermediate species leading to the formation of ^{13}C propionaldehyde from adsorbed ^{13}CO can be expressed as

$$\tau_{\text{C}_2\text{H}_5^{13}\text{CHO}} = \int_0^{\infty} t E_{\text{C}_2\text{H}_5^{13}\text{CHO}}(t) dt - \tau_{^{13}\text{CO}} \quad (2)$$

Figure 3 shows the deuterated propionaldehydes response to a 10 cm^3 pulse of D_2 into the H_2 flow during steady-state ethylene hydroformylation (14). The lag of the deuterated propionaldehydes response with respect to that of D_2 indicates that the hydrogenation of acyl intermediates is a rate-determining step.

DISCUSSION

The mechanism for the formation of propionaldehyde from $\text{CO}/\text{H}_2/\text{C}_2\text{H}_4$ reaction has been postulated from analogy with the homogeneous hydroformylation reaction (12,15). The general accepted mechanism of the reaction is shown in Table 1 (12). The approach for kinetic analysis of a heterogeneous catalytic reaction involves the postulation of a rate-determining step and express the rate in terms of the concentrations of the reaction intermediates in that step. The concentrations of the intermediates must then be related to the gas phase concentration of the reactants and products (adsorption isotherms). The simplest theoretical expression for an adsorption isotherm is the Langmuir isotherm, on which the LHHW formalism is based.

Different rate-determining steps, RDS, yield different forms of the rate equations so that they can be distinguished from each other. The best fit of the data is when step 6 in Table 1 is considered as the RDS for propionaldehyde formation. Step 6 as the RDS is supported by D_2 pulse studies as shown in Figure 3. The relation between $\text{TOF}_{\text{C}_2\text{H}_5\text{CHO}}$, $\text{TOF}_{\text{C}_2\text{H}_6}$, $\theta_{\text{C}_2\text{H}_5\text{CO}}$, and θ_{CO} , and partial pressure of the reactants can be derived from LHHW formalism with step 6 as RDS, as shown below.

$$\theta_{\text{C}_2\text{H}_5\text{CO}} = \frac{\sqrt{K_1 K_2 K_3 K_4 K_5 P_{\text{CO}}} \sqrt{P_{\text{H}_2}} P_{\text{C}_2\text{H}_4}}{1 + K_2 P_{\text{CO}} + \sqrt{K_1 P_{\text{H}_2}} + K_3 P_{\text{C}_2\text{H}_4}} \quad (3)$$

$$\theta_{\text{CO}} = \frac{K_2 P_{\text{CO}}}{1 + K_2 P_{\text{CO}} + \sqrt{K_1 P_{\text{H}_2}} + K_3 P_{\text{C}_2\text{H}_4}} \quad (4)$$

$$\text{TOF}_{\text{C}_2\text{H}_5\text{CHO}} = \frac{k_6 K_1 K_2 K_3 K_4 K_5 P_{\text{CO}} P_{\text{H}_2} P_{\text{C}_2\text{H}_4}}{(1 + K_2 P_{\text{CO}} + \sqrt{K_1 P_{\text{H}_2}} + K_3 P_{\text{C}_2\text{H}_4})^2} \quad (5)$$

$$\text{TOF}_{\text{C}_2\text{H}_6} = \frac{k_1 K_1 K_3 K_4 P_{\text{H}_2} P_{\text{C}_2\text{H}_4}}{(1 + K_2 P_{\text{CO}} + \sqrt{K_1 P_{\text{H}_2}} + K_3 P_{\text{C}_2\text{H}_4})^2} \quad (6)$$

The above rate law and isotherm equations derived from LHHW were found to accurately describe the rate and isotherm data.

CONCLUSION

Four independent quantities, $\text{TOF}_{\text{C}_2\text{H}_5\text{CHO}}$, $\text{TOF}_{\text{C}_2\text{H}_6}$, $\theta_{\text{C}_2\text{H}_5\text{CO}}$, and θ_{CO} were measured as a function of partial pressure of reactants during steady-state ethylene hydroformylation over Rh/SiO_2 . The results of this study demonstrate that the coverage of acyl intermediate determined from the dynamic response of an isotopic tracer is quantitatively consistent with that calculated from LHHW formalism; the coverage of $^*\text{CO}$ measured from IR spectroscopy is qualitatively consistent with that obtained from LHHW formalism. This study also shows that the measurement of coverage of adsorbates by both transient and IR techniques provides essential information to verify a proposed mechanism and kinetic model.

REFERENCES

- Hougen, O., and Watson, K., *Ind. Eng. Chem.*, **35**, 529 (1943).
- Tempkin, M., *Adv. Catal.*, **28**, 173 (1979).
- Smith, J., *Ind. Eng. Chem. Fundam.*, **21**, 327 (1982).
- Bourdart, M., and Djeda-Mariadassou, G., *Kinetics of Heterogeneous Catalytic Reactions*, Princeton University Press, Princeton, N.J., 1984.
- Weller, S., *Catal. Rev. Sci. Eng.*, **34**(3), 227 (1992).
- Hougen, O., and Watson, K., *Chemical Process Principles Part III-Kinetics and Catalysis*, John Wiley & Sons, New York, 1947.
- Hill, C., Jr., *An Introduction to Chemical Engineering Kinetics and Reactor Design*, John Wiley & Sons, New York, 1977.
- Kiperman, S., *Chem. Eng. Comm.*, **100**, 3 (1991).

9. Weller, S., *Adv. Chem Ser.*, **148**, 26 (1975).
10. Srinivas, G., Chuang, S., and Balakos, M., *AIChE J.* **39** 530 (1993).
11. Balakos, M., Chunag S., in press *J. Catal.* (1995).
12. Chuang, S., and Pien, S., *J. Catal.* **135**, 618 (1992).
13. Fogler, H., *Elements of Chemical Reaction Engineering*, 2 ed., Prentice Hall, Englewood Cliffs, 1992.
14. Brundage, M., M.S. Thesis, The University of Akron (1994).
15. Chuang, S., Tian, Y., Goodwin, J., and Wender, I., *J. Catal.* **96**, 449 (1985).

Table 1. The Proposed Mechanism for Heterogeneous Hydroformylation of Rh/SiO₂.

(Step 1)	$H_{2(g)} + 2^*$	$\xrightleftharpoons{K_1} 2^*H$
(Step 2)	$CO_{(g)} + ^*$	$\xrightleftharpoons{K_2} ^*CO$
(Step 3)	$C_2H_{4(g)} + ^*$	$\xrightleftharpoons{K_3} ^*C_2H_4$
(Step 4)	$^*C_2H_4 + ^*H$	$\xrightleftharpoons{K_4} ^*C_2H_5 + ^*$
(Step 5)	$^*C_2H_5 + ^*CO$	$\xrightleftharpoons{K_5} ^*C_2H_5CO + ^*$
(Step 6)	$^*C_2H_5CO + ^*H$	$\xrightarrow{k_6} ^*C_2H_5CHO + ^*$
(Step 7)	$^*C_2H_5 + ^*H$	$\xrightarrow{k_7} C_2H_6_{(g)} + 2^*$
(Step 8)	*C_2H_5CHO	$\xrightarrow{k_8} C_2H_5CHO_{(g)} + ^*$

K_i is the equilibrium adsorption parameter, $i=1,2,\dots$
 k_{i+} is the forward rate constant; k_{i-} is the backward rate constant.

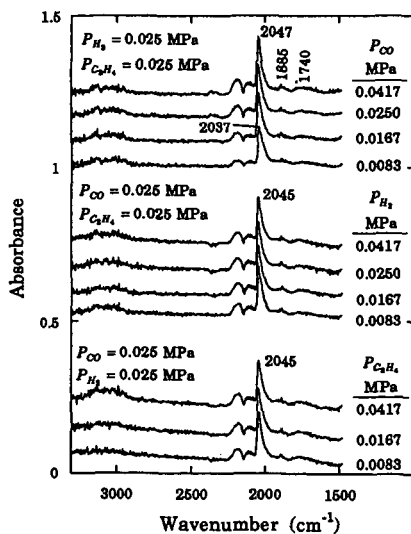


Figure 1. *In Situ* IR spectra of heterogeneous ethylene hydroformylation on 4 wt% Rh/SiO₂ at 513 K and 0.1 MPa at varying partial pressures of reactants.

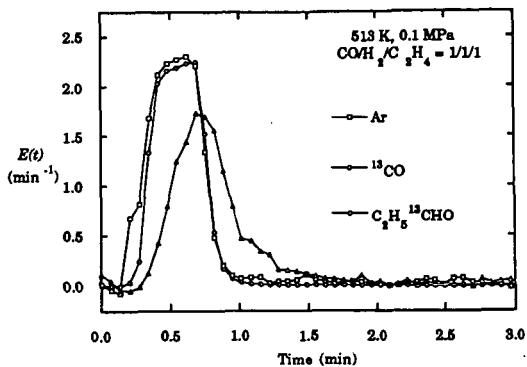


Figure 2. The Transient response of Ar, ^{13}CO , and $\text{C}_2\text{H}_5^{13}\text{CHO}$ to a 1 cm^3 pulse of ^{13}CO in a ^{12}CO flow during ethylene hydroformylation on 4 wt% Rh/SiO₂ at 513 K and 0.1 MPa.

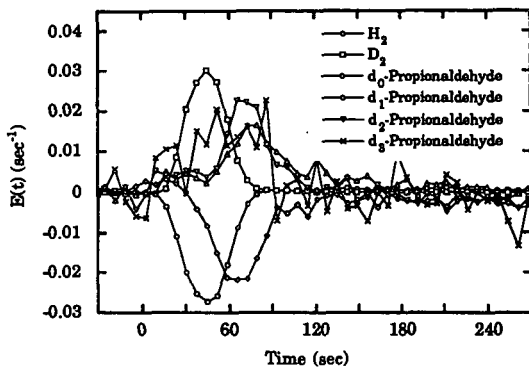


Figure 3. Transient Response of Deuterated Propionaldehydes to a 10 cm^3 pulse of D_2 into a H_2 flow during ethylene hydroformylation on 4 wt% Rh/SiO₂ at 513 K and 0.1 MPa.

DETAILED MECHANISTIC OF THE SYNTHESIS OF OXYGENATES FROM CO/H₂

Alessandra Beretta, Enrico Tronconi, Luca Lietti, Pio Forzatti, Italo Pasquon
Dipartimento "G. Natta", Politecnico, 20133 Milano-Italy

KEYWORDS: HAS, Reaction Network, Mechanistic Model

INTRODUCTION

The traditional interest for the synthesis of higher oxygenates from CO and H₂ mixtures has been recently focused on the accomplishment of high selectivities towards α -branched alcohols, such as 2-methyl-propanol and 2-methyl-butanol, which can be exploited as precursors for the synthesis of ethers (MTBE, TAME) with high octane properties [1]. Indeed isobutanol is the most abundant product of Higher Alcohol Synthesis (HAS); however, more than 100 other compounds are formed by hydrogenation of CO [2], among which commercially undesired oxygenates are also included. HAS product distribution is strongly affected by the operating conditions under which the reaction is carried out: contact time, temperature, feed composition control, in fact, the yield and selectivity of the different classes of species produced. The development of an industrial process for the synthesis of branched alcohols calls for a rational optimization of the operating conditions, which may be accomplished only by means of a reliable kinetic treatment of the reacting system. Detailed kinetic models of HAS have been proposed for both the low-temperature [3] and the high-temperature [4] modified methanol catalysts; however, so far no kinetic analysis has been published which can predict the whole distribution of HAS products as a function of all the operating variables.

In the following we present the development of a mechanistic kinetic model of HAS over Cs-promoted Zn/Cr/O catalysts aimed to design purposes; the model translates the bulk of independent observations concerning the mechanism and the thermodynamic constraints involved in the chain-growth process.

HAS REACTION NETWORK

An extensive study was performed in the past on the evolution and reactivity of the surface intermediates involved in HAS, consisting in steady-state microreactor experiments, Temperature Programmed Desorption (TPD) and Surface Reaction (TPSR) of a wide variety of oxygenated C₁-C₃ probe molecules [5, 6]; three major chemical routes were thus identified as responsible of the chain growth process:

- 1) the *aldol-type condensation* between carbonylic species, giving rise to the formation of branched higher aldehydes or ketones according to a "normal" or "oxygen-retention reversal" (ORR) evolution of the surface intermediate [7];
- 2) the so-called *α -addition* of a C₁ nucleophilic specie to higher aldehydes;
- 3) the *ketonization reaction*, responsible of the formation of ketones *via* decarboxylative condensation of two aldehydes.

Together with a first C₁->C₂ step, such reactions can explain the whole variety of observed under synthesis conditions.

While the chain growth proceeds in a kinetic regime, other reactions also involved in HAS have been proved to be governed by chemical equilibrium. They include: the methanol synthesis, the hydrogenation of aldehydes and ketones to primary and secondary alcohols respectively, the ketonization reactions, the water gas shift reaction and the synthesis of methyl-esters [8].

DEVELOPMENT OF A MECHANISTIC KINETIC MODEL OF HAS

The reaction network above presented has been validated on a quantitative basis by the formulation of a kinetic analysis [4] able to reproduce HAS product distribution for specified values of the operating conditions. Such original treatment has been recently modified and adapted to optimization purposes, that is to obtain a comprehensive and predictive description of the reacting system as function of the major operating variables. The development of the final

kinetic model can be schematized as follows in three subsequent steps:

1) **Identification of the reacting species.** Based on the experimental evidences, classes of reactants have been defined for each reaction included in the kinetic scheme. Namely, for the case of aldol condensations a nucleophilic behavior has been attributed to all the carbonylic species with no α -branching, while an electrophilic behavior has been attributed to the C_1 - C_6 aldehydes, both linear and branched. The nature of formaldehyde has been assumed for the C_1 intermediate involved in α -additions, which have been considered to interest the whole class of aldehydes as possible electrophilic reactants. Finally, for each ketone a contribute of formation via ketonization has been included.

2) **Chemical lumping.** Reaction rates and specie reactivities have been diversified along the line of the experimental observations. In the case of aldol condensations an intrinsic kinetic constant (function of reaction temperature, only) has been defined, but a set of further relative rate constants has been introduced in order to characterize the possible chain growth pathway (Normal or ORR), the nature of the nucleophilic reactant (aldehyde or ketone), the structure of the electrophilic agent (linear or branched). Similar diversification has been applied to the cases of α -additions and ketonizations.

3) **Formulation of model equations.** Mass balances have been written for all the reacting species; the rate expressions were based on a Langmuir-Hinshelwood mechanism taking into account the competitive adsorption of water on the catalyst active sites. Assumed an isothermal PRF model for the synthesis reactor, the model resulted in 42 differential mass balances for carbonyl species, 42 algebraic equations accounting for the hydrogenation equilibria between carbonyl species and corresponding alcohols, the balances for CO , H_2 , H_2O , CO_2 .

RESULTS

The model parameters were estimated from multiresponse non linear regression on 11 kinetic runs performed over a Cs-doped Zn/Cr/O catalysts. The comparison between experimental and calculated effects of H_2/CO feed ratio, CO_2 feed content and reaction pressure are reported in Fig. 1-3 (symbols = experimental data, lines = model calculations).

* **Effect of H_2/CO feed ratio.** As shown in Fig. 1a methanol concentration is maximum when a stoichiometric mixture of H_2 and CO is fed. The model reproduces correctly the experimental data, due to the assumption of chemical equilibrium for methanol synthesis. Higher alcohol concentrations present smooth maximum-wise trends with growing values of H_2/CO feed ratio in the range 0.5-1.5; the model predicts with accuracy that the highest productivities can be obtained for H_2/CO values close to 1. and 0.5, in the cases of primary alcohols (Fig. 1a-b) and ketones (Fig. 1c) respectively. Both experimental data and model calculations indicate that at high values of hydrogen partial pressures, a significant drop in the formation of the C_2 oxygenates occur.

* **Effect of CO_2 feed content.** The presence of CO_2 in the feed stream causes an overall decreasing of higher alcohols production (Fig. 2a-c). Such effect is however mostly emphasized in the case of the oxygenates with terminal behavior (isobutanol), while modest in the case of the intermediates species (ethanol): thus, the product distribution changes, with increasing fraction of CO_2 , in the direction of a growing molar ratio between low and high molecular weight components. These features are well reproduced by the kinetic treatment that can explain the inhibiting effect of CO_2 on HAS by accounting for the competitive adsorption of water on the catalyst active sites; notably, water concentration increases significantly with growing CO_2 partial pressure due the thermodynamic equilibrium which governs the water gas shift reaction.

* **Effect of reaction pressure.** A slight promotion of HAS is obtained by increasing the reaction pressure in the range 85-100 atm (Fig. 3a-c). Experimental and calculated results show, however, that such promotion is accompanied by a significant loss in the relative selectivity higher alcohol/methanol; methanol formation is, in fact, strongly enhanced at high pressures. The model fitting appears satisfactory. We note that the adoption of a first order dependence with respect to CO partial pressure for the kinetics of the $C_1 \rightarrow C_2$ reaction has been decisive for a proper simulation of the pressure effect; this results on the contrary overestimated when the formation of the first C-C bond is described by second order kinetics, in analogy with the chain-growth reactions (e. g. aldol condensations).

The match between experimental data and model previsions is extremely satisfactory and suggests an overall adequacy of the kinetic model (reaction mechanism, kinetic expressions, diversification of the reactivities). However, we have verified to a more stringent level the chemical costistency of our treatment by adopting of a perturbative approach: we have infact applied the model to the simulation of chemical enrichment experiments. The comparison between calculated and experimental effect of adding an oxygenate (ethanol, propanol, 2-butane) to the feed stream turned out to be highly informative on the accuracy with which reaction mechanism and the relative reactivities of the intermediates are decribed.

* *Addition of ethanol.* In this case a global promotion of HAS is experimentally observed. If compared to reference conditions where only syngas if fed to the reactor, the products mixture obtained with an ethanol-containing feed stream presents higher amounts of linear and branched primary alcohols, as well as of ketones (Fig. 4-a). This is in line with the well known high reactivity of the C₂ intermediate. Simulating the addition of ethanol, also the calculated product mixture distribution changes towards an increased amount of all the major classes of products (Fig. 4-b); such result proves that the model is able to reproduce correctly the key role of the intermediate specie and the network of chemical patterns which spread from it involving the whole reacting system. It is on the other hand evident that the model tends to overestimate the promotion of ketones formation, which has been related to an overestimation of the role of ketonization reactions in the kinetic scheme. We note, however, that ketones are only secondary products of HAS, their outlet concentration being usually one order of magnitude lower than the concentration of primary alcohols.

CONCLUSIONS

A mechanistic kinetic model of HAS over Cs-promoted Zn/Cr/O catalysts has been developed, the final aim being its application to process design purposes. The model adequacy has been tested by comparison with a set of kinetic data obtained under typical synthesis conditions and with the results of chemical enrichment experiments; the former are specifically demanding for a quantitative adequacy of the kinetic scheme, the latter are instead more informative on the accuracy with which the details of the reaction mechanism are taken into account. A satisfactory description of the reacting system has been obtained over a wide operational field; in line with the experimental results, the model calculations suggest that an equimolar H₂/CO feed ratio and absence of CO₂ in the feed stream are optimal conditions for the synthesis of branched oxygenates. Increments of the total pressure are then estimated to lead to a lowering of the relative higher alcohol/methanol selectivity.

ACKNOWLEDGEMENT

This research was supported by SNAMPROGETTI SpA.

REFERENCES

1. Zou, P., Summary of the HAS workshop, U.S. Dept. of Energy, Febr. 1994.
2. Forzatti, P., Tronconi, E., and Pasquon, I., *Catal. Rev. - Sci. Eng.* **33**, 109-168 (1991).
3. Smith, K. J., Young, C. W., Hermann, R. G., and Klier, K., *Ind. Eng. Chem. Res.*, **29**, 61 (1991)
4. Tronconi, E., Lietti, L., Gropi, G., Forzatti, P., and Pasquon, I., *J. Catal.* **135**, 99-114 (1992).
5. Lietti, L., Forzatti, P., Tronconi, E., and Pasquon, I., *J. Catal.* **126**, 401-420 (1990).
6. Lietti, L., Tronconi, E., and Forzatti, P., *J. Catal.* **135**, 400-419 (1992).
7. Nunan, J., Bogdan, C. E., Klier, K., Smith, K. J., Young, C. W., and Hermann, R. G., *J. Catal.* **116**, 195-221 (1989).

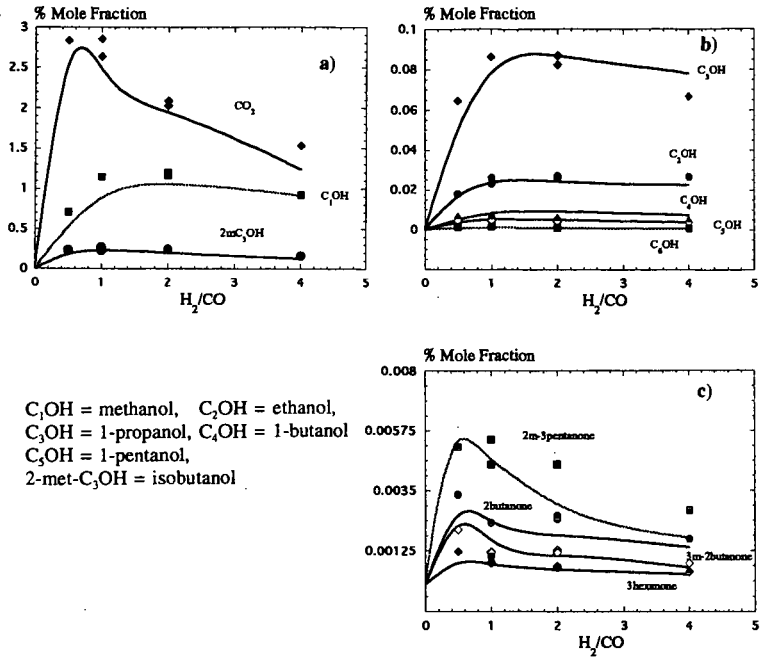


Fig 1. Calculated (lines) and experimental (symbols) effect of H_2/CO feed ratio on HAS product distribution. $T = 405^\circ C$, $P = 85$ atm, $CO_2 = 0\%$, $GHSV = 8000$ h^{-1} .

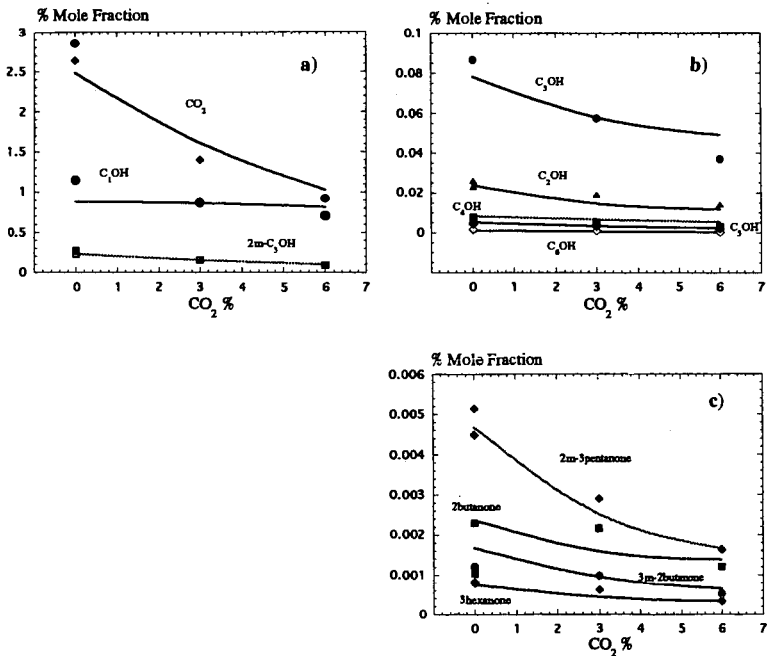


Fig. 2. Experimental and calculated effect of CO_2 feed content. $T = 405^\circ C$, $P = 85$ atm, $H_2/CO = 1$, $GHSV = 8000$ h^{-1} .

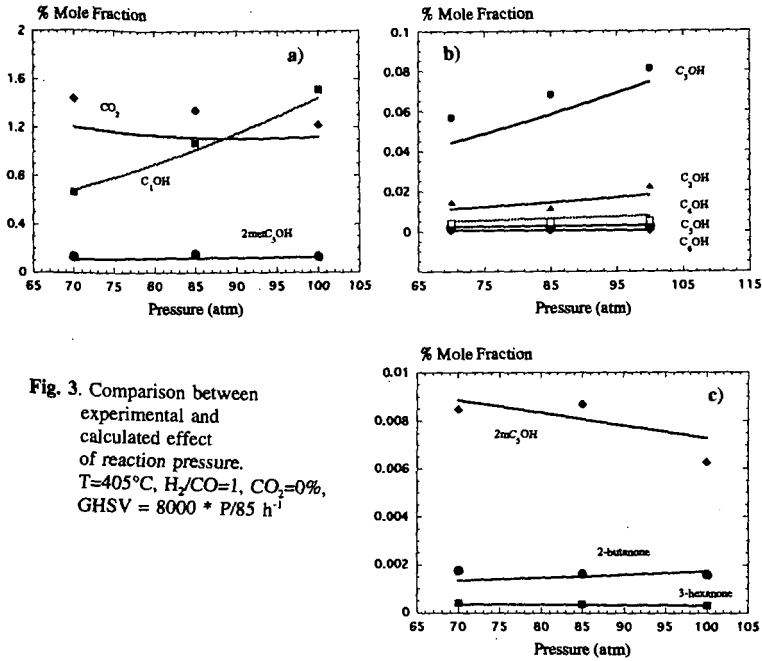


Fig. 3. Comparison between experimental and calculated effect of reaction pressure. $T=405^{\circ}\text{C}$, $\text{H}_2/\text{CO}=1$, $\text{CO}_2=0\%$, $\text{GHSV} = 8000 \cdot P/85 \text{ h}^{-1}$

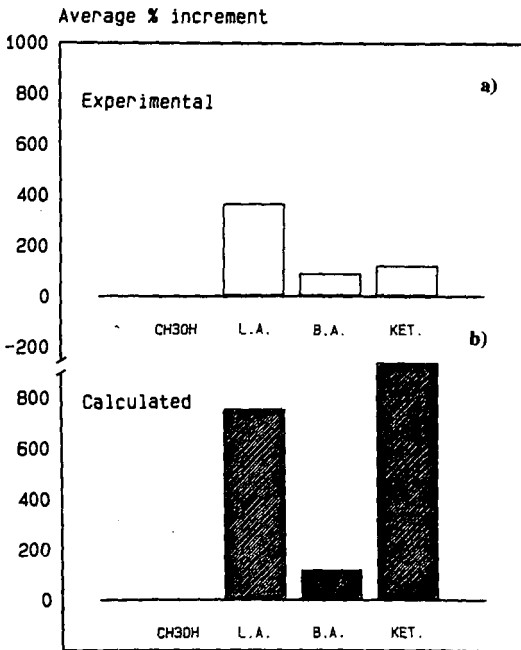


Fig. 4. Experimental versus calculated effect of ethanol addition on grouped HAS product distribution. $T = 405^{\circ}\text{C}$, $P = 85 \text{ atm}$, $\text{H}_2/\text{CO} = 1$, ethanol = 2 %, $\text{CO}_2 = 0 \%$, $\text{GHSV} = 8000 \text{ h}^{-1}$. The effect is expressed as average percentage increment of the molar fraction with respect to absence of ethanol in the feed stream for L.A.=linear alcohols (ethanol excluded), B.A.=branched alcohols, KET.=ketones.

MECHANISTIC STUDIES OF THE PATHWAYS LEADING TO ETHERS *via* COUPLING OF ALCOHOLS

Qun Sun, Luca Lietti, Richard G. Herman, and Kamil Klier
Zettlemoyer Center for Surface Studies and Department of Chemistry
7 Asa Drive, Lehigh University, Bethlehem, PA 18015, U.S.A.

Keywords: Alcohols, Ethers, Resin and HZSM-5 Catalysts, S_N2 reactions

ABSTRACT

The reaction mechanisms for the solid acid-catalyzed dehydrative coupling of methanol and ethanol with isobutanol and 2-pentanol to form ethers were examined by using isotope labelling and chiral inversion experiments. When the reactions were carried out at 110°C and 1 MPa with ^{18}O -ethanol and ^{16}O -isobutanol over the Amberlyst-35 resin catalyst, 95% of the major product ethyl isobutyl ether (EIBE) contained ^{16}O , while 96% of the minor product ethyl tertiarybutyl ether (ETBE) contained ^{18}O . Similar results were obtained with methanol and isobutanol over Nafion-H and Amberlyst-35 catalysts, with methyl isobutyl ether (MIBE) and methyl tertiarybutyl ether (MTBE) as the products. These results indicate that EIBE (MIBE) was produced by a surface-catalyzed S_N2 reaction, while the ETBE (MTBE) product arose *via* a carbenium intermediate. The analogous reaction carried out over Nafion-H and HZSM-5 catalysts with chiral 2-pentanol verified the surface-mediated S_N2 reaction, wherein chiral inversion of the product ether was observed relative to the S- and R-2-pentanol reactants. In addition, a remarkable shape selectivity with chiral inversion was observed over the HZSM-5 zeolite to selectively form 2-ethoxypentane but not 3-ethoxypentane.

INTRODUCTION

The dehydrative coupling of alcohols to form ethers is practiced on an industrial scale for symmetric ethers with small alkyl groups. In solution phase with an acid catalyst such as H_2SO_4 , it is generally believed that the synthesis of ethers from secondary and tertiary alcohols follow the S_N1 pattern, while synthesis from primary alcohols follow the S_N2 pathway [1]. Mechanistic studies of alcohol dehydration over solid oxide acid catalysts to form olefins and ethers *via* a consecutive-parallel pathway was reported by Knozinger et al. [2]. A series of studies on butanol dehydration over the HZSM-5 catalyst was performed by Makarova et al. [3,4], and ether formation was proposed to proceed *via* a surface- $\text{O}-\text{C}_4\text{H}_9$ intermediate.

Recently, we have explored some possible new routes for synthesizing high value oxygenates, e.g. fuel-grade C_3 to C_6 ethers such as MIBE, MTBE, EIBE, ETBE, ethyl isopropylether (EIPE) and diisopropylether (DIPE), from non-petroleum feed stocks [5-7] owing to the potential use of these ethers as effective anti-knock replacements for leaded gasoline. The $\text{CH}_3^{18}\text{OH}$ /isobutanol coupling reaction over the Nafion-H catalyst was studied, and a S_N2 reaction mechanism was suggested for the production of MIBE [6]. The present work extends the mechanistic study to other alcohol reactants, e.g. ethanol, isopropanol, and chiral 2-pentanol, as well as other solid acid catalysts, i.e. Amberlyst-35 and HZSM-5, and provided additional more generalized mechanistic features of the solid acid-catalyzed ether formation from the corresponding alcohols, $\text{ROH} + \text{R}'\text{OH} \rightarrow \text{ROR}' + \text{H}_2\text{O}$. Experiments were carried out using reactant mixtures in which one of the alcohols (i) was isotopically labelled with ^{18}O or (ii) contained a chiral center.

EXPERIMENTAL

The solid acid catalysts employed in the present study were the commercial Nafion-H with 0.9 meq H^+ /g, Amberlyst-35 from Rohm and Haas with 5.2 meq H^+ /g, and HZSM-5 from Mobil Corporation with a Si/Al ratio of 32/1. The ^{18}O -MeOH and ^{18}O -EtOH reagents with greater than 97% ^{18}O content were purchased from MSD Isotopes. The S-2-pentanol and R-2-pentanol were purchased from Aldrich Chemicals. The experiments were carried out at 90-110°C and 1 MPa total pressure in a gas phase downflow stainless steel tubular reactor with on-line GC analysis of reactants and products to determine alcohol conversion and product selectivities. Typically, the reactant feed contained 3.6 ml/hr liquid alcohol mixture, 88 ml/min He and 12 ml/min N_2 , where the reactant conversion was limited to less than 5%. The liquid products were trapped in a glass cold trap cooled with liquid nitrogen and examined for the source of the ether oxygen by GC/MS and for chirality by a Chirasil-CD column of fused silica column coated with beta-cyclodextrin. The reference compound R-2-ethoxypentane was prepared by using the Williamson synthesis method starting with R-2-pentanol and sodium metal. For comparison, the chiral experiment was also carried out in liquid phase at 100°C and ambient pressure for 1 hr with concentrated H_2SO_4 as the catalyst and the molar ratio of ethanol/2-pentanol/ $\text{H}_2\text{SO}_4 = 4.0/1.0/0.4$.

RESULTS

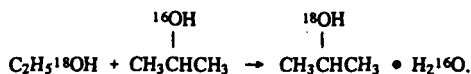
Isotope Labelling Studies of Ether Formation Over Amberlyst-35 Catalyst. The reactants in four experiments where the incorporation of the labelled oxygen into the ether products was monitored were the following:

1. $\text{CH}_3^{18}\text{OH} + (\text{CH}_3)_2\text{CHCH}_2^{16}\text{OH}$
2. $\text{CH}_3\text{CH}_2^{18}\text{OH} + (\text{CH}_3)_2\text{CHCH}_2^{16}\text{OH}$
3. $\text{CH}_3^{18}\text{OH} + \text{CH}_3\text{CH}_2^{16}\text{OH}$
4. $\text{CH}_3\text{CH}_2^{18}\text{OH} + (\text{CH}_3)_2\text{CH}^{16}\text{OH}$.

The labelling results involving isobutanol as a reactant over the Amberlyst-35 catalyst, shown in Tables 1 and 2, were similar to those for the coupling of $\text{CH}_3^{18}\text{OH}$ /isobutanol over the Nafion-H catalyst where the reactions were carried out at 90°C and ambient pressure [6]. In particular, DME (Table 1) and DEE (Table 2) contained almost only ^{18}O , indicating that no oxygen scrambling occurred with the acid catalyst, while MIBE and EIBE retained the ^{16}O of the isobutanol. MIBE and EIBE appear to be formed by the isobutanol attacking the acid-activated methanol and ethanol, respectively, while the methanol and ethanol attacking the isobutanol might be steric hindered. MTBE and ETBE contained ^{18}O , suggesting that these ethers were formed by the coupling of isobutene and the corresponding light alcohols. The isotope distributions in the products are not sensitive to the reaction conditions, e.g. temperature, pressure and relative concentration of the reactant alcohols, nor to the particular resin catalyst employed.

In contrast, the $\text{CH}_3^{18}\text{OH}/\text{CH}_3\text{CH}_2^{16}\text{OH}$ experiment showed that there was no steric (or other) preference in the coupling reaction over Amberlyst-35, and ^{16}O and ^{18}O were found with equal abundance in methyl ethylether (MEE) (Table 3). Again, the isotopic composition of DME and DEE demonstrated that no oxygen scrambling occurred.

In the experiment with ^{18}O -ethanol and ^{16}O -isopropanol (a secondary alcohol), with a 1.0/1.5 molar ratio respectively, the observed products were DIPE, propene, EIPE and DEE, given in order of decreasing selectivity. The isotopic distributions shown in Table 4 clearly showed that the mixed ether EIPE was formed via a mechanism wherein the ^{18}O from the ethanol was retained, while the ^{16}O of the reactant isopropanol molecule was predominantly lost, i.e.



These mechanistic studies utilizing $\text{CH}_3^{18}\text{OH}$ and $\text{CH}_3\text{CH}_2^{18}\text{OH}$ to couple with higher alcohols over the resin catalysts, Nafion-H and Amberlyst-35, indicated that ether synthesis proceeds mainly via a $\text{S}_{\text{N}}2$ reaction pathway to form methyl and ethyl ethers.

Ether Formation From Ethanol and Chiral 2-Pentanol. The definitive proof of a $\text{S}_{\text{N}}2$ reaction mechanism is the observation of the configuration inversion of the product with respect to the reactant. The experiments were carried out with S- or R-2-pentanol and $\text{CH}_3\text{CH}_2^{18}\text{OH}$ over the Nafion-H and HZSM-5 catalysts under the reaction conditions similar to those utilized in the previously described isotope labelling experiments.

The dehydrative coupling of ^{18}O -ethanol and S-2-pentanol produced self-coupling products DEE and di-2-amylether (D2AE), cross-coupling products 2-ethoxypentane (2-EP) and 3-ethoxypentane (3-EP), and the dehydration product 2-pentene but not ethene. The ^{18}O content and chirality of the cross-coupling products are presented in Table 5. For the acid-catalyzed cross-coupling of EtOH and 2-pentanol, the product 2-ethoxypentane can, in principle, be formed either by EtOH attacking the activated 2-pentanol or vice versa. The experiment with Et ^{18}OH was designed to determine the contributions from these two distinct routes. Data in Table 5 demonstrated that the EtOH attack of the acid activated 2-pentanol was the predominant pathway where ^{18}O was retained in the product ether. The true configuration inversion for the ether formation due to EtOH attack of the activated 2-pentanol is given in the last column of Table 5.

The combined ^{18}O retention and the R-/S- chirality results demonstrate that the axial rear-attack $\text{S}_{\text{N}}2$ mechanism dominates (97% over HZSM-5 and 77% over Nafion-H) in this heterogeneous acid-catalyzed dehydrative coupling of alcohols. It is probably due to the steric hindrance that HZSM-5 produced remarkably higher configuration inversion than either the Nafion-H and the H_2SO_4 . The Nafion-H resin catalyst behaved like an acid solution, possibly due to its flexible backbone of the acid groups. The OH group of 2-pentanol is the preferred leaving group, after being activated by the surface H^+ and subjected to the concerted nucleophilic attack by the light alcohol.

The minor paths (23% over Nafion-H and 3% over HZSM-5) can be accounted for by a less efficient carbenium ion (C⁺) or olefin (C⁻) intermediate mechanism. These minor paths are corroborated by observations of the 3-ethoxypentane product, which could only be formed via carbenium ion or olefinic intermediates, over Nafion-H. However, 3-ethoxypentane was not observed as a product with the HZSM-5 catalyst, indicating that the formation of 3-ethoxypentane could be further minimized by shape selectivity in the zeolite pore. The 3-ethoxypentane is more branched and is expected to pass through the HZSM-5 channel (0.55 nm) [8] at a slower rate than 2-ethoxypentane, even if it were formed by the carbenium ion or the olefin reactions at channel intersections.

CONCLUSIONS

The solid acid, Nafion-H, Amberlyst-35 and HZSM-5 zeolite, catalyzed direct coupling of alcohols to form ethers proceeds primarily through a surface-mediated S_N2 reaction pathway that is far more efficient than either a carbenium or olefin pathway. The surface-S_N2 reaction gives rise to high selectivity to configurationally inverted chiral ethers when chiral alcohols were used. This is especially observed in the case of the HZSM-5 catalyst, in which the minor C⁺ or C⁻ paths were further suppressed by "bottling" of 3-ethoxypentane by the narrow zeolite channels.

Acknowledgements

We thank the U.S. Department of Energy for financial support of this research, Rohm and Haas for providing the Amberlyst-35 catalyst, and Mobil Corporation for providing the ZSM-5 sample. Thanks to Professor J. Benbow for helpful suggestions on analysis of chiral products.

References

- Morrison, R.T., and Boyd, R.N., *Organic Chemistry*; Chapter 17, Allyn and Bacon, Inc., Boston, (1972).
- Knozinger, H., and Kohne, R., *J. Catal.*, 5, 264 (1966).
- Makarova, M.A., Williams, C., Thomas, J.M., and Zamaraev, K.I., *Catal. Lett.*, 4, 261 (1990).
- Makarova, M.A., Paukshtis, E.A., Thomas, J.M., Williams, C., and Zamaraev, K.I., *J. Catal.*, 149, 36 (1994).
- Nunan, J., Klier, K., and Herman, R.G., *J. Chem. Soc., Chem. Commun.*, 676 (1985).
- Herman, R.G., Klier, K., Feeley, O.C., and Johansson, M.A., *Preprints, Div. Fuel Chem., ACS*, 39 (2), 343 (1994).
- Herman, R.G., Klier, K., Feeley, O.C., Johansson, M.A., Sun, Q., and Lietti, L., *Preprints, Div. Fuel Chem., ACS*, 39 (4), 1141 (1994).
- Olson, D.H., Kokotailo, G.T., Lawton, S.L., and Meier, W.M., *J. Phys. Chem.*, 85 2243 (1981).

Table 1. Percent isotopic composition ($\pm 2\%$) of O-containing products from the reaction of CH₃¹⁸OH/¹⁶O-isobutanol over Amberlyst-35 catalyst at 110°C and 1 MPa.

Isotope	MIBE	MTBE	DME
¹⁸ O	2	93	94
¹⁶ O	98	7	6

Table 2. Percent isotopic composition ($\pm 2\%$) of O-containing products from the reaction of CH₃CH₂¹⁸OH/¹⁶O-isobutanol over Amberlyst-35 catalyst at 110°C and 1 MPa.

Isotope	EIBE	ETBE	DEE
¹⁸ O	<5	96	>93
¹⁶ O	>95	4	<7

Table 3. Percent isotopic composition ($\pm 2\%$) of O-containing products from the reaction of $\text{CH}_3^{18}\text{OH}/\text{CH}_3\text{CH}_2^{16}\text{OH}$ over Amberlyst-35 catalyst at 110°C and 1 MPa.

Isotope	DME	DEE	MEE
^{18}O	<98	<2	50
^{16}O	>2	>98	50

Table 4. Percent isotopic composition ($\pm 2\%$) of O-containing products from the reaction of $\text{CH}_3\text{CH}_2^{18}\text{OH}/^{16}\text{O}$ -isopropanol over Amberlyst-35 catalyst at 90°C and 1 MPa.

Isotope	EIBE	ETBE	DEE
^{18}O	89	<2	>98
^{16}O	11	>98	<2

Table 5. Product selectivities ($\pm 2\%$) (taking into account 2- and 3-ethoxypentane only) from the reaction of Et^{18}OH and S-2-pentanol over Nafion-H and HZSM-5 catalysts at 100°C and 1 MPa, and in concentrated H_2SO_4 solution at 100°C and ambient pressure, where the true inversion = $\%X/(X+Y-Z)$.

Acid Catalyst	Product selectivity (%)			Ratio for R-2-EP/S-2-EP (X/Y)	$^{16}\text{O}/(^{16}\text{O}+^{18}\text{O})$ % in 2-EP (Z)	Inversion (%)
	S-2-EP	R-2-EP	3-EP			
HZSM-5	14.0	86.0	0.0	86/14	11.0	97
Nafion-H	32.9	60.9	6.2	65/35	16.0	77
H_2SO_4	33.6	64.0	2.4	66/34	18.0	80

HIGHER ALCOHOL SYNTHESIS OVER A Cs-Cu/ZnO/Cr₂O₃ CATALYST: EFFECT OF THE REACTION TEMPERATURE ON PRODUCT DISTRIBUTION AND CATALYST STABILITY

Alessandra Beretta, Qun Sun, Richard G. Herman, and Kamil Klier
Zettlemoyer Center for Surface Studies and Department of Chemistry
7 Asa Drive, LEHIGH UNIVERSITY, Bethlehem, PA 18015

Keywords: catalyst, higher alcohols, synthesis gas, stability

ABSTRACT

The influence of reaction temperature on methanol and higher alcohol synthesis has been investigated in the range of 310-340°C. Optimal conditions for selective production of 2-methyl primary alcohols was identified with $T = 340^\circ\text{C}$ and synthesis gas $\text{H}_2/\text{CO} = 0.75$. Deactivation features were observed after 300 hr on stream, but no significant growth of Cu crystals or reduction in surface area was observed for the catalyst after testing.

INTRODUCTION

The Cu/ZnO/M₂O₃ systems (M = trivalent metal) are well-known catalysts for methanol and higher alcohol synthesis (HAS) [1-4]; their performances are reported in the literature with particular attention being paid to the optimization of both the catalyst composition (amount of alkaline dopant, metal ion ratios) and the operating conditions [2-5]. The application of these catalysts is commonly limited to reaction temperatures not exceeding 310-325°C in order to avoid sintering phenomena that are recognized as the major constraint and drawback of all the copper-containing catalysts. At these temperatures, methanol formation is highly favored, and only by carrying out the reaction at low H_2/CO ratios can significant quantities of C₂⁺ oxygenates be obtained. No specific studies have so far addressed the thermal stability of Cu/ZnO-based systems at high temperatures. However, the strong demand for selective production of branched higher oxygenates supports more extensive exploration of the range of allowable reaction temperatures that can be utilized with copper-based catalysts. Indeed, an increment in the temperature is expected to result in the desired promotion of higher alcohol production and a concurrent decrease in methanol formation. In the following, a study of the effect of reaction temperature on HAS over a Cs-doped Cu/ZnO/Cr₂O₃ catalyst is presented, and the principal interests are the changes in the product distribution and the catalyst thermal stability.

EXPERIMENTAL

Catalyst Preparation. The methodology has been described by Nunan et al. [3,6], which consists of the precipitation of a hydrotalcite-like precursor $\text{Cu}_{2.4}\text{Zn}_{3.6}\text{Cr}_2(\text{OH})_{16}\text{CO}_3 \cdot 4\text{H}_2\text{O}$ [7], followed by stepwise calcination to 350°C to give the mixture of oxides, CuO/ZnO/Cr₂O₃. Cesium doping was achieved by adding the catalyst to a N₂-purged aqueous solution of CsOOCH, which was then slowly evaporated to dryness under flowing N₂. The amount of dopant (3 mol%) was chosen on the basis of previous studies of the optimal catalyst composition with respect to higher alcohol synthesis [3]. The catalyst was finally reduced with a 2 mol% H₂/N₂ mixture at 250°C.

Activity Tests. The apparatus has been extensively described elsewhere [8]. It is noted that charcoal and molecular sieve traps, an internally copper-lined stainless-steel reactor, as well as a copper thermocouple-well were used during the catalytic testing to prevent the formation and deposition of iron-carbonyls, which are well-known deactivating agents [9,10]. The catalysts were tested under steady state conditions at 7.6 MPa with synthesis gas of various H₂/CO compositions flowing with a gas hourly space velocity of 5300 l/kg cat/hr. The reaction temperature was varied between 310 and 340°C.

The exit product mixture was sampled every 30-60 min using an in-line, automated, heated sampling valve and analyzed in a Hewlett-Packard 5390 gas chromatograph. The products were analyzed via a Poraplot-Q capillary column alternatively connected to a flame

ionization detector and to a thermal-conductivity detector (TCD) and a Molsieve capillary column connected to TCD. The sensitivity factors of the instrument were determined on the basis of calibrated mixtures. The gas-phase on-line analyses were coupled with the analysis of liquid samples collected downstream from the reactor (atmospheric pressure) by liquid nitrogen cooled traps. The identification of the products (more than 50 components) was obtained by comparison of their retention times with those of known standards and from analysis of the liquid samples by a HP GC/MS instrument. All of the experimental data were obtained in a steady-state regime that was reached about 6-8 hr after setting the operating conditions.

Catalyst Characterization. BET measurements and XRD analyses were performed at each stage of the catalyst preparation and after testing to determine the catalyst surface area and crystalline phases, respectively.

RESULTS

Effect of the Reaction Temperature on the Product Distribution. In Fig. 1, the productivities of the most abundant oxygenated products are reported as a function of the reaction temperature, which was increased from 310°C up to 340°C over a period of about 160 hr. As the temperature was increased, a decrease of methanol productivity was observed, in line with the thermodynamic constraints that govern methanol synthesis. As shown in Fig. 1(a), the productivities of all the linear higher alcohols exhibited decreasing trends with increasing reaction temperature. In fact, the product mixture tends to become depleted in intermediate species (ethanol, propanol) and more enriched in the branched oxygenates that play a terminal role in the chain-growth process. At 325°C, a promotion of all the 2-methyl alcohols was observed (Fig. 1-b). It is noted that the molar ratio between methanol and the totality of α -branched alcohols passed from a value of about 16 at 310°C to the value of about 5 at 340°C. In the case of secondary alcohols (whose productivities are summed in Fig. 1-c with those of the corresponding ketones), it is observed that high temperatures favor the formation of high molecular weight species (e.g. 2-methyl-3-pentanol) at the expense of the intermediate species (e.g. 2-butanol).

The formation of methane and C_2^+ hydrocarbons was also observed to increase with increasing reaction temperature (Fig. 2). The overall production of hydrocarbons, equal to 15.7 g/kg cat/hr at 310 °C, grew to the value of 39.4 g/kg cat/hr at 340°C. It is worth noticing that, contrary to the case of oxygenates, hydrocarbons appear to keep an almost constant relative product distribution, which could support the hypothesis of a formation pattern independent from the higher alcohol chain-growth process.

Finally, it is noted that the productivities of all the methyl-esters detected in the product mixture decreased monotonically with increasing reaction temperature. This trend was especially evident in the case of methyl-formate and methyl-acetate, while it was less pronounced for the higher homologs (methyl-propionate, methyl-isobutyrate, methyl-butyrate).

High Reaction Temperature: Effect of H_2/CO Ratio. At the reaction temperature of 340°C, kinetic runs were performed to investigate the combined effects of high temperature and H_2/CO feed ratio on HAS product distribution. The results are reported in Fig. 3, and the data show that an excess of H_2 exclusively promoted methanol formation. The production of higher oxygenates appears to be significantly inhibited at high H_2/CO ratios. Specifically, all of the primary alcohols tended to show a maximum in productivity, with the highest value being associated with the H_2/CO value of 0.75 (Fig. 3 a-b).

With respect to the formation of hydrocarbons, the data reported in Fig. 4 indicate that while the synthesis of C_2^+ hydrocarbons is strongly slowed down by decreasing CO partial pressure, methane productivity was approximately constant as a function of the H_2/CO ratio.

High Reaction Temperature: Catalyst Stability. The operating conditions of $T = 340^\circ\text{C}$, $H_2/CO = 0.45$, 7.6 MPa, and GHSV = 5300 $\ell/\text{kg cat/hr}$ were periodically reproduced in order to check the stability of the catalyst. The results of the experiments are

reported in Fig. 5, where the averaged FID signals, in arbitrary units, for the most abundant products have been plotted vs the time of testing. As previously noted, a period of about 160 hr occurred before reaching the final temperature of 340°C, and at this high temperature a stable catalytic activity was observed during 125 hr. Subsequently, a slow loss of selectivity of the higher oxygenates in favor of an increment in methanol productivity was detected. Similar results were obtained in the past when studying deactivation caused by the deposition of iron-carbonyls onto Cu/ZnO catalysts [9]. Even though the cause of the origin of the behavior shown in Fig. 5 cannot be assessed, Cu sintering can be excluded as playing a major role, where the XRD pattern of the tested catalyst (300 hr on stream at 340°C) revealed the presence of metallic copper with crystallite size in the range of 100Å, which is comparable with the dimension of Cu crystallites observed in the binary Cu/ZnO systems after the reduction stage and before testing [9]. Moreover, BET measures showed that no reduction in the catalyst surface area occurred during the kinetic runs, being 85 m²/g and 89 m²/g the surface area values before and after testing, respectively.

CONCLUSIONS

The presented experimental results suggest that:

- (1) the productivity of α -branched species benefits significantly from an increment of the reaction temperature to 325°C. For further increments of temperature, the productivities of higher alcohols are almost constant but the methanol/higher alcohols molar ratio increases progressively.
- (2) at high temperature, the H₂/CO feed ratio of 0.75 is optimal with respect to higher oxygenate formation. Under such conditions, an equal amount of methanol but *twice* the amount of branched higher alcohols can be obtained, compared to the optimal low temperature conditions (T = 310°C, H₂/CO = 0.45).
- (3) no significant Cu sintering or surface area reduction occurred upon testing at the reaction temperature of 340°C; but iron-carbonyl formation and deactivation of the catalysts under high temperature conditions needs to be studied further.

ACKNOWLEDGMENT

This research was partially supported by the U.S. Department of Energy-Pittsburgh Energy Technology Center (contracts DE-AC22-90PC90044 and -90PC90018) and by a Fullbright Scholarship (A.B.).

REFERENCES

1. Natta, G., Colombo, U., and Pasquon, in "Catalysis," Vol. 5, Chap. 3, ed. by P. H. Emmett, Reinhold (1957).
2. Smith, K. J. and Anderson, R. B., *J. Catal.*, **85**, 428 (1984).
3. Nunan, J. G., Herman, R. G., and Klier, K., *J. Catal.* **116**, 222 (1989).
4. Herman, R. G., in "New Trends in CO Activation," ed. by L. Guzzi, Elsevier, Amsterdam, 265 (1991).
5. Boz, I., Sahibzada, M., and Metcalfe, I., *Ind. Eng. Chem. Res.* **33**, 2021 (1994).
6. Nunan, J. G., Himelfarb, P. B., Herman, R. G., Klier, K., Bogdan, C. E., and Simmons, G. W., *Inorg. Chem.*, **28**, 3868 (1989).
7. Busetto, C., Del Piero, G., Manara, G., Trifiro, F., and Vaccari, A., *J. Catal.*, **85**, 260 (1984).
8. Nunan, J. G., Bogdan, C. E., Klier, K., Smith, K. J., Young, C.-W., and Herman, R. G., *J. Catal.* **116**, 195 (1989).
9. Bogdan, C. E., Nunan, J. G., Santiesteban, J. G., Herman, R. G., and Klier, K., in "Catalysis-1987," ed. by J. W. Ward, Elsevier, Amsterdam, 745 (1988).
10. Hindermann, J. P., Hutchings, G. J., and Kiennemann, A., *Catal. Rev.-Sci. Eng.*, **35**, 1 (1993).

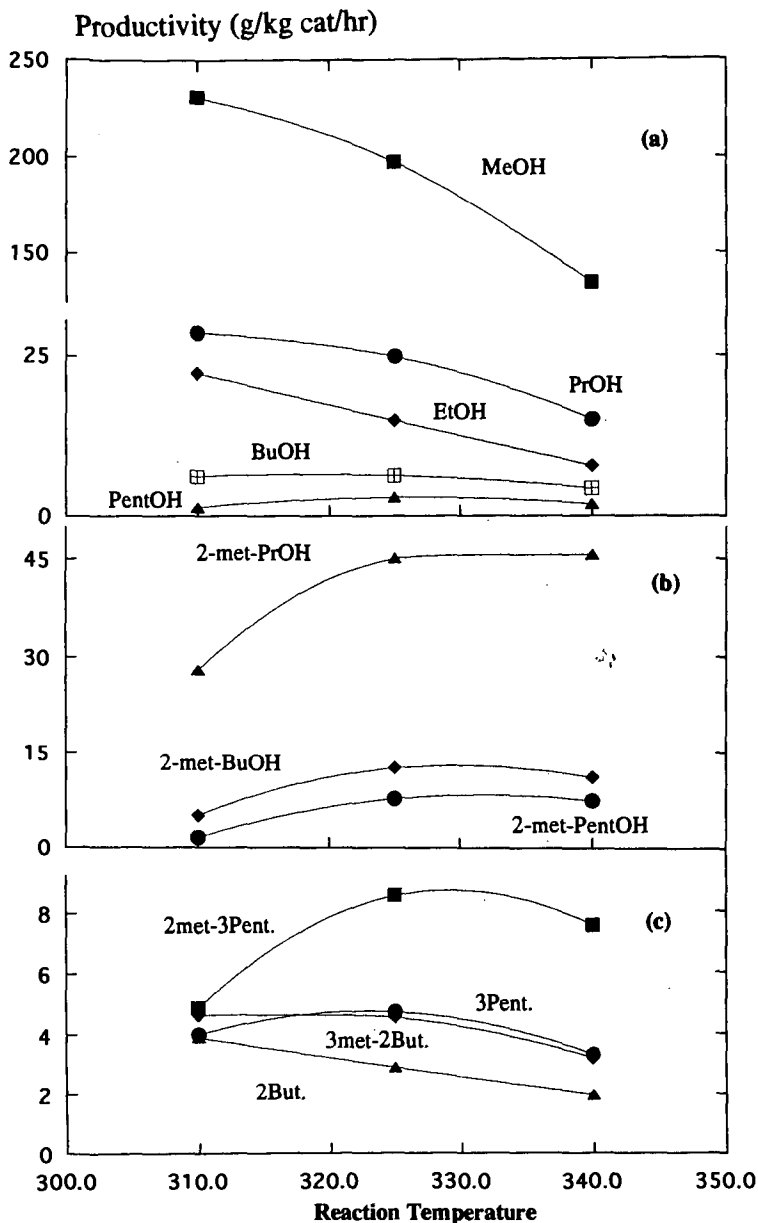


Fig. 1. Experimental effect of reaction temperature on methanol and higher oxygenates productivities. In 1-c: 2met-3Pent = 2methyl-3-pentanol + 2-methyl-3-pentanone, 3-Pent. = 3-pentanol + 3-pentanone, 3met-2But. = 3-methyl-2-butanol + 3-methyl-2-butanone, 2-But. = 2-butanol + 2-butanone. Operating conditions: $H_2/CO=0.45$, $P=7.6$ MPa, $GHSV=5300$ l/kg cat/hr.

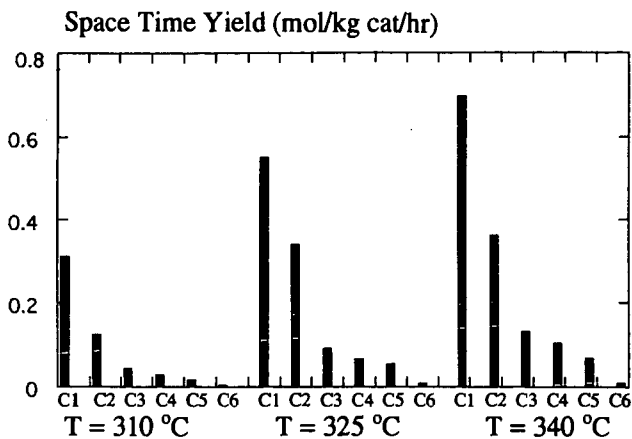


Fig. 2. Effect of temperature on C_1 - C_6 hydrocarbon production and distribution.

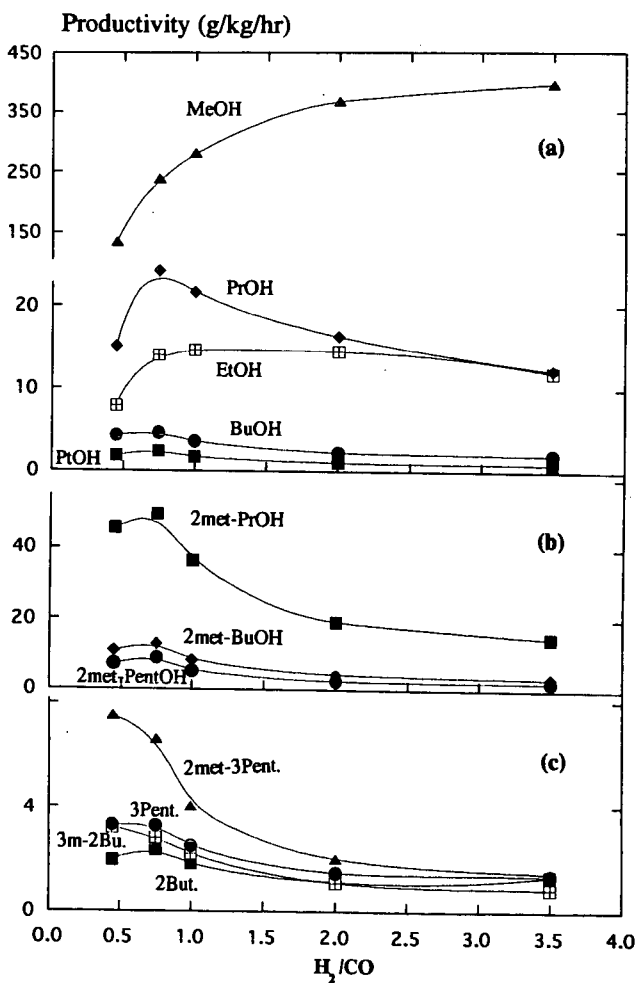


Fig. 3. Effect of H_2/CO ratio; $T = 340^\circ C$, $P = 7.6$ MPa, $GHSV = 5300$ l/kg cat/hr.

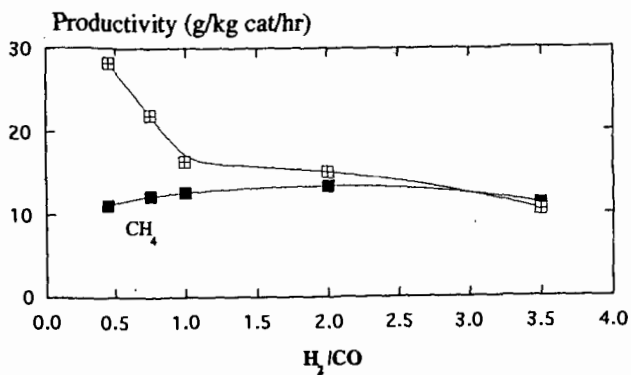


Fig. 4. Effect of H₂/CO ratio hydrocarbon formation. Conditions as in Fig. 3.

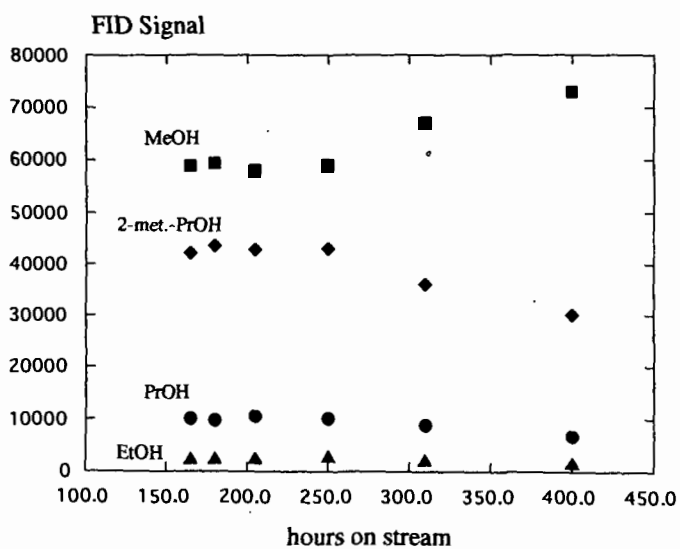


Fig. 5. Change of product distribution with time as detected by FID.

SYNTHESIS OF ALCOHOLS FROM SYNGAS AND ALCOHOL CHAIN GROWTH OVER COPPER-COBALT BASED CATALYSTS

Wei CHU*, Guoxing XIONG

State Key Laboratory of Catalysis, Dalian Institut of Chemical Physics,
Academia Sinica, P.O. Box 110, Dalian 116023, China

ABSTRACT: The alcohols synthesis were studied over copper-cobalt catalysts from syngas under pressure (6.0 MPa). The higher alcohols formation was enhanced with the cobalt content, caused probably by an increase of the number of Co-Cu bisites, and the higher hydrocarbons augmented simultaneously, explained by common reactional intermediates. The cobalt quantity on the surface influences the chain growth evolving into alcohols or hydrocarbons. It was shown that an augmentation of CO insertion and a modification of the hydrogenation property of system could be responsible of these effects, as supported by the tests of reactivities and those of probe molecules. It was illustrated that some strong interactions existed between cobalt and copper, and the influences of different pretreatments were also investigated.

1. INTRODUCTION

The syngas conversion remains one of the most interesting reactions in heterogeneous catalysis. Especially since the two energy crisis in the world, the more effective utilisations of syngas have attracted much attention [1,2]. With different catalysts and operational conditions, it could be oriented into methanolation, methanation, olefin production via Fischer-Tropsch reactions, synthesis of ethanol or acetyl aldehyde over Rhodium catalysts, or synthesis of mixed alcohols, etc. In that mixed alcohols production, the main problems were carbon chain growth, high alcohol activity and good selectivity. Several catalytic systems have been proposed [2], the copper-cobalt catalysts seem to be the most promising [1-3].

In this work, the influences of cobalt additives onto copper based catalysts were investigated, as well as the effects of pretreatments and those of supports, the temperature programmed reduction (TPR) and CO chemisorption were performed for the catalyst characterizations, the results of probe molecule tests were also discussed.

2. EXPERIMENTAL

2.1. Catalyst preparation: the supports were prepared by the coprecipitation method[4], referred as CuLaZr(i). The catalysts were prepared by impregnating the support with an aqueous solution of $\text{Co}(\text{NO}_3)_2 \cdot 6\text{H}_2\text{O}$ to a desired content. The impregnates were dried at 70°C in a flux of argon, and calcined at 350°C in a flux of argon or in air for 5h. They are referred as x%Co/CuLaZr(i).

2.2. Syngas reactions: hydrogenation of CO was carried out in a continuous flow reactor consisting of a 6 mm ID stainless steel tube containing 0.5 g of catalyst under the reaction conditions: P = 6.0 MPa, T = 250-280°C, $\text{H}_2/\text{CO} = 2$, D = 4 l/h/g. The reaction products were analysed by gas chromatography.

2.3. Probe molecule tests: the samples (0.5g) were reduced in hydrogen over night, then brought into contact with synthesis gas (P = 0.1 MPa, T = 225°C). After reaching a stationary state, a small amount (2 mol%) of probe molecules (C_2H_4) were sent into the CO/H_2 stream and the generated gases were analysed by gas chromatography with flame ionization detector [5,6].

3. RESULTS AND DISCUSSION

3.1. Influence of cobalt additive

The alcohols synthesis were studied over cobalt modified copper catalysts, six samples with different cobalt content were prepared and investigated. For the monometallic copper sample CuLaZr(1), it has almost no chain growth, the higher alcohol fraction was only 0.2%. With the cobalt addition, the higher alcohols (C_{2+} OH) formation was enhanced, and it increases with the

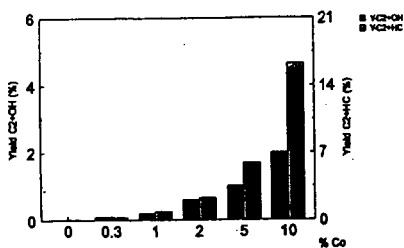


Fig. 1a. Yields in C_{2+} OH and in C_{2+} HC — Influence of cobalt content

rise of cobalt content, as does the yield into higher hydrocarbons (C_{2+} HC) and that of total hydrocarbons. The simultaneous augmentation of C_{2+} OH and C_{2+} HC (Fig. 1a) was explained as that there were common intermediates for their formation [7,8].

As suggested, during the growth of hydrocarbonated chain, there is a competition between the CH_2^* addition (formed on cobalt) which leads to the hydrocarbons formation, and the insertion of oxygenated species (formyl or CO, formed on copper) which results in alcohols. Thus the cobalt quantity on the surface influences the chain growth evolving into the alcohols or the hydrocarbons.

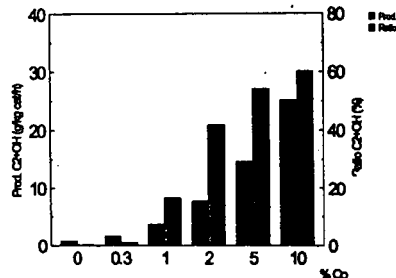


Fig. 1b. Higher alcohols productivity and ratio in total alcohols — Influence of cobalt content

In the case of the production into higher alcohols C_{2+} OH and their fraction in total alcohols, both increase with the rise of the cobalt content (Fig. 1b).

3.2. Effect of pretreatment

A pretreatment of the precursor after impregnation may be favorable to the decomposition of $Co(NO_3)_2$ and the formation of Co_3O_4 , which results in a modification of the reducibility of the catalyst and eventually the formation of mixed oxides. We have compared the pretreatments operating at the temperatures between 350°C and 700°C, in an inert flux (argon) or in air environment (21% O_2).

As illustrated in Fig. 2, the catalytic activity decreases while the calcination temperature rises, and the best results of the alcohol production and the higher alcohol ratio (C_{2+} OH/ROH) have been obtained by calcinating at 350°C. When calcinated in air rather than in argon, the catalytic system orient the reactions much more selectively to the alcohols, and the alcohols productivity is also better for the previous system (calcinated in air). So the pretreatment at 350°C in air has been used for the continuation of the work.

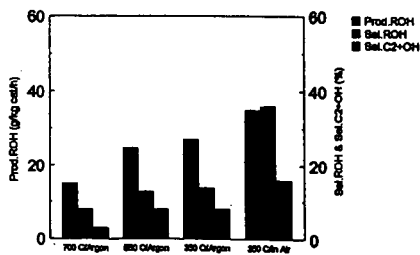


Fig. 2. Effect of pretreatment on activities of the catalysts

3.3. Influence of support

In our previous work, several copper based catalysts were investigated. It is the sample CuLaZr(2) which is the most favorable for the methanolation, and it was then utilised as a support in the place of CuLaZr(1) for the preparation of the bimetallic catalyst. In fact, the catalyst 5%Co/CuLaZr(2) gives better results.

The effects of reaction temperature were also studied. It was shown that both yields of alcohols and of hydrocarbons increased with the reaction temperature, and that the selectivity to alcohols pass a maximum of 38.4% at 270°C (Fig.3), and the alcohols productivity was 35.8 g/kg cat/h with higher alcohols ratio of 51.6%.

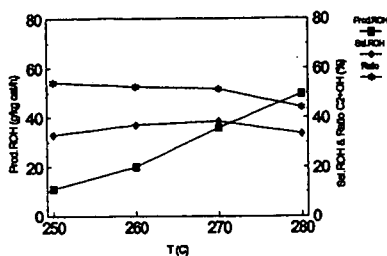


Fig.3. Influence of reaction temperature

3.4. CO chemisorption and TPR

The chemisorption of reactants like CO or H₂ was the slow step in CO/H₂ reactions. The quantity and the form of CO adsorbed are often in relation to the rate and the orientation of the reaction. And the study on CO chemisorption may also give some information of the accessible metallic area after the reduction[9].

The tests of CO chemisorption were made on three types of catalysts (CuLaZr, Co/LaZr, Co/CuLaZr) and the quantities of CO chemisorbed at ambient temperature are compared. It is shown that the addition of cobalt onto CuLaZr decreases the accessible metallic area of the catalyst, as explained by a covering of copper sites by cobalt oxide (more difficultly reducible) on the surface of the catalyst.

The temperature programmed reduction (TPR) tests were performed to see the influence of cobalt additive on the catalyst reducibilities, and the TPR spectra of the above three catalysts were compared. The maximum of the reduction peak of cobalt catalysts were at 316°C and that of copper system was at 218°C. And for the bimetallic system (Co/CuLaZr), there was only a reduction peak with a maximum at 255°C. This phenomenon suggested that there was an interaction between cobalt and copper, which resulted in a simultaneous reduction and a decrease of the Co₃O₄ reduction temperature. This interaction was also reported by Mouaddib [10].

3.5. Probe molecule tests

The effect of ethylene addition is illustrated in Fig.4. It is shown that C₂H₄ addition leads to a great augmentation of propanol, with a diminution of methanol. Propanol (propionic aldehyde) increases simultaneously. This result suggested that there is an insertion of the methanol precursor (like formyl species or CO) to the chemisorbed olefins. The other formed products (like CH₄, C₃H₆₋₈ and C₄H₈₋₁₀, not represented in the figure) change only a little.

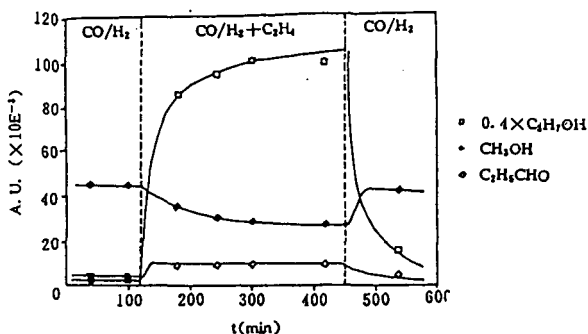


Fig. 4. Effect of C_2H_4 addition to syngas stream as a probe molecule

As discussed by Chuang et al.^[5], the insertion of C_1 oxygenated species (CO or formyl) into hydrocarbonated entities has particular importances as an indication of the growth of the oxygenated products. The comparison with the results of monometallic system is represented in Fig. 5. It is observed that only over bimetallic catalyst a great augmentation of the C_3H_7OH formation has been achieved. It means that the simultaneous presence of copper and cobalt is important for a good chain growth formation into the alcohols.

The ratios $C_2H_6/(C_2H_4+C_2H_6)$ and C_3H_7OH/C_2H_5CHO may be good indications for the hydrogenating properties of the systems. It is observed that ethane represents 99.7% of total C_2 hydrocarbon over the catalyst CuLaZr, which indicates a great hydrogenating property of the system. However, the chain growth on this system is very low. For the catalyst Co/LaZr, the ratio of $C_2H_6/(C_2H_4+C_2H_6)$ is 2.1%, which indicates a weak hydrogenating property of the system, which may be in relation to its weak activity. In the case of Co/CuLaZr, the ratio of $C_2H_6/(C_2H_4+C_2H_6)$ is 20.5%, and C_3H_7OH/C_2H_5CHO is 30, which indicated a good hydrogenating property of the system.

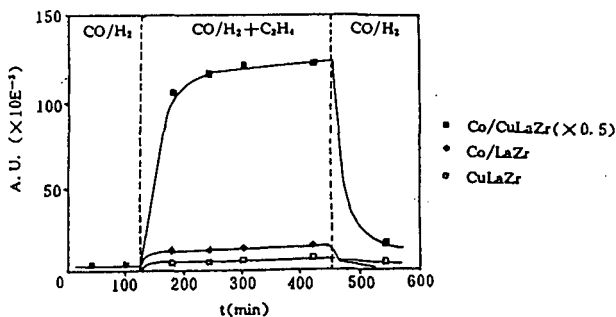


Fig. 5. Effect of C_2H_4 addition to syngas on C_3H_7OH formation

4. CONCLUSION

It was shown that there were some strong interactions between cobalt and copper, and their simultaneous presence was important for a good orientation for the alcohol formation. And the addition of cobalt onto CuLaZr system may have three important effects on the higher alcohol production: an increase of the formation of hydrocarbonated species, an augmentation of the CO insertion property of the system, and a modification of the hydrogenating property of the catalyst, as supported by the tests of reactivities and those of probe molecules. With different pretreatment, the results show that the calcination at 350°C in air was most favorable.

REFERENCES

1. P.Courty, A.Forestiere, N.Kawata, T.Ohno, C. Raimbault, M.Yoshimoto, 191st ACS National Meeting, New York, 328, 42-60, 1986
2. Xu Xiaoding, E.B.Doesburg, J.J.F. Scholten, *Catal. Today*, 2, 125, 1987
3. P.Courty, D.Durand, J.C.Guibett, N.Kawata, T.Yasuda, M.Yoshimoto, *Revue IFP*, 42, 243, 1987
4. W.Chu, R.Kieffer, A. Kiennemann, *React. Kinet. Catal. Lett.*, 48, 627, 1992
5. S.C.Chuang, Y.H.Tian, J.G. Goodwin, I.Wender, *J.Catal.*, 96, 396, 1985
6. A.Kiennemann, C.Diagne, J.P.Hindermann, P.Chaumette, P.Courty, *Appl. Catal.*, 53, 197, 1989
7. M. Ichikawa, *J.Chem. Soc. Chem. Commun.*, 566, 1978
8. A.Takeuchi, J.R.Katzer, G.C.A.Schuit, *J.Catal.*, 82, 447, 1983
9. T.Fortin, PhD thesis, Poitiers University, France, 1986
10. N.Mouaddib, V.Perrichon, *Proc. 9th ICC, Calgary*, II-521, 1988

MÖSSBAUER STUDY OF IRON-CARBIDE GROWTH AND FISCHER-TROPSCH ACTIVITY

K.R.P.M. Rao, F.E. Huggins, G.P. Huffman, R.J. O'Brien[#], R.J. Gormley¹, and B.H. Davis[#]

341, Bowman Hall, University of Kentucky, Lexington, KY 40506-0059

[#]Center for Applied Energy Research, University of Kentucky, Lexington, KY 40511,

¹Pittsburgh Energy Technology Center, Department of Energy, Pittsburgh, PA 15236

Key words: Mössbauer spectroscopy, χ -carbide, Fischer-Tropsch synthesis

ABSTRACT: There is a need to establish a correlation between the Fischer-Tropsch (FT) activity of an iron-based catalyst and the catalyst phase during FT synthesis. The nature of iron phases formed during activation and FT synthesis is influenced by the gas used for activation. Mössbauer investigations of iron-based catalysts subjected to pretreatment in gas atmospheres containing mixtures of CO, H₂, and He have been carried out. Studies on UCI 1185-57 catalyst indicate that activation of the catalyst in CO leads to the formation of 100% magnetite and the magnetite formed gets rapidly converted to at least 90% of χ -Fe₅C₂ during activation. The χ -Fe₅C₂ formed during activation gets partly (\approx 25%) converted back to Fe₃O₄ during FT synthesis and both χ -Fe₅C₂ and Fe₃O₄ reach constant values. On the other hand, activation of the catalyst in synthesis gas leads to formation of Fe₃O₄ and which is slowly converted to χ -Fe₅C₂ and ϵ -Fe_{2.2}C during activation, and both carbide phases increase slowly during FT synthesis. FT synthesis activity is found to give rise to \approx 70% (H₂+CO) conversion in the case of CO activated catalyst as compared to \approx 20% (H₂+CO) conversion in the case of synthesis gas-activated catalyst.

INTRODUCTION: Pretreatment is an important step in the development of an efficient catalyst. It affects the distribution of iron phases that are formed during the pretreatment and changes that take place during synthesis. It is controlled by the type of gas, temperature (T), pressure (P) and gas space velocity (S.V.) used. The FT activity and possibly selectivity may be related to the iron phases present in the catalyst; however the role of any specific phase on the FT synthesis is not yet clearly understood.

Mössbauer characterization of two iron based catalysts, viz., UCI 1185-57 and UCI 1185-149 has been carried out with a view to identify and quantify the iron phases that are present in the activated and spent catalysts and define their influence on Fischer-Tropsch (FT) synthesis. The catalysts were activated in (i) CO or (ii) H₂/CO (syngas) and then subjected to FT synthesis.

EXPERIMENTAL:

CO-ACTIVATED UCI 1185-57 CATALYST: The UCI 1185-57 catalyst (64%Fe₂O₃/5%CuO/1%K₂O/30% Kaolin) was pretreated under CO at 270°C and then subjected to FT run conditions with a syngas of H₂/CO=0.7. Catalyst samples were withdrawn at various times during the pretreatment and FT synthesis. The phase distributions are given in Table I. The χ -Fe₅C₂ is formed rapidly during activation in CO.

SYNGAS-ACTIVATED UCI-1185-57 CATALYST: The UCI 1185-57 catalyst was preheated in He up to 200°C, then heated in H₂+CO at 280°C during the remainder of a 24 hour period and then subjected to a FT run with a syngas of H₂/CO=0.7. The catalyst samples were withdrawn at various times during pretreatment and FT synthesis. The phase distribution determined is given in Table II. As compared to the CO pretreatment, activation in synthesis gas leads to the formation and a slow increase of χ -carbide and ϵ -carbide at the expense of Fe₃O₄. The carbides are formed in proportion to the pretreatment and synthesis duration; in addition to magnetite, some substituted magnetite and a small fraction of superparamagnetic iron oxide.

RESULTS AND DISCUSSION: As can be seen from the data in Table I, the hematite is converted into magnetite (Fe₃O₄) during heating the catalyst in CO up to 270°C in 2 hrs 43 min. The magnetite is converted into χ -Fe₅C₂ during further pretreatment under CO at 270°C; this phase represents 90% at the end of 24hrs of pretreatment. The remaining 10% of magnetite is converted into superparamagnetic (spm) phase. Low temperature (12°C) measurement on RJO-139J has revealed that the spm phase is magnetite. During FT synthesis part of the χ -Fe₅C₂ (\approx 25%) converted again to Fe₃O₄ and spm phase. However, after about 20 hrs of FT synthesis, the amounts of χ -Fe₅C₂, Fe₃O₄ and the spm phases do not change further. The FT activity remains essentially constant at \approx 70% H₂+CO during these changes.

The activity of the catalyst is higher when activated in CO than in synthesis gas. As compared to the CO pretreatment, the synthesis gas pretreatment leads to a slow increase in the χ -Fe₅C₂ and

ϵ -Fe_{2.2}C phases at the expense of Fe₃O₄ and the conversion = 30% (H₂+CO) at the end of 24 hrs of activation. The χ -Fe₅C₂ and ϵ -Fe_{2.2}C continue to grow during FT synthesis while Fe₃O₄ continues to decrease indicating that magnetite converts into carbides, a trend which is opposite to that seen in the case of CO-activated catalyst (Fig. 1a). It may be noted that there is no ϵ -Fe_{2.2}C detected in samples withdrawn during either pretreatment or FT synthesis in the case of the CO pretreated catalyst.

The (CO+H₂) conversion for the two types of pretreatment is shown in Fig. 1b. The (CO+H₂) conversion is maintained at ≈70% in the case of CO pretreated catalyst. On the other hand, in the case of synthesis gas pretreated catalyst, the conversion reaches ≈ 60% during activation but drops to ≈ 30% at the start of FT run when process conditions are changed. Some carbides were formed during activation and they continue to increase during the FT run.

We have also carried out Mössbauer investigations on the low α catalyst, UCI 1185-149 (2nd preparation) (57.2Fe/9.3Cu/0.05K) that had been subjected to pretreatment in (i) CO and (ii) H₂/CO. The pretreatment and FT synthesis conditions are given below and the results of are given in Tables III and IV.

CO-ACTIVATED UCI 1185-149 (2ND): This catalyst was pretreated in CO at 270°C, 175 psig, for 22hrs in 1.4 nL CO/g-Fe hr. FT synthesis was carried out with 10% catalyst loading in distilled Allied-Signal heavy wax at 270°C, 175psig, 2.4 nL syngas/g-Fe hr, at 1000rpm.

The activation is not complete during pretreatment. As can be observed from the Table III, the amount of χ -carbide continues to increase during FT synthesis and the FT activity decreases with increasing time on stream.

SYNGAS-ACTIVATED UCI 1185-149 (2ND): This catalyst was pretreated in H₂/CO at 280°C, 175 psig, for 14hrs in 1.4 nL CO/g-Fe hr. FT synthesis was carried out in C28 wax with 10% catalyst loading at 270°C, 175psig, 2.4 nL syngas/g-Fe hr, at 1000rpm. For this catalyst also the carbiding is not complete during pretreatment. As can be observed from the data in Table IV, the χ -carbide continues to increase during FT synthesis and the FT activity decreases with increasing time on stream, similar to the other catalyst used in this study. It may be noted that the FT activity is low even when the χ -Fe₅C₂ present in the spent catalyst is as much as 91%. This indicates that the absolute amount of χ -Fe₅C₂ present in the catalyst is not significant for FT activity.

Zarochak and McDonald [1] have carried out studies on the effects of pretreatment on the slurry phase FT synthesis activity and selectivity of a potassium-promoted precipitated iron catalyst and characterized the catalyst by Mössbauer spectroscopy measurements. They carried out two kinds of activation for the potassium promoted catalyst ((i) in CO and (ii) in syngas) were used and then the materials were subjected to FT synthesis. The catalyst activated in CO for 24 hrs gets completely converted into χ -Fe₅C₂ while the catalyst activated in syngas was converted partly to ϵ -Fe_{2.2}C during 24hrs of activation, and was completely converted to this phase only after 503 hrs of synthesis. The FT activity of the catalyst subjected to CO pretreatment was found to be higher than that found for the catalyst activated in syngas and the decrease in the FT activity with time on stream was slower for the CO pretreated sample.

- References:** [1] M.F.Zarochak and M.A. McDonald
Slurry-Phase Fischer-Tropsch Synthesis
6th DOE Indirect Liquefaction Contractor's Meeting
Dec 1-9, 1987, Pittsburgh Energy Technology Center, Pittsburgh

Table I†

CO-activated UCI 1185-57 catalyst:

Sample		%Fe ₃ O ₄	% χ -carbide	Spm Phase
Preheat conditions:				
RJO139A	Heating up to 270°C under CO in 2hr 43min	100	---	--
RJO139B	2.5hr under CO@270°C	95	---	5
RJO139C	6.5hr under CO@270°C	62	26	12
RJO139D	10.5hr under CO@270°C	33	56	11
RJO139E	18.5hr under CO@270°C	12	78	10
RJO139F	24hr under CO@270°C	--	90	10

Synthesis conditions

RJO139G	6hr of synthesis	--		87		13
RJO139H	19.75hr synthesis	8		69		23
RJO139I	27.75hr synthesis	10		67		23
RJO139J	48.75hr synthesis	13		62		25
RJO139K	140 hr synthesis	16		66		18

Spm= Superparamagnetic

Pretreatment conditions: Ramped up to 270°C @ 1.5°C/min. under CO @ 175 psig. Maintained at 270°C and 175psig with CO flow for 24 hr.

Synthesis conditions: H₂/CO=0.7, space velocity=3.4nL/hr/g(Fe)
T=270°C and pressure 175psig.

Table II†

(H₂, CO) activated UCI 1185-57 catalyst:

Sample	α -Fe ₂ O ₃	Fe ₃ O ₄	S-Fe ₃ O ₄	χ -Carbide	ϵ -carbide	Spm
RJO-140A taken after heating to 200°C in He in 2hr 43 min	94	--	--	2	--	4
RJO-140C 7hr in (CO+H ₂) Taken at 250C during heat upto 280 C 150psig, TOS ^o =7hr, S.V.=2.	--	93	7	--	--	--
RJO-140E Taken after reaching 280°C, TOS=11.2hr	--	85	5	--	5	5
RJO-140F taken 3.75h after reaching 280°C, TOS=15hr	--	69	5	6	13	7
RJO-140G Taken 12.5hr after reaching 280°C TOS=23.75hr	--	44	5	12	23	17

**FT synthesis
conditions:**

RJO-140H Taken 3.25hr after switching to synthesis conditions, S.V=2.5, 200psig, TOS=27hr	--	25	4	27	33	11
RJO-140I Taken after 26.5hr under synthesis conditions, TOS=50.25hr	--	17	--	35	42	6

TOS= time on stream

S-Fe₃O₄ = substituted magnetite

† Catalyst preparation and FT synthesis runs were carried out CAER

Table III

UCI 1185-149 2nd catalyst activated in CO:

SAMPLE	χ -Fe ₃ C ₂	Fe ₃ O ₄	Spm	(H ₂ +CO) Conv%*
CW-S3-11-D TOS=84HRS	40	37	23	84.0
CW-S3-11-J TOS=235HRS	60	30	10	67.7
CW-S3-11-M TOS=305	68	27	5	51.2

* Catalyst preparation and FT synthesis runs were carried out at PETC, Pittsburgh

Table IV

UCI 1185-149 2nd catalyst activated in syngas:

Sample	χ - Fe ₃ C ₂	Fe ₃ O ₄	Spm phase	(H ₂ +CO)* conversion
CW-S3-10- ACT Activated for 14hrs	36	48	16	--
CW-S3-10-A FT run for 26hrs	84	14	2	16
CW-S3-10-B FT run for 49hrs	91	7	2	6

* Catalyst preparation and FT runs were carried out at PETC, Pittsburgh

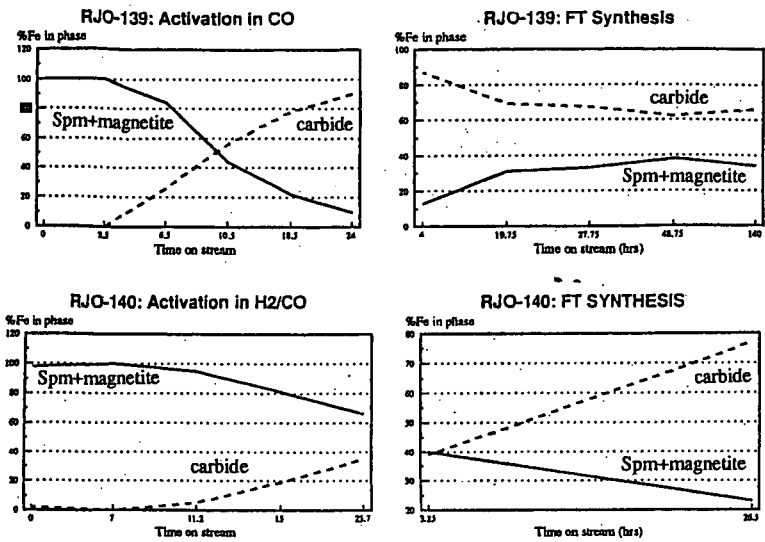


Fig.1a Variation of iron phases with time on stream

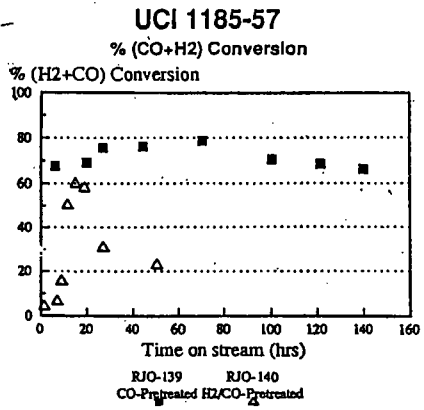


Fig.1b (H2+CO) conversion dependence on pretreatment

FINE DETAILS ON THE SELECTIVITY AND KINETICS OF THE FISCHER-TROPSCH SYNTHESIS OVER PRECIPITATED COBALT CATALYSTS BY COMBINATION OF QUANTITATIVE GAS CHROMATOGRAPHY AND MODELLING.

Ronald S. Hurlbut, Imre Puskas and Daniel J. Schumacher
Amoco Corporation, Naperville, Illinois 60566, (708) 653-4897

Keywords: Fischer-Tropsch, chain growth, kinetics, diffusion.

INTRODUCTION.

This report summarizes a part of our work carried out on the conversion of natural gas-derived synthesis gas to liquid fuels. Particularly, we were interested to find a catalyst which can convert dilute synthesis gas -such as obtainable from natural gas by partial oxidation with air- to predominantly liquid products at low pressures. For this purpose we needed to generate fundamental kinetic information on the controllability of the molecular weight distribution, which is defined by the chain growth probability of the reaction, because relatively little information is available on the subject (1-5). A wealth of information suggests, that with some exceptions in the low molecular weight regimes (1,6), the product distributions can be described by Anderson-Schulz-Flory (ASF) kinetics, using either a single chain growth probability, or separate chain growth probabilities for the light and heavy products (7). The causes of the "dual" chain-growth probabilities still have not been defined. Three causes have been suggested which could account for the dual chain growth probabilities: 1./ Differences in the catalytic sites (8,9); 2./ transport-enhanced 1-olefin readsorption and incorporation into the heavy product fractions (10); 3./ operating characteristics of the reactor (3).

To aid with our objectives, we have developed an approach for product analyses which is based on a combination of quantitative gas chromatography and modelling. This resulted in instantaneous determinations of the complex product mixtures, providing an opportunity to generate instantaneous information on the selectivity and the kinetics of the reaction. The influence of experimental parameters (feed, pressure, space velocity and temperature) on the chain growth probability and on the rate was studied by this analytical approach. The results shed new information on the causes of the deviations from the ASF kinetics. Furthermore, the kinetic data also provide evidence for diffusional limitations of the reaction rates. Finally, the instantaneous analyses may aid in future research to link the kinetics and the selectivity of the reaction which seem to be interdependent and hence should require simultaneous treatment.

EXPERIMENTAL SECTION.

The methods of catalyst preparation, characterizations, evaluations and product analyses have been outlined in previous publications (6, 11-13). Full details are given in the unabbreviated version of this paper.

RESULTS AND DISCUSSIONS.

1./ Feed composition studies.

The addition of extra hydrogen to the feed was evaluated on Catalyst 1 in an experiment conducted at 197°C, 156 kPa. Table 1 gives the detailed results. Table 1 also serves to illustrate the type of information generated by the GC-modelling combination. The data show that an increase of the H₂ to CO feed ratio from 2.0 to 3.1 resulted in substantial increase of the reaction rate as indicated by the catalyst productivities, and a modest decrease in the growth factor. The data also illustrate how the C₁ to C₄ product selectivities, expressed in percentage of the theoretical ASF predictions, change with the H₂ to CO feed ratio. The C₁ selectivity is very dependent on the feed ratio. However, the C₂ to C₄ selectivities are only little influenced by the feed ratio. This is in line with our earlier findings (6), that over Co catalysts, the fraction of C₂ to C₄ olefin incorporation by telomerization is nearly constant and little influenced by the experimental variables. The data of Table 1 suggest, that high H₂ to CO feed ratio promotes the hydrogenation of the C₂-C₄ olefins slightly more than their telomerization.

We considered the possibility that physisorbing inert components of the feed may also impact on the value of the growth factor by

creating "steric impediment" to propagation on the surface of the catalyst. This possibility was studied by nitrogen dilution of the feed on Catalyst 2, at 202°C, 168 kPa. The highlights of the results are shown in Figure 1. Indeed, nitrogen dilution of the feed resulted in decreased growth and decreased rate (productivity). Since nitrogen dilution also resulted in increased space velocity, specifically from 131 to 177 VHSV, the possibility need to be considered that the observed changes may have been caused by space velocity changes rather than by nitrogen dilution. It will be demonstrated later, that increased feed space velocity results in increased rate, without affecting the growth factor. Hence we can conclude that nitrogen dilution was the cause of the lower reaction rate and lower growth factor.

If nitrogen dilution affects the chain growth, it is expected, that the hydrocarbon products of the synthesis may also have a similar effect. The effect of hydrocarbon dilution was studied by comparing the reaction products from one-pass operations and from recycle mode operations. In this latter mode, the reaction products were passed through an air-cooled condenser to condense out the liquids. Part of the uncondensed gases were pumped back into the reactor after mixing with fresh feed. Catalyst 3 was used in the experiments, at 200.5°C, 103 kPa, with identical fresh feed flows. In the once-through operations, we obtained 60.4% CO conversion, 11.8% methane selectivity, 0.732 growth factor and 0.0235 g/g/hr catalyst productivities. During recycle operations, with 1.9 to 1 volumetric recycle to fresh feed ratio, we obtained 58.2% CO conversion, 13.2% methane selectivity and 0.0223 g/g/hr catalyst productivity. Unfortunately, the gas chromatographic effluent analysis was not adoptable for the determination of the growth factor on the basis of the C₁ to C₁₀ products, because these were partially removed by the recycle operations. We estimate 0.725 growth factor for the recycle operations on the basis that it yields the same selectivity balance as obtained in the once-through operations. We believe that these results qualitatively demonstrate that hydrocarbon dilution of the feed results in decreased growth and decreased rate, because the inert diluents successfully compete with the chemisorbing reagents for the catalytic sites.

2./ Pressure effects.

Table 2 illustrates the effect of small pressure changes at constant temperatures and constant feed flow rates on three different catalysts. In all cases, significant increases in the growth factor and also in the rates (catalyst productivities) were caused by small pressure increases. The C₁ to C₄ carbon selectivities (not shown in the Table) followed the trends defined by the growth factors. However, the C₁ to C₄ selectivities expressed in percent of their theoretical values did not appear to change. The small scatter of data is attributable to analytical error; no trend can be recognized with the pressure changes.

3./ Space velocity effects.

The effect of space velocity changes was studied on Catalyst 6 in atmospheric experiments at 195°C. The results are summarized in Figures 2 to 8. As Figure 2 shows, in this series of experiments we obtained essentially 100% selectivity balances, indicating that the ASF model extrapolation adequately accounted for the heavy products. Figure 2 also shows that the space velocity had little, if any effect on the growth factor. The data of Figure 3 illustrate another interesting point. While the CO conversion increased with increasing contact time (i.e. decreasing space velocity), the catalyst productivity decreased. Since the reaction occurs on the catalyst surface, and the feed composition, temperature and pressure were identical in this series of experiments, the change in catalyst productivity (rate) must have been caused by changes in the diffusion rates of the reagents to reach the catalyst surface. Faster space velocity provided faster diffusion rates. From these results, diffusional limitations of the reaction rates can be inferred.

Figures 4 to 8 show the C₁ to C₄ product selectivity dependencies on the contact time. These appear to be independent of the contact time. However, as expected, the distribution of the C₃ and C₄ products changes. The propylene and 1-butene contents decrease with increasing contact time due to hydrogenations to

propane and butane, respectively, and, in case of 1-butene, also to isomerizations to cis- and trans-2 butenes (Figures 6 to 8).

4./ Temperature effects.

The effect of temperature changes was studied at constant pressure (156 kPa) and constant space velocity (120 VHSV) on Catalyst 1. As Figure 9 illustrates, in the 190-205°C region, the growth factor steeply increased with decreasing temperature. However, below about 180°C, the measured growth factors did not seem to change with decreasing temperature. The carbon selectivity balances, also shown in Figure 9, may shed some information about the causes of these observations. Above about 190°C, the carbon balances were in the 91-95 percent range, suggesting that extrapolation by the ASF model underestimated the heavy product formation. Below about 185°C, the heavy product formation was substantially underestimated as revealed by the balance data. Hence we infer, that at decreasing temperature, heavier products with very high value of growth factor may have continued to form, but these had little impact on the relative amounts of C₁ to C₁₀ products which provided the basis for the determination of the growth factor. The data seem to support the theories, that the measured growth factor is a composite of a wide range of actual growth factors.

Figures 10 to 12 illustrate, that the methane selectivities, expressed in percent of the theoretical, increase with increasing temperature, but the C₂, C₃ and C₄ selectivities are unaffected. However, temperature affects the C₂ and C₄ distributions. At higher temperatures less propene (Figure 11) and less 1-butene (Figure 12) were found.

Figure 13 shows the temperature dependance of the CO conversions and the catalyst productivities. Surprisingly, the results suggest a linear correlation between temperature (T) and rate (-r), except for the high temperature (high conversion) regions:

$$-r = k K (T - T_i) \quad (1)$$

where k is the rate constant, K is another constant characteristic for the conditions and T_i is the temperature of the start of the reaction. This means that the Arrhenius equation is not valid in this surface reaction. Nevertheless, in Figure 14, we present a pro-forma Arrhenius plot which is curved. (For the plot, we used CO conversion data in lieu of rate constants from the linear region of Figure 13). The results may not be surprising, because theoretical considerations have demonstrated that non-linear Arrhenius plots can be obtained in transport-limited catalytic reactions (14, 15). From the data, we estimate pro forma activation energies ranging from 16 to 31 kcal/mole, which cover the bulk of the previously reported values.

CHAIN GROWTH PROBABILITY AND PRODUCT SELECTIVITY.

We propose that the chain growth probability (α) is defined by the nature of the catalyst surface (C), the surface concentrations of the adsorbed species (S₁ to S_n) -which include chemisorbing reagents and non-reactive adsorbed species- and the temperature of the surface:

$$\alpha = f(C, S_1, \dots, S_n, T) \quad (2)$$

It may be expected, that the nature of the catalytic metal, the size of the metal crystallites, metal-support interactions may influence the chain growth probability. Indeed, different catalytic sites were postulated in the past to give different chain growth (8,9). However, providing evidence for this was elusive, but scientific interest continues in the subject. Our results demonstrated, that not only the chemisorbing reagents, but also the physisorbing inerts can affect the chain growth probability. The surface concentrations of the adsorbed species will depend on their respective concentrations in the gas phase, on the pressure, on their rate of chemisorption, and on the diffusional conditions.

Even though it may be a long way to define an explicit form for Equation 2, the Equation may be useful for some qualitative predictions. Even if a specific catalyst were to possess only one type of catalytic site, a common plug-flow type reactor will produce a multiplicity of growth factors due to changes in the relative surface concentrations of the adsorbing species along the reactor axis arising from gas-phase compositional changes.

and due to minor temperature gradients on the surfaces. We have modelled these possibilities and some results with relevant assumptions are shown. Figure 15 gives the calculated ASF plot of a product mixture with growth factor evenly changing from 0.70 to 0.80. For all practical purpose, the product mixture can be described by a single growth factor. However, a careful examination reveals a slight break in the ASF plot at C_9 - C_{10} . Figure 16 gives the ASF plots of two assumed mixtures. In one of the mixtures, the growth factor continuously changes from 0.60 to 0.85, in the other one from 0.60 to 0.95. In both examples, there is a break in the ASF plot around C_{10} . However, the C_6 to C_{10} data from the two plots are nearly parallel, yielding nearly identical growth factor values by the conventional measurements. With this example, we have simulated an explanation for the finding that the measured growth factor did not increase with decreasing temperature below about 185°C.

The above discussion makes it clear that the operating characteristics of the reactor can result in molecular weight distributions with non-linear ASF plots. However, our results do not provide any indication that "transport enhanced olefin readsorption" can lead to increased growth probability and to non-linear ASF plots, as postulated recently (10). In our work, we have found evidence only for C_2 - C_4 olefin incorporation, and possibly very little C_5 incorporation, but the degree of these incorporations was fairly constant and independent of the residence time.

REFERENCES.

1. Henrici-Olive, G., and Olive, S., *Angew. Chem. Intl. Ed. Engl.* 15, 136 (1976).
2. Dry, M. E., in "Catalysis Science and Technology" (J. R. Anderson and M. Boudart, Eds.), Springer Verlag, Berlin, 1981, p. 159. See also Idem, *Catal. Today*, 6, 183 (1990).
3. Matsumoto, D. K., and Satterfield, C. N., *Energy & Fuels* 3, 249 (1989).
4. Dictor, R. A., and Bell, A. T., *J. Catal.* 97, 121 (1986).
5. Krishna, K. R., and Bell, A. T., *J. Catal.* 139, 104 (1993).
6. Puskas, I., Hurlbut, R. S., and Pauls, R. E., *J. Catal.* 139, 139 (1993).
7. For a review, see Davis, B. H., *Preprints, ACS, Fuel Division*, 37, 172 (1992).
8. Huff, G. A., and Satterfield, C. N., *J. Catal.* 85, 370 (1984).
9. Stenger, H. G., *J. Catal.* 92, 426 (1985).
10. Iglesia, E., Reyes, S. C., Madon, R. J. and Soled, S. L., in "Advances in Catalysis" (D. D. Eley, H. Pines and P. B. Weisz, Eds.), Academic Press, Inc., Vol. 39, 1993, p. 221.
11. Puskas, I., Fleisch, T. H., Hall, J. B., Meyers, B. L., and Roginski, R. T., *J. Catal.* 134, 615 (1992).
12. Puskas, I., *Catal. Lett.* 22, 283 (1993).
13. Puskas, I., Meyers, B. L., and Hall, J. B., *Catalysis Today*, 21, 243 (1994).
14. Weisz, P. B., and Prater, C. D., in "Advances in Catalysis" (W. G. Frankenburg, V. I. Komarewsky and E. D. Rideal, Eds.), Academic Press, Inc., Vol. 6, 1954, p. 143.
15. Rajadhyaksha, R. A., and Doraiswamy, L. K., *Catal. Rev. - Sci. Eng.* 13, (20), 209, (1976).

FIGURE 1

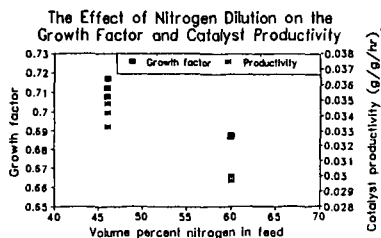


FIGURE 2

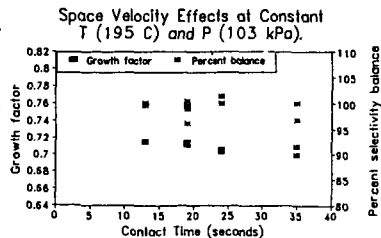


TABLE 1. Changes in Catalyst Performance and Product Selectivities with Changes in the H₂ to CO Feed Ratio.^a

H ₂ /CO ratio	2.0	2.0	2.5	2.5	3.1	3.1
VHSV	120	120	131	131	141	141
% CO conv.	60.3	59.4	77.3	77.5	91.5	93.5
Productivity	0.0285	0.0281	0.0367	0.0367	0.0436	0.0443
Growth factor	0.752	0.756	0.733	0.732	0.720	0.712
% Balance	96.2	95.8	93.1	93.9	96.6	97.7
% Selectivities						
CO ₂	2.9	2.8	2.6	2.7	2.2	2.7
C ₁	8.9	8.8	11.5	11.8	16.2	18.7
C ₂ -s	2.1	2.1	2.5	2.7	3.4	3.7
C ₃ -s	7.1	7.0	7.0	7.3	7.7	8.0
C ₄ -s	9.0	8.7	9.0	9.2	9.7	9.8
% of theoretical						
C ₁	151	153	167	171	213	233
C ₂ -s	24.4	24.6	26.4	28.0	34.1	32.4
C ₃ -s	69.7	70.0	66.1	68.5	71.4	73.4
Propene	38.8	39.8	23.2	23.1	9.0	6.5
Propane	30.8	30.2	42.9	45.4	62.4	66.9
C ₄ -s	87.2	85.8	87.1	89.1	93.3	95.7
1-Butene	23.7	23.5	14.7	14.8	9.8	9.9
n-Butane	33.6	33.1	42.6	43.8	58.9	62.8
t-2-Butene	14.3	13.7	16.2	16.6	14.9	14.5
c-2-Butene	15.6	15.5	13.7	13.9	9.7	8.5

^aCatalyst 1 at 197+1°C, 156 kPa. The volumetric feed compositions were 18-38-46, 16-41-43 and 15-47-38 CO-H₂-N₂, respectively.

TABLE 2. The Effect of Small Pressure Changes on Catalyst Performance and Product Selectivities.

Catalyst ID NO	2		4		5	
	203		193		202	
Temperature, °C						
Pressure, kPa	169	241	104	170	170	202
VHSV	131	131	286	286	220	220
Contact time (sec.)	46	65	13	21	27	32
% CO conversion	79.7	90.0	32.7	39.9	68.9	78.8
Productivity (g/g/hr)	0.034	0.039	0.014	0.016	0.043	0.050
Growth factor	0.703	0.736	0.739	0.789	0.648	0.696
% Balance	99.4	98.1	96.1	102.6	96.3	93.5
% CO ₂ selectivity	4.0	4.9	3.1	2.3	2.9	3.2
Selectivities, % of theoretical						
C ₁	144	142	191	215	135	122
C ₂	24.4	23.4	23.8	25.6	26.0	22.3
C ₃	68.1	65.6	69.6	76.5	70.4	62.8
Propene	22.8	21.4	40.0	44.7	25.8	21.2
Propane	45.2	44.2	29.5	31.7	44.5	41.6
C ₄	93.6	90.2	88.6	93.9	95.4	86.4
1-Butene	13.4	11.6	21.0	23.9	14.2	11.4
n-Butane	43.7	43.0	33.2	38.0	40.4	38.4
t-2-Butene	21.0	19.9	19.3	17.0	23.8	21.4
c-2-Butene	15.6	15.6	15.1	15.0	17.0	15.2

FIGURE 3

Space Velocity Correlation with CO Conversion and Catalyst Productivity

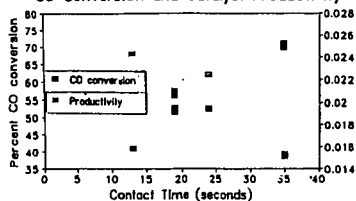


FIGURE 4

Contact Time-C₁ and C₂ Selectivity Correlations

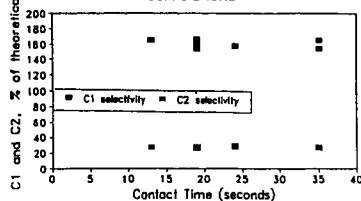


FIGURE 5
Contact Time-C3 Selectivity Correlations

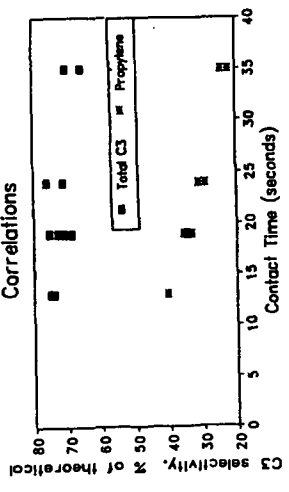


FIGURE 6
Contact Time-C4 Selectivity Correlations

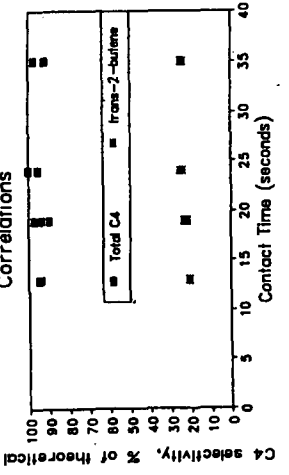


FIGURE 7

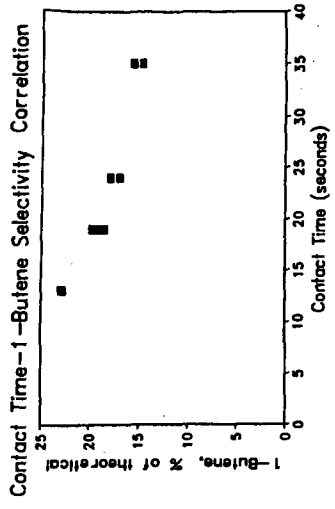


FIGURE 8
Contact Time-C4 Selectivity Correlations

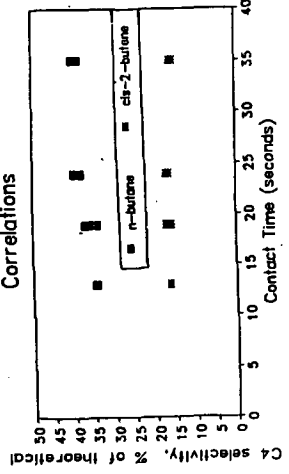


FIGURE 9
Growth Factors and Carbon Balances versus T at Constant P and SV.

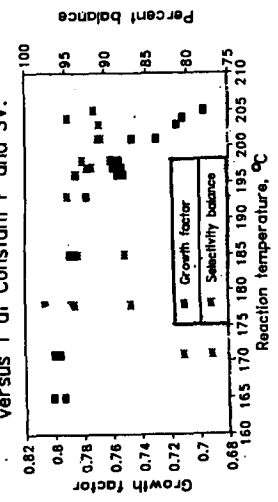


FIGURE 10

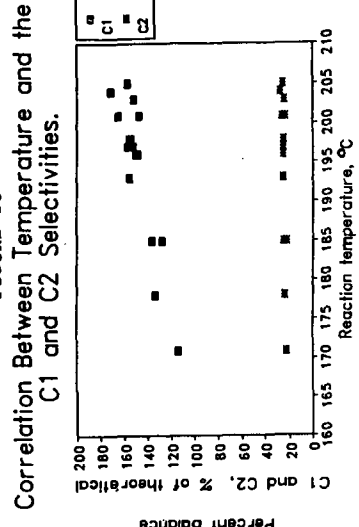


FIGURE 5
Contact Time-C3 Selectivity Correlations

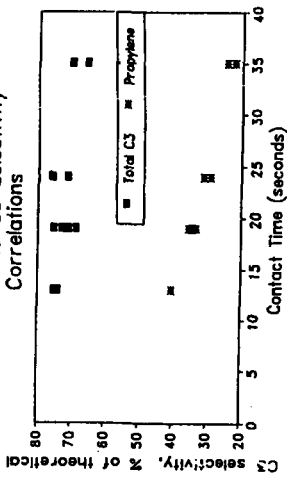


FIGURE 6
Contact Time-C4 Selectivity Correlations

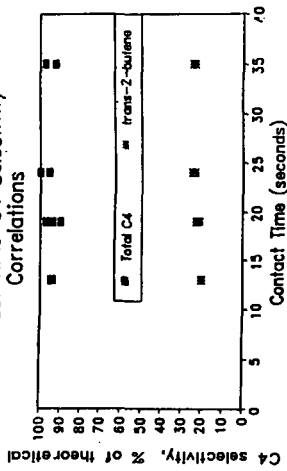


FIGURE 7

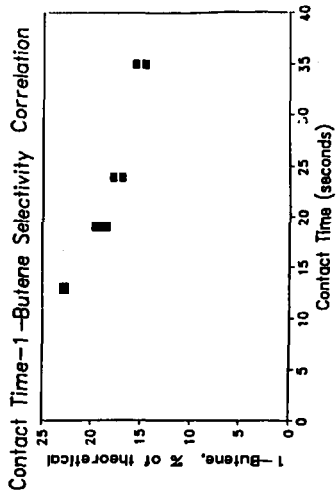


FIGURE 8
Contact Time-C4 Selectivity Correlations

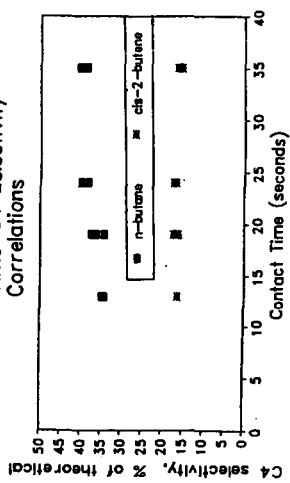


FIGURE 9
Growth Factors and Carbon Balances versus T at Constant P and SV.

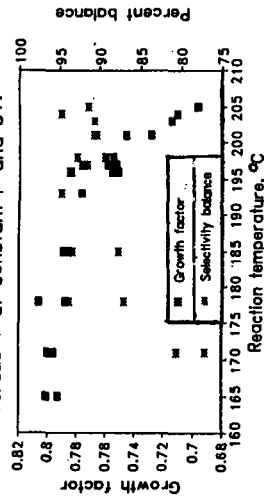


FIGURE 10

Correlation Between Temperature and the C1 and C2 Selectivities.

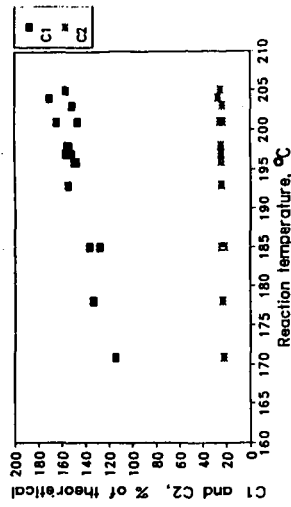


FIGURE 11

Correlation Between Temperature and the C3 Selectivities.

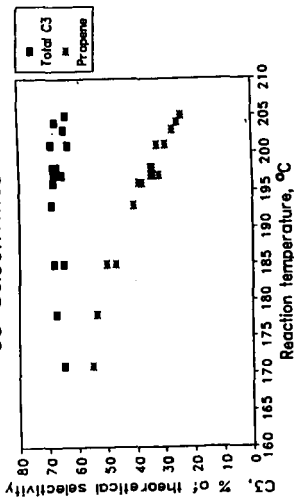


FIGURE 12

Correlation Between Temperature and the C4 Selectivities.

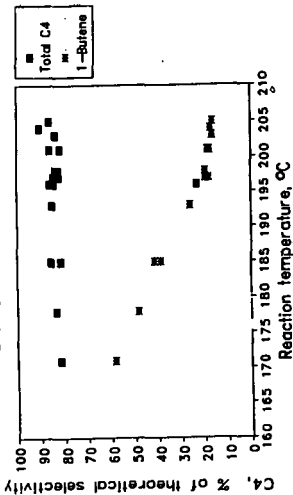


FIGURE 13

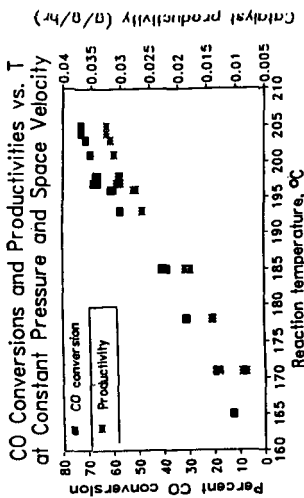


FIGURE 14. Arrhenius Plot.

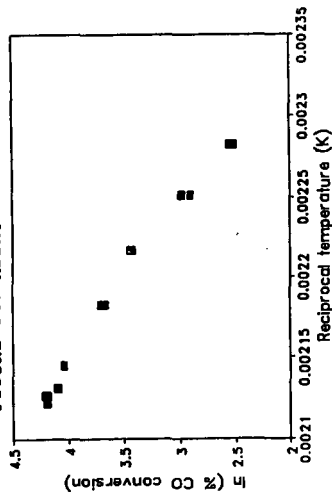


FIGURE 15. Calculated ASF Plot of a Product Distribution Continuously Changing in Alpha from 0.7 to 0.8

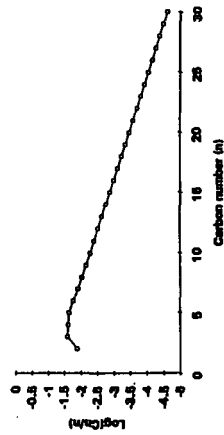


FIGURE 16. Calculated ASF Plots with Alpha Ranging from 0.60 to 0.85 and from 0.60 to 0.95

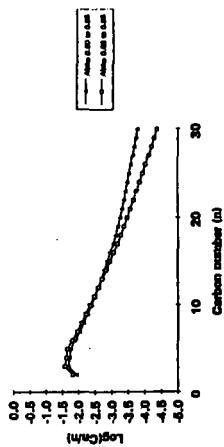


FIGURE 11

Correlation Between Temperature and the C3 Selectivities.

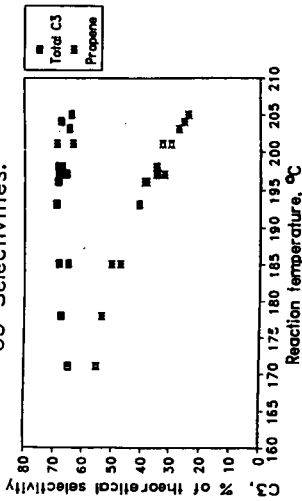


FIGURE 12

Correlation Between Temperature and the C4 Selectivities.

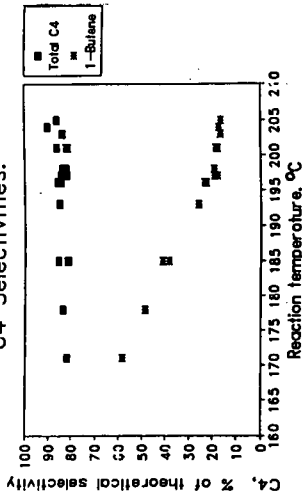


FIGURE 13

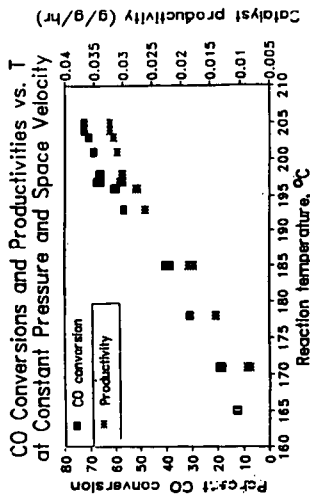


FIGURE 14. Arrhenius Plot.

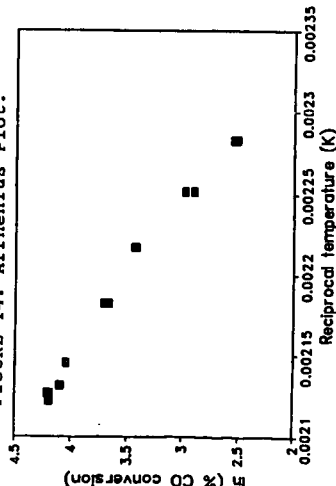


FIGURE 15. Calculated ASF Plot of a Product Distribution Continuously Changing in Alpha from 0.7 to 0.8

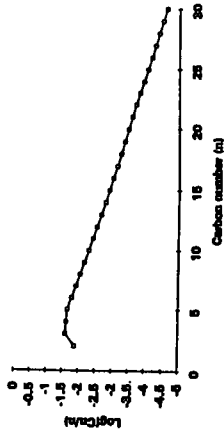
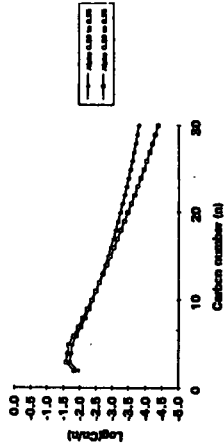


FIGURE 16. Calculated ASF Plots with Alphas Ranging from 0.60 to 0.85 and from 0.60 to 0.95



REOXIDATION AND DEACTIVATION OF SUPPORTED COBALT FISCHER-TROPSCH CATALYSTS

D. Schanke², A.M. Hilmen¹, E. Bergene², K. Kinnari³, E. Rytter³, E. Adnanes² and A. Holmen¹

¹Department of Industrial Chemistry, Norwegian Institute of Technology, University of Trondheim, N-7034 Trondheim, Norway

²SINTEF Applied Chemistry, N-7034 Trondheim, Norway

³Statoil Research Centre, N-7005 Trondheim, Norway

Keywords: Fischer-Tropsch synthesis, cobalt catalysts, deactivation

INTRODUCTION

As a result of the highly exothermic nature of the Fischer-Tropsch reaction, heat transfer considerations limit the maximum conversion per pass in fixed-bed processes, whereas slurry reactors can operate at higher conversions (1). During Fischer-Tropsch synthesis on cobalt catalysts, high conversions will generate high partial pressures of water at the reactor exit, due to the low water gas shift activity of cobalt. In addition, the extensive back-mixing in slurry reactors will give a relatively uniform concentration profile in the reactor, characterized by a high concentration of water and low reactant concentrations. From the commercial iron-catalyzed Fischer-Tropsch synthesis in fixed-bed (Arge) reactors it is known that the catalyst deactivates by oxidation of iron by CO₂ and H₂O near the exit of the reactor (2). Although bulk oxidation of cobalt during Fischer-Tropsch synthesis is not thermodynamically favored, it was early speculated that surface oxidation of cobalt could occur during Fischer-Tropsch synthesis (3).

The purpose of the present work is to describe the influence of water on the deactivation behavior of Al₂O₃ supported cobalt catalysts. The possibility of cobalt oxidation during Fischer-Tropsch synthesis was investigated by model studies.

2. EXPERIMENTAL

2.1 Catalysts

Cobalt catalysts containing (by weight) ~20% Co, 1% Re and optionally 1% rare earth oxides (designated RE) on γ -Al₂O₃, were prepared by incipient wetness coimpregnation of the support with aqueous solutions of Co(NO₃)₂·6H₂O, HReO₄ and (optionally) the RE-oxide precursor. The rare earth oxide precursor was supplied as nitrates (Molycorp 5247) and contained 66% La₂O₃ after calcination, the remainder being other rare earth oxides. The catalysts were dried in air overnight at 393 K before calcination in air at 573 K for 2 hours. The alumina supports had a specific surface area of 174 - 182 m²/g and 0.7-0.9 cm³/g pore volume. The extent of cobalt reduction was ~80% after reduction at 623 K for 14-16 hours (measured by O₂ titration at 673 K), and the cobalt dispersion (H_{ads}:Co) was estimated to 7-8% by temperature programmed desorption of H₂.

2.2 Kinetic experiments

Deactivation studies were carried out in a 0.9 cm I.D. stainless steel fixed-bed reactor heated by a fluidized sand bath. 3 g of catalyst (38-53 μ m) was diluted with an inert material (non porous SiC) in a 1:3 weight ratio to minimize temperature gradients. The catalyst was reduced in flowing hydrogen (5000 cm³ (STP)/(g_{cat}·h)) at atmospheric pressure at 623 K for 16 hours (heating rate from ambient temperature: 1 K/min). After reduction, the catalyst was cooled to 443 K in flowing H₂ and purged with He before increasing the pressure to 20 bar and switching to a feed mixture containing 97 mol% synthesis gas with H₂/CO = 2.1 and 3 mol% N₂. The reaction temperature was then slowly increased to the desired initial reaction temperature. On-line GC samples were taken at regular intervals and analyzed for N₂, CO, CO₂ and C₁+ hydrocarbons on a HP 5890 gas chromatograph. Space velocity was varied to give 20-70% CO conversion. High water partial pressures were obtained by addition of steam to the reactor inlet.

2.3 Gravimetric experiments

Reoxidation experiments were performed in a Sartorius 4436 high pressure microbalance (4). Before reduction, the catalyst was dried for 24 hours at a temperature 50 K higher than the reduction temperature to ensure minimal weight losses due to removal of water from the catalyst during reduction. After cooling to ambient temperature, the catalyst was reduced in flowing H_2 (1 K/min. to 623 K, 16 hours hold time). After reduction, the temperature was adjusted to 523 K and a feed consisting of H_2 , He and H_2O (as steam) was added to the reactor for a period of 16-17 hours.

2.4 X-ray Photoelectron Spectroscopy (XPS)

XPS studies were conducted in a VG ESCALAB MkII instrument equipped with a non-monochromatic Al $K\alpha$ source (1486.6 eV). The catalyst samples were treated in an integrated high pressure pretreatment cell before being transferred to the analysis chamber without exposure to air. The catalysts were analyzed in the unreduced state, after reduction and after treatment with a H_2O/H_2 mixture.

3. RESULTS AND DISCUSSION

3.1 CO hydrogenation experiments

Fig. 1. shows a typical example of the deactivation behavior of an alumina supported, Re-promoted cobalt catalyst. The results are obtained after a 50 h period of stable operation at 463 and 473 K and the CO conversion was adjusted to 31-33% before and after the period where water was added to the feed, in order to allow direct comparison of the catalyst activities. The sharp decrease in reaction rate when water is introduced into the feed is a result of a reversible kinetic effect caused by the change in feed composition and is recovered when water is removed from the feed. The drop in reaction rate is apparently greater than predicted by 1. order kinetics, meaning that the change in reaction rate can only partly be explained by the decreased partial pressure of H_2 when the feed is diluted with H_2O . The reversible part of the decrease in reaction rate must therefore also contain an inhibition term associated with the concentration of water which is not accounted for in the simple 1. order (in H_2) kinetics. Similar behavior has been reported for iron catalysts (5). The contribution of the water inhibition term is likely to be larger than indicated in Fig. 1, since the pressure order for Fischer-Tropsch synthesis on cobalt has been shown to be less than 1.0 (6).

In addition to the inhibition effect, the presence of high water partial pressures also results in relatively rapid deactivation of the catalyst. It is shown that the rate of deactivation is further increased when the inlet partial pressure of water is raised from 5 to 7.5 bar. Virtually no further deactivation was observed after the water had been removed from the feed. From comparison of rates or rate constants before and after the period where water was added to the feed, the catalyst has lost approximately 30% of its initial activity. There is a tendency for decreased rate of deactivation towards the end of the period where water was added to the feed, indicating that the rate of deactivation depends not only on the partial pressure of water, but also on the remaining activity. This is the expected behavior in the case of a parallel poisoning reaction.

The influence of water on the deactivation can also be shown indirectly by monitoring the change in reaction rate at different conversions for a fresh catalyst. Fig. 2. shows that a stable activity is obtained at ~34 and ~52% CO conversion, whereas deactivation is evident when the conversion is raised to an initial value of ~70%. These conversions correspond to H_2O partial pressures of approximately 3, 5 and 7 bar respectively at the reactor outlet. However, these partial pressures are not directly comparable to the situation where water is added to the feed. In the latter case, a uniform concentration profile of water in the reactor is obtained. In the case where all of the water is produced by the Fischer-Tropsch reaction, the concentration of water will be high only near the reactor exit.

3.2 Model studies

Model experiments at non-reacting conditions with various H_2O/H_2 feeds were carried out in order to test the hypothesis of cobalt oxidation as being responsible for the observed deactivation.

Results from the gravimetric studies are shown in Fig. 3. In the series of experiments shown here, catalysts without rare earth oxides (RE) have been used. Although this precludes direct comparison with the deactivation studies, we have generally experienced that this low level of RE loading does not influence the deactivation behavior significantly.

A common feature of all of the curves shown in Fig. 3 is the initial rapid weight increase of ≈ 20 mg/g. Blank experiments using unreduced catalyst (curve 1 in Fig. 3) and the pure support (not shown) also showed the same initial weight increase. It is therefore concluded that the initial behavior is caused by adsorption of water on the porous support. The water adsorption equilibrium is rapidly established and the blank experiments therefore serve as a baseline for measuring weight gains associated with the possible oxidation of cobalt.

Exposure of the reduced $CoRe/Al_2O_3$ catalyst to a H_2O/He mixture (without H_2) resulted in a large weight increase, corresponding to almost complete bulk reoxidation of cobalt (curve 4 in Fig. 3). The situation is markedly different when the feed contains even small amounts of H_2 , as shown for the case with $H_2O/H_2 = 10$ where the weight curve indicates only a limited extent of reoxidation (curve 3 in Fig. 3). This H_2O/H_2 ratio would represent a very high conversion and a stronger deactivation potential than in the kinetic experiments. At the same partial pressure of water but at a higher H_2 partial pressure ($H_2O/H_2 = 1.5$), which could be considered a more realistic case, an even lower weight increase suggests almost negligible bulk reoxidation (curve 2 in Fig. 3).

Significant bulk oxidation of metallic cobalt was therefore considered to be unlikely under Fischer-Tropsch reaction conditions. In view of the strong deactivating effect of water shown in Fig. 1, the possibility of surface oxidation was therefore considered.

XPS spectra of a $20\%Co-1\%Re-1\%RE/\gamma-Al_2O_3$ catalyst are shown in Fig. 4. The peak at 781.5 eV, which is the dominant peak in the XPS spectrum of the calcined catalyst (curve a in Fig. 4), is assigned to cobalt oxides, and is accompanied by a shake-up satellite at 787-788 eV, probably representing Co^{2+} . In the reduced catalyst (curve b in Fig. 4), the XPS peak representing cobalt metal (778 eV) is visible, but the XPS-spectrum is still dominated by the oxide peak at 781.5 eV. In general, the extent of reduction measured by XPS (given as the intensity ratio $Co^0/(Co^{2+/3+}+Co^0)$) is significantly lower than estimated by bulk methods. This is most likely caused by the presence of multiple cobalt oxide phases with widely different dispersion and reducibility, ranging from large Co_3O_4 crystallites to an atomically dispersed surface cobalt aluminate (7,8). The latter is unreducible at the temperatures used in this study but will dominate the XPS-spectrum due to the high dispersion.

Treatment of the reduced catalyst with a 1:4 H_2O/H_2 mixture, gave clear indications of reoxidation of cobalt metal to Co^{2+} or Co^{3+} , as shown by the decreased $Co^0/Co^{2+/3+}$ intensity ratio (curve c in Fig. 4). The intensity of the satellite peak appears to increase slightly, indicating some formation of Co^{2+} .

Thermodynamic calculations show that bulk cobalt metal will not reoxidize in H_2O/H_2 mixtures (3). However, highly dispersed phases or surface layers can be expected to show deviations from bulk behavior. The gravimetric studies indicated a relatively small extent of bulk reoxidation of $CoRe/Al_2O_3$ even at $H_2O/H_2 = 10$, and an even more modest effect at $H_2O/H_2 = 1.5$. The latter conditions are probably more representative of the conditions used in the fixed-bed deactivation studies. In contrast, XPS indicated significant reoxidation already at $H_2O/H_2 = 0.25$. From the comparison of results from surface and bulk techniques it is reasonable to suggest that surface oxidation or preferential oxidation of highly dispersed phases occurs in H_2O/H_2 or $H_2O/H_2/CO$ mixtures.

4. CONCLUSIONS

The presence of high water partial pressures during Fischer-Tropsch synthesis increases the rate of deactivation of a Co-Re-RE/ γ -Al₂O₃ catalyst. In simulated high conversion conditions using H₂O/H₂ feeds, bulk reoxidation of cobalt occurs only to a very limited extent, even at high H₂O/H₂ ratios. However, XPS studies indicated that surface oxidation or oxidation of highly dispersed cobalt phases are responsible for the observed deactivation.

ACKNOWLEDGEMENT

The authors gratefully acknowledge Statoil for financial support and for the permission to publish these results.

REFERENCES

- (1) Fox, J.M., Catal.Rev.-Sci.Eng., 35(2), 169 (1993).
- (2) Dry, M.E., Catal. Lett., 7, 241 (1990).
- (3) Anderson, R.B., in P.H. Emmett (ed.) "Catalysis" Vol.IV, Rheinhold Publ. Comp., New York (1956)
- (4) Holmen, A., Schanke, D. and Sundmark, D., Appl. Catal., 50, 211 (1989)
- (5) Satterfield, C.N., Hanlon, R.T., Tung, S.E., Zou, Z.-M. and Papaefthymiou, G.C., Ind. Eng. Chem. Prod. Res. Dev., 25, 407 (1986).
- (6) Iglesia, E., Reyes, S., Madon, R.J. and Soled, S.L., Adv. Catal., 32, 221 (1993).
- (7) Stranick, M.A., Houalla, M. and Hercules, D.M., J. Catal., 102, 151 (1987).
- (8) Arnoldy, P. and Moulijn, J.A., J. Catal. 93, 38 (1985).

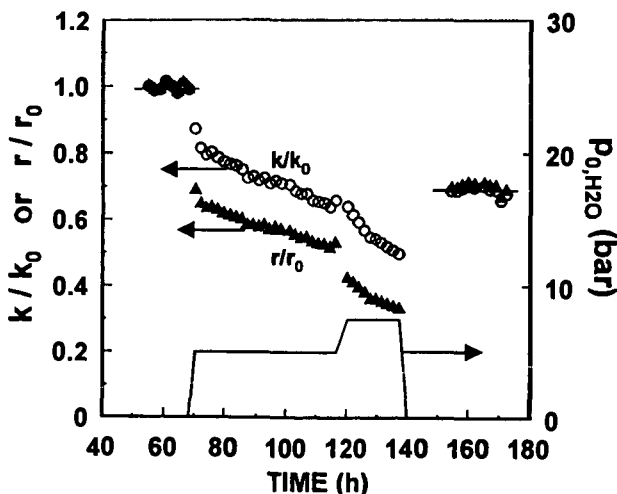


Fig. 1. Activity change during simulated high conversion conditions using a 20%Co-1%Re-1%RE/ γ -Al₂O₃ catalyst. T = 483 K, P = 20 bar, H₂/CO = 2.1.

k/k_0 = (Observed rate constant)/(Initial rate constant at 483 K)
 r/r_0 = (Observed rate)/(Initial rate at 483 K)

k = pseudo 1. order rate constant for H₂ conversion in a plug-flow reactor (contraction factor = -0.5). r = hydrocarbon formation rate (reactor average). P_{0,H_2O} = partial pressure of water at the reactor inlet.

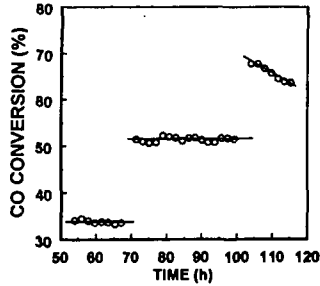


Fig. 2. Conversion vs. time using a 20%Co-1%Re-1%RE/ γ -Al₂O₃ catalyst. Step changes in conversion have been obtained by changing the space velocity. T = 483 K, P = 20 bar, H₂/CO = 2.1.

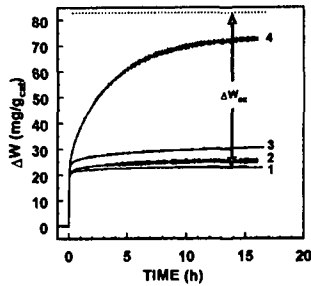


Fig. 3. Weight changes recorded by the microbalance during exposure of 21%Co-1%Re/ γ -Al₂O₃ to H₂O/H₂/He or H₂O/He at 523 K and 10 bar. W_{ox} = weight increase corresponding to total reoxidation of cobalt to Co₃O₄, assuming 80% initial extent of reduction.

1. Unreduced catalyst (P_{H2O}:P_{H2}:P_{He} = 5.5:0:4.5 (bar))
2. Reduced catalyst (P_{H2O}:P_{H2}:P_{He} = 5.5:3.7:0.8 (bar))
3. Reduced catalyst (P_{H2O}:P_{H2}:P_{He} = 5.5:0.55:4.0 (bar))
4. Reduced catalyst (P_{H2O}:P_{H2}:P_{He} = 5.5:0:4.5 (bar))

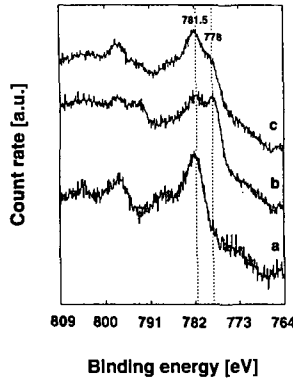


Fig. 4. Co 2p XPS spectra of 20%Co-1%Re-1%RE/ γ -Al₂O₃.
 a. Calcined catalyst.
 b. Catalyst reduced at 723 K for 13 h
 c. Reduced catalyst exposed to -20 vol% H₂O in H₂ for 18 h
 (P = 20 bar, T = 513 K)

A PRELIMINARY UNIFIED APPROACH TO THE STUDY OF FISCHER-TROPSCH KINETICS

Rafael L Espinoza
Sastech (Pty) Ltd
P.O. Box 1, Sasolburg 9570
South Africa

Keywords: Fischer-Tropsch, kinetics, modelling

INTRODUCTION

The standard approach to the study of Fischer-Tropsch (FT) kinetics is mainly based on statistical techniques. The rate expression is chosen on the grounds of the "best data fitting" as measured by the correlation factor in parity plots.

For each FT metal (like Co or Fe), there are different - and sometimes conflicting - rate expressions proposed in the literature. The development of a rate expression based on well designed experimental data is a relatively simple task. Therefore we are inclined to believe that - at least most - of the proposed rate expressions are basically correct for the catalyst used to generate the experimental data.

The objective of this study was to ascertain what role the specific characteristics of the FT catalyst plays in its kinetic behaviour. Once the main parameter(s) that affect this behaviour are identified, it should be possible to propose a general rate expression. The results of such a study are presented in this paper, in which a "unified" kinetic approach was taken and a single kinetic expression is proposed for all the different FT metals.

METHODOLOGY

The necessary data were obtained in two ways:

- Simulation of the data from well known kinetic expressions, and
- Using experimental data from the literature.

Use is made of a new kinetic technique, the "Singular kinetic path"¹ (SKP), to study kinetic data available in the literature for different FT metals. In short, the SKP technique discriminates between kinetic expressions based on the relative conversion path. This technique needs little experimental data, in the form of pairs of data points obtained at different space velocities. The two space velocities are selected to be in a ratio of 1 to 4 and this ratio is kept constant through the study. Because the data are relative and normalized, the reconstruction of the conversion path can be performed using pairs of data points obtained at different temperatures, pressures, pairs of space velocities (at a constant ratio) and feed compositions.

Use is also made of a simplified general kinetic model for the generation of the conversion path, based on the pairs of datum point mentioned above. This model is a simple stochastic model in which the feed composition generates large numbers of input molecules. These molecules go through many iterations in which they are converted into products according to the path dictated by the particular rate expression used. The new numbers and species of molecules are updated between iterations. The retention time is simulated by the number of iterations, while the space velocity is simulated by the initial numbers of molecules. Other inputs are the pressure and temperature. Factors like transport phenomena, temperature profiles, etc. do not have an effect on this study due to the relative and normalized handling of the data by the SKP technique¹.

KINETIC ANALYSIS

The following kinetic expressions were used to generate the data for the construction of the SKP plot:

Case 1. "Standard" precipitated Fe catalyst, Anderson²:

$$-r_{\text{CO} + \text{H}_2} = a P_{\text{H}_2} P_{\text{CO}} / (P_{\text{CO}} + b P_{\text{H}_2\text{O}}) \quad (1)$$

Case 2. "Standard" cobalt catalyst, Satterfield³:

$$-r_{\text{CO} + \text{H}_2} = c P_{\text{CO}} P_{\text{H}_2} / (1 + d P_{\text{CO}})^2 \quad (2)$$

Case 3. High Water-Gas-Shift (WGS) Fe catalyst, Ledakowicz⁴:

$$-r_{\text{CO} + \text{H}_2} = e P_{\text{H}_2} P_{\text{CO}} / (P_{\text{CO}} + f P_{\text{CO}_2}) \quad (3)$$

Case 4. Ruthenium catalyst, Everson⁵:

$$-r_{\text{CO} + \text{H}_2} = g P_{\text{H}_2} P_{\text{CO}}^{-0.36} \quad (4)$$

Case 5. In addition, we used experimental data⁶ for a Co-Mn catalyst that exhibited a similar degree of WGS as a typical potassium promoted precipitated iron catalyst.

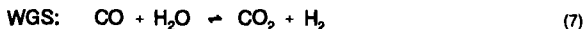
The SKP plot for these 5 cases is shown in Figure 1. In this figure, the ratio of the space velocities is an arbitrary 4 to 1. Notice that the two iron catalysts (cases 1 and 3) follow a different path. The same comment applies to the two cobalt catalysts (cases 2 and 5). The most noticeable difference between these catalysts is their WGS activity.

In the case of iron catalysts, the well known Anderson equation has a water partial pressure term in the denominator. That is, the accumulation of water has a negative effect on the rate of reaction. The Anderson equation is not able to reproduce Ledakowicz's data, since almost all the reaction water disappears due to the very high WGS activity of his catalyst. To solve this problem, Ledakowicz used a CO_2 term in the denominator of his kinetic expression. Notice that both the Anderson and Ledakowicz kinetic expressions can be considered particular cases of the more general rate expression:

$$-r_{\text{CO} + \text{H}_2} = h P_{\text{H}_2} P_{\text{CO}} / (P_{\text{CO}} + i P_{\text{H}_2\text{O}} + j P_{\text{CO}_2}) \quad (5)$$

Where for the "standard" iron, $j = 0$, and for the very high WGS iron, $i = 0$.

The FT and WGS equations can be represented by:



From equations (6) and (7), it is evident that the extent of the $(\text{CO} + \text{H}_2)$ conversion is proportional to the generation of $\text{CO}_2 + \text{H}_2\text{O}$. Therefore, it should be possible to use the $(\text{H}_2 + \text{CO})$ conversion (CONV) in the denominator of the rate expression, instead of the CO_2 and H_2O terms.

Such an approach was used to reproduce the SKP paths shown in Figure 1. We found that it was necessary to use the square root of the CO term in the numerator. The expression to reproduce the SKP paths is:

$$-r_{\text{CO} + \text{H}_2} = m P_{\text{H}_2} P_{\text{CO}}^{0.5} / (P_{\text{CO}} + k \text{CONV}) \quad (8)$$

In this expression, the conversion can be represented in terms of the partial pressures of the H₂, CO and the generation of H₂O and CO₂.

The k constants for the different catalysts are:

Ruthenium catalyst:	about	0.01 - 0.02
"Standard" cobalt catalyst:	about	0.01 - 0.02
"Standard" precipitated iron catalyst:		0.3 - 0.5
"High" WGS cobalt catalyst:		0.4 - 0.5
High WGS iron catalyst:		3.5

The WGS activity of typical ruthenium and cobalt catalysts is very low compared to typical precipitated iron catalysts⁷. The WGS activity of the high WGS cobalt catalyst is very similar to that of precipitated iron catalysts⁸, while the WGS activity of the high WGS iron catalyst⁹ was so high that practically all the water reacted to CO₂. It seems therefore that the k constant in equation (8) is a function of the WGS activity of the catalyst.

This observation is reinforced by the fact that two different FT catalysts that have similar WGS activity (the cobalt catalyst of case 5 and the "standard" iron catalyst of case 1) follow the same specific kinetic equation of Anderson².

Equation (8) shows that it is possible to express the interaction of the reactants or SKP path for different FT catalysts using a single equation. The next step is to consider the activation energy.

The activation energies proposed in the literature are not so different from each other, even for different FT metals. Most of the published activation energies for cobalt are between 93 - 103 kJ/mol³. For iron, the range for the published activation energies is somewhat larger⁸, mainly from 70 - 100 kJ/mol; while for ruthenium, Everson³ proposes 80 kJ/mol.

Since these activation energies overlap, as a first approximation a figure of 93 kJ/mol will be assumed for use in equation (8). The general equation would then be:

$$-r_{\text{CO} + \text{H}_2} = n e^{(-93/RT)} P_{\text{H}_2} P_{\text{CO}}^{0.5} / (P_{\text{CO}} + k \text{ CONV}) \quad (9)$$

The accuracy of the proposed general equation (9) was tested by comparing it with experimental data or kinetic rate expressions and SKP path for the 5 different catalysts described previously. The range of operating conditions used in the comparison is shown in Table 1.

The results are plotted in Figure 2 in the form of a parity plot. This figure shows that the general FT equation reproduces the experimental data or the predicted conversions using specific equations in an acceptable manner. There are some deviations which could be due to the fact that the proposed equation (9) is still not the optimal one. In addition, some deviations from proposed kinetic expressions are usually present due to experimental error.

CONCLUSIONS

It seems to be possible to model the conversion shown by different FT catalysts using a single kinetic rate expression. This expression applies to different metals and for catalysts that, despite having the same FT metal, exhibit different kinetic behaviour. This general kinetic expression is a first approximation, and it should be possible to improve it. Its objective was to ascertain the feasibility of a unified kinetic approach to FT kinetics.

The only variable in this expression is a term that is a function of the WGS activity of the specific catalyst being modelled. We can only speculate about this relationship at present. There may be an overlap for the sites responsible for the FT and the WGS reactions, which could explain the intimate relationship between the FT and WGS activities (besides the one due to the effect of FT and WGS on partial pressures) and its impact on the FT kinetic rate expression.

Should this be the case, then the path followed by the FT reaction is more dependent upon the reduced/oxidized state of the surface than on the chemical composition of the FT catalyst under consideration.

The applicability of the general kinetic rate expression means that there is still much to be done in FT catalysis, particularly in the surface field, in the understanding of the nature of the active sites for the FT and the WGS reactions, and in their interaction.

The results from this study also point out that perhaps different FT metals should not be studied in isolation and that more insight could be gained from an unified research approach.

REFERENCES

1. Espinoza, R.L., *Preprints, Int. Conf. on Catalysis & Catalytic Processing*, pp 391 -402, 1993, Cape Town, South Africa.
2. Anderson, R.B., *Catalysis, Emmet, P.H., (Ed) Vol 4, Reinhold*, 1956, New York.
3. Satterfield, C.N., Yates, I.C., *Energy & Fuels*, 1991, 5, 168 - 173.
4. Ledakowicz, S.; Nettelhoff, H.; Kokuun, R.; Deckwer, W.-D., *Ind. Eng. Chem. Process Des. Dev.*, 1985, 24, 1043 -1049.
5. Everson, R.C.; Mulder, H.; Keyser, M.J. *Proceedings of 7th Nat. Meeting of the South African Institution of Chem. Engineers*, pp 840 - 848, 1994, Esselen Park, South Africa.
6. Keyser, M., Ph.D. Thesis, Potchefstroomse University, Thesis submitted.
7. Dry, M.E., *The Fischer-Tropsch Synthesis, Catal. Science and Technology*, Anderson, J.R. and Boudart, M. (Eds), Vol 1, Springer-Verlag, 1981.
8. Huff, G.A.; Satterfield, C.N., *Ind. Eng. Chem. Process Des. Dev.*, 1984, 23, 696 -705.

TABLE 1: Range of operating conditions for the comparison of the proposed General Kinetic expression versus experimental data or specific kinetic equations for the 5 cases under study.

Catalyst	Pres. (bar)	Temp. (°C)	H ₂ /CO (in)	Mode of comparison
Case 1	20 - 35	220 - 260	1 - 3	Anderson eq.
Case 2	20 - 35	210 - 240	0.5 - 3	Satterfield eq.
Case 3	10	220 - 260	0.7 - 0.8	Exp. data
Case 4	20 - 35	210 - 240	0.5 - 2	Everson eq.
Case 5	5 - 20	220	1 - 5	Exp. data

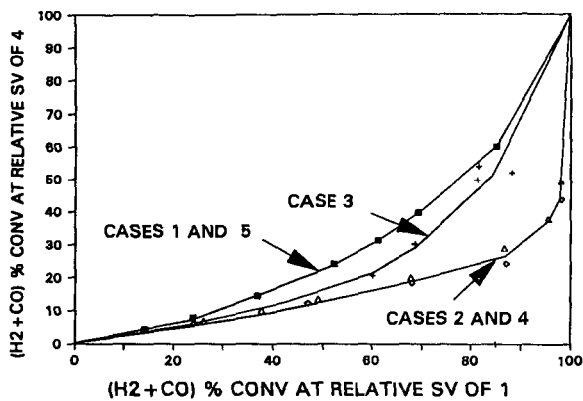


Figure 1. SKP Plot for the 5 different catalysts

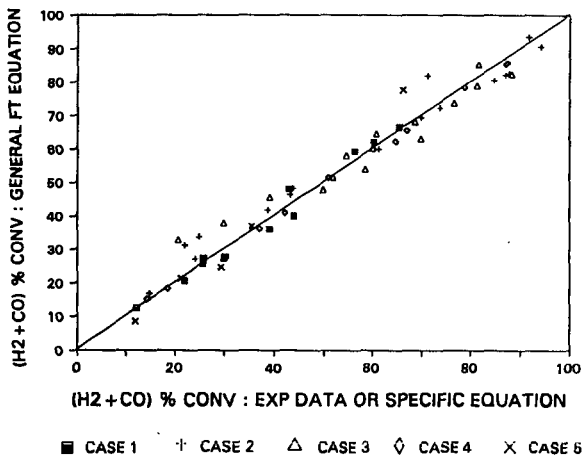


Figure 2. Parity plot between the general FT equation and specific FT equations or experimental data for the 5 cases under study

ROLE OF CO₂ IN THE INITIATION OF CHAIN GROWTH DURING THE FISCHER-TROPSCH SYNTHESIS

Burtron H. Davis, Liguang Xu, Shiqi Bao, Li-Min Tau,
Birbal Chawla and Hossein Dabbagh

Center for Applied Energy Research, University of Kentucky, 3572 Iron
Works Pike, Lexington, KY 40511

Keywords: Fischer-Tropsch Synthesis, Isotopic Tracer, Iron Catalyst

ABSTRACT

Data are presented to show that alcohols produce hydrocarbons during the Fischer-Tropsch Synthesis (FTS) that are not consistent with a simple initiation mechanism. CO₂ is produced directly from the alcohol, and not by the reverse of the carbonylation reaction. CO₂ also initiates chain growth in the FTS, and the initiation intermediate is presumed to be the same intermediate as in the water-gas-shift reaction.

INTRODUCTION

The Fischer-Tropsch Synthesis involves the production of many hydrocarbon and oxygenate products from CO and H₂. This makes the analysis of the products very difficult and adds much complexity to the interpretation of the data to develop a consistent mechanism for the reaction. In an effort to obtain data to aid in understanding this complex system, isotopic tracer studies have been utilized. One approach has employed ¹⁴C-labeled intermediates (1-6). The early results from the use of ¹⁴C-labeled intermediates led to the proposal of an oxygen containing structure that is considered to be responsible for the initiation of the growing chain on the surface of iron catalysts (1-3). With the advent of surface analytical instrumentation, the presence of carbon, but not a significant amount of oxygen on the catalyst surface led workers to question the role of the oxygenated intermediate, and revived the carbide mechanism. However, this latter carbide mechanism differed from that of the one advanced by Fischer and Tropsch (7), where the synthesis was postulated to occur by utilizing the bulk carbide as an intermediate, since the carbide is now believed to be restricted to a surface metal carbide structure (8).

EXPERIMENTAL

The catalyst utilized for all but one of the experiments described below was a C-73 fused iron catalyst manufactured by the United Catalyst, Inc. Prior to use the catalyst was reduced at 400°C in flowing hydrogen and passivated after decreasing the temperature of the catalyst to room temperature. The passivated catalyst was slurried in octacosane in a one liter continuously stirred tank reactor (CSTR) and again reduced at 262°C for three days. The reaction was conducted using a CO/H₂ ratio of 1, 262°C, 8 atm. total pressure and a flow rate of synthesis gas to provide 60% conversion of CO. The ¹⁴C-tracer compound was added, using a piston pump or as a CO₂/CO gas mixture, so that the carbon added in the tracer was 3 or less atomic % of the total carbon added to the CSTR. Liquid products were collected and analyzed for radioactivity as detailed in an earlier report (9).

Experiments with the ¹⁴CO₂ were conducted by adding the labeled-gas to the synthesis gas prior to entering a 1-liter mixing vessel. The catalyst utilized in this synthesis was a proto-type catalyst containing 0.03% K, 12% CuO and the remainder Fe₂O₃. The experimental conditions were otherwise similar to those reported for the C-73 catalyst.

RESULTS

The results for the radioactivity in liquid alkane fractions show that the normal primary alcohol is incorporated to a much greater extent than the corresponding alpha olefin (Figure 1). This result, as did earlier data, suggests that the oxygen-containing compound is a potential chain initiator.

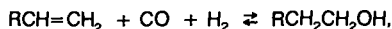
One of the puzzling aspects of the tracer studies was the observation that the radioactivity/mole of alkane decreased approximately as the logarithm of the carbon number. It was postulated that this was a result of the FTS involving two surface chains.

Furthermore, one chain produced alkanes, alkenes and oxygenates and was initiated by the added alcohol or alkene while the other chain was not initiated by the alcohol and produced only alkanes. These two chains could not have a common intermediate and would therefore occur on different catalytic sites (10).

Another puzzling aspect of the results obtained during the addition of the ^{14}C -labeled alcohol is the production of CO_2 that contains more ^{14}C /mole than the CO . It is generally believed that the CO_2 that is formed during the FTS with an iron catalyst is formed by the water-gas-shift reaction:

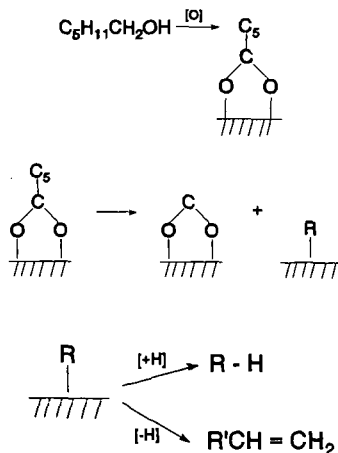


If the primary alcohol formed CO through the reverse carbonylation reaction,



and this CO then underwent the water-gas-shift reaction, the CO_2 would have the same radioactivity/mole as the CO . However, when $1\text{-}^{14}\text{C}\text{-}1\text{-pentanol}$ was added to the synthesis gas the radioactivity/mole of the CO_2 was much greater than that of the CO (Figure 2). This means that the CO_2 could not have been formed by decarbonylation followed by the water-gas-shift reaction. In order to ensure that the results with $1\text{-}^{14}\text{C}\text{-}1\text{-pentanol}$ were reliable, $2\text{-}^{14}\text{C}\text{-}1\text{-hexanol}$ was synthesized and added to the synthesis gas under reaction conditions that were identical to those utilized with $1\text{-}^{14}\text{C}\text{-}1\text{-pentanol}$. As can be seen from the data in Figure 2, the radioactivity of both CO and CO_2 are below the detection limit while that of pentane is high compared to that of 1-pentene. The radioactivities/mole of the C_3 and C_4 hydrocarbons are below the detection limit. The results in Figure 2 clearly show that the added alcohol has undergone conversion to produce CO_2 that is derived from the carbonyl carbon and that the alkyl group remaining has been converted directly to the alkane rather than to the 1-alkene which is then hydrogenated to the alkane.

The data in Figure 2 are consistent with a mechanism in which the adsorbed alcohol reacts with a surface oxygen; thus, it appears that the reaction can be adequately described by the following mechanism:



Additional data to support the above mechanism has now been obtained by adding $^{14}\text{CO}_2$ to the synthesis gas. If the FTS chains are initiated by species derived only from CO then the hydrocarbon products produced from the experiment with $^{14}\text{CO}_2$ could not have a radioactivity/mole that was greater than that of CO . The $^{14}\text{CO}_2$ was added so that it contained only 0.3% of the carbon that was added; thus, the composition of the gases in the CSTR was not altered significantly by the added $^{14}\text{CO}_2$. The radioactivity/mole of the CO , CO_2 , CH_4 , and C_2H_6 are given in Table 1.

If the methane had been formed only from CO then the radioactivity/mole of methane and ethane could not have exceeded that of the CO since the experiment was conducted in a CSTR where all of the catalyst particles are exposed to the same gas composition. The

methane has an activity that approaches that of the added CO₂, rather than that of the CO. This requires the formation of methane to be initiated from CO₂. The activity of ethane is also close to that of the CO₂ showing that it is the FTS that is initiated to a large extent by an intermediate derived from CO₂, and not just the formation of methane.

Data for the C₁-C₉ hydrocarbons formed during the addition of ¹⁴C₂ are presented in figure 3. The CPM/mole for the CO and CO₂ in the exit gas are shown by the solid triangles labeled by CO and CO₂, respectively. It is apparent that the CO₂ has a much higher radioactivity than does the CO. The broken line passing through the radioactivity for the CO represents the increase in radioactivity with carbon number of the hydrocarbon products if they were formed only from CO. In this case each hydrocarbon, C_n, would contain the radioactivity of n carbons derived from the CO. It is clear that the radioactivity of each of the products is much higher than could result from synthesis using CO only. The radioactivity of the hydrocarbon products are shown in open circles, resulting from analysis using the gas analyzer, and open squares, resulting from analysis using a Porpack column that permits the analysis of hydrocarbons of higher carbon numbers. For the moment, we concentrate on the radioactivities of the C₃-C₉ products. The solid line representing these data is parallel to the broken line passing through the radioactivity for CO. For the C₃-C₅ hydrocarbons, the radioactivity measured using the different g.c. instruments show good agreement. Furthermore, the line defined by the C₃-C₉ hydrocarbons extrapolates to a radioactivity of about 0.8 x 10³ CPM/mole. The slope of the solid line in figure 3 indicates that chain growth is primarily due to addition of carbon units derived from CO; the similar slopes of the solid and the broken lines are considered to require this conclusion. However, it appears that about 60% of the hydrocarbon chains that lead to C₃-C₉ hydrocarbon products are derived from CO₂. From the higher activity of the C₂ and C₁ hydrocarbons, it appears that even more than 60% of these products are derived from CO₂ initiation. It therefore seems clear that the data in figure 3 require the species that is responsible for the chain initiation be different from the species that is responsible for chain propagation. Furthermore, the species responsible for chain initiation is derived from both CO₂ and CO but the species that is responsible for chain propagation is derived from CO. Thus, it is concluded that the species that is responsible for chain initiation retains some oxygen, and in this respect is similar to the postulates of Emmett and coworkers.

CONCLUSION

It appears that the FTS mechanism with an iron based catalyst involves an oxygenate species that can be derived from both CO and CO₂. The data generated from the above studies involving the addition of CO₂ or alcohol are consistent with a reaction mechanism that involves reactions as shown above for the alcohol. Thus, the intermediate that is involved in the water-gas-shift reaction is postulated to be an initiator for chain growth for the FTS reaction.

ACKNOWLEDGMENT

This work was supported with funding from the Commonwealth of Kentucky and the U.S. Department of Energy, Pittsburgh Energy Technology Center, through Contract No. DE-AC22-84PC70029 and DE-AC22-94PC94055.

REFERENCES

1. G. Blyholder and P. H. Emmett, *J. Phys. Chem.*, **63**, 962 (1959).
2. W. K. Hall, R. J. Kokes and P. H. Emmett, *J. Am. Chem. Soc.*, **82**, 1027 (1960).
3. W. K. Hall, R. J. Kokes and P. H. Emmett, *J. Am. Chem. Soc.*, **79**, 2983 (1957).
4. L-M. Tau, H. A. Dabbagh and B. H. Davis, *Catal. Lett.*, **7**, 141 (1990).
5. L-M. Tau, H. A. Dabbagh and B. H. Davis, *Energy & Fuels*, **5**, 174 (1991).
6. L-M. Tau, H. A. Dabbagh, J. Halasz and B. H. Davis, *J. Mol. Cat.*, **71**, 37 (1992).
7. F. Fischer and H. Tropsch, *Brennst. Chem.*, **4**, 276 (1923).
8. K. Kishi and W. M. Roberts, *J. Chem. Soc. Faraday Trans. 1*, **71**, 1715 (1975).
9. L. M. Tau, H. Dabbagh, B. Chawla and B. H. Davis, Final Report, E-AC22-84PC70029, January, 1988.
10. L. M. Tau, H. Dabbagh, S. Bao and B. H. Davis, *Catal. Lett.*, **7** (127) (1990).

Table 1. Radioactivity/mole of Effluent Gas Products

Compound	Radioactivity, Counts/Min./Mole
CO	0.12×10^{-3}
CO ₂	1.31×10^{-3}
CH ₄	1.12×10^{-3}
C ₂ H ₆	1.28×10^{-3}

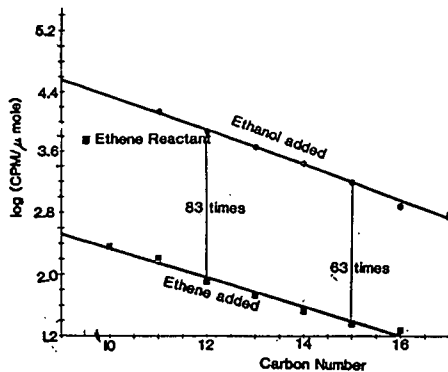


Figure 1. The ¹⁴C activity in the alkane products formed when 1-pentanol (●) or 2-pentene (■) was added to the syngas feed to a C-73 catalyst (CSTR, 262°C, 8 atm).

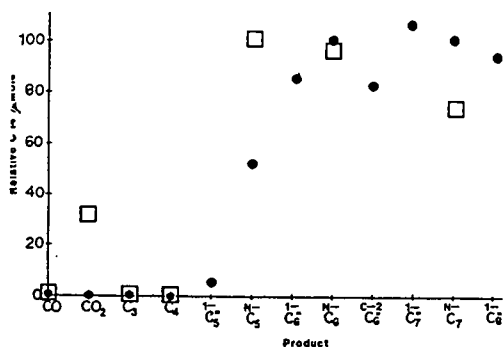


Figure 2. Products (gas phase) from the conversion of a syngas containing either 2-¹⁴C-1-hexanol (●) or 1-¹⁴C-1-pentanol (□) with a C-73 catalyst at 262°C and 8 atm (total) in a CSTR.

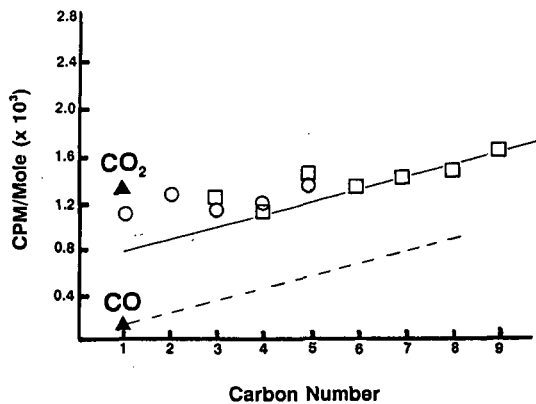


Figure 3. The ^{14}C activity in the alkane products formed when $^{14}\text{CO}_2$ is added to the synthesis gas fed to the UCI proto-type iron catalyst (CSTR, 270°C, 8 atm).

ZIRCONIA PROMOTION OF FISCHER-TROPSCH COBALT CATALYSTS: BEHAVIOR IN FIXED-BED AND SLURRY BUBBLE COLUMN REACTORS

R. Oukaci, J.G. Goodwin, Jr., G. Marcelin, and A. Singleton¹
Chemical & Petroleum Engineering Department
University of Pittsburgh
Pittsburgh, PA 15261

¹ Energy International Corporation, 135 William Pitt Way, Pittsburgh, PA 15238.

Keywords: Fischer-Tropsch Synthesis, CO Hydrogenation, Cobalt Catalysts.

ABSTRACT

A series of cobalt-based F-T catalysts supported on alumina and silica were prepared with different loadings of Zr and different sequence of impregnation of Co and Zr. All catalysts were extensively characterized by different methods. The catalysts were evaluated in terms of their activity and selectivity both in fixed bed and slurry bubble column reactors. Addition of ZrO₂ to both Co/SiO₂ and Co/Al₂O₃ catalysts resulted in at least a twofold increase in the catalyst activity for F-T synthesis in the fixed bed reactor. In the slurry bubble column reactor, a similar promotion effect was observed for the SiO₂-supported catalysts, while the addition of Zr to a cobalt/alumina catalyst had a less significant effect.

INTRODUCTION

Cobalt has been one of the most commonly used metals for Fischer-Tropsch catalysts since the 1930's because of its high activity (1). It has received a lot of attention recently (2-8) due to its usefulness in converting CO to liquid hydrocarbons. While many promoters for Fischer-Tropsch (F-T) synthesis, such as the alkali series, have been extensively studied, others such as Zr have not. A number of studies of F-T synthesis over ZrO₂-supported Co (1,9), Ni (9), Ni/Co (9), and Pd (10) have been reported in the literature. The use of ZrO₂ as the support for these different active metals has been found to increase the higher hydrocarbon selectivity. Recently, a number of patents by Shell (11-13) have involved Zr promotion of Co/SiO₂. Addition of up to 15 wt% ZrO₂ promotor was found to increase the overall activity of the Co catalyst without affecting the selectivity for higher hydrocarbons.

A series of cobalt-based F-T catalysts supported on alumina and silica were prepared with different loadings of Zr and different sequence of impregnation of Co and Zr in order to investigate the role of ZrO₂ on affecting the F-T reaction in both fixed bed and slurry bubble column reactors.

EXPERIMENTAL

All catalysts compared in this study consisted of 20 wt% cobalt and different amounts of zirconia (up to 15 wt% Zr), the support being alumina (Vista B) or silica (Davison 952). The supports, calcined at 500°C for 10 hours prior to catalyst preparation, were loaded with Co and/or Zr by either a single or 2-step impregnation method. Aqueous solutions of cobalt nitrate and/or zirconium nitrate were used to prepare all the catalysts except in the case of S[Co/8.5Zr(O)]/SiO₂, where a solution of zirconium tetra-n-propoxide in a mixture of n-propanol, toluene, and acetyl acetone was used to impregnate the Zr in the initial impregnation step. In the case of single step impregnations, the SiO₂-supported catalysts were prepared by kneading (11-13) the aqueous metal precursor solution-support mixture for 3.5 hours. For the sequentially impregnated SiO₂-supported catalysts, kneading was used in the initial step for the addition of Co, followed by use of the incipient wetness method for the impregnation of Zr (11-13). For the other sequentially impregnated SiO₂-catalysts and all the alumina-supported catalysts, the incipient wetness method was used in both steps. After the first impregnation step, the catalyst was dried in an oven for 5 hours at 115°C with occasional stirring. Then, it was calcined in air by raising its temperature to 300°C with a heating rate of 1°C/min and holding for 2 hours. Also, after the second step of impregnation (if used) the catalyst was dried and calcined identically as in the first step. The catalysts are listed in Table 1 with the corresponding preparation methods.

Prior to H₂ chemisorption or reaction, the catalysts were reduced in H₂ at 250°C for the SiO₂-supported catalysts and 350°C for the Al₂O₃-supported catalysts, for 10 hours following a 1°C/min ramp. They have all been extensively characterized by different methods, including elemental analysis, BET physisorption, particle size distribution, X-ray diffraction, hydrogen chemisorption, temperature programmed reduction. Table 2 summarizes the relevant characterization data.

The catalysts were evaluated in terms of their activity and selectivity both in a fixed bed reactor and in a slurry bubble column reactor. Typically, 0.15 to 0.35 g of prereduced

catalyst were charged into the fixed bed reactor tube and rereduced overnight at 300°C. The reaction was carried out at 220°C, 1 atm, H₂/CO ratio of 2.0, and a total flow rate of 90 cm³/min. No inert diluent was used. Sample analyses were taken after approximately 2, 5, 9, and 24 hours on-stream. In some cases the temperature was varied between 210 and 240°C in order to calculate an Arrhenius activation energy. Product analysis for C1 to C20 hydrocarbons was performed by on-line gas chromatography. CO conversion rates were calculated based on the GC analysis of the products. Anderson-Schultz-Flory (A-S-F) distributions were plotted and the chain growth probability, α , calculated using the C4 to C16 data.

For the slurry bubble column tests, the catalyst was first reduced *ex-situ* in a fluidized bed assembly and then transferred into a glove box for weighing and subsequent transfer into the slurry bubble column reactor. Approximately 15 g of catalyst and 200 g of liquid medium were used in a run. Typically, the reaction was carried out at 240°C, a total pressure of 450 psi, H₂/CO ratio of 2, and 60% N₂ diluent. Analysis of the gas products, CO, CO₂, and C1 to C5, was performed hourly. Liquid products were collected at the end of each 24 hour period, blended, and submitted for analysis. A-S-F plots of the liquid products were used to determine α . After reaching steady-state under these conditions, temperature, pressure, and H₂/CO ratio were varied in turn to study the effect of process conditions. A typical complete run lasted about 10 days. Only the base Co catalysts (non-promoted Co/SiO₂ and Co/Al₂O₃) and the most active catalysts in the fixed bed reactor were tested in the slurry bubble column reactor.

RESULTS AND DISCUSSION

From XRD measurements, it was found that the average diameter of the Co oxide crystallites for all catalysts varied within a narrow range (ca. 20-30 nm), regardless of the amount of Zr present or the support used. In addition, the XRD results suggest that Zr was highly dispersed on Co/SiO₂ since no Zr compound phases were detected.

The TPR results show little difference in the degree of reduction for all the catalysts with the exception of Cl[0.7Zr+Co]/SiO₂ and S[Co/8.5Zr]/Al₂O₃ which exhibited the lowest and the highest reducibility, respectively. The Al₂O₃-supported catalysts had in general higher reducibilities than their silica-supported analogs. It was also found that all the catalysts used in this study were reduced to the maximum degree (defined as % Co reduced during TPR to 900°C) during the standard reduction procedure at 250°C.

The sequentially-impregnated Zr/Co on SiO₂ catalysts showed an increase in the amount of total hydrogen chemisorbed compared to that for [Co]/SiO₂. On the other hand, for the sequentially-impregnated Co/Zr on SiO₂ catalysts, the Zr addition did not influence significantly the amount of H₂-chemisorption. The co-impregnated catalyst (Cl[8.5Zr+Co]/SiO₂ had almost twice as much H₂ uptake as either Cl[0.7Zr+Co]/SiO₂ or [Co]/SiO₂. The opposite effect was observed with the Al₂O₃-supported catalysts. The sequentially-impregnated Co/Zr on Al₂O₃ catalyst and the co-impregnated catalyst with low Zr loading (Cl[1.4Zr+Co]/Al₂O₃ had the highest H₂ uptakes.

Table 3 shows selected data obtained from fixed bed reaction which indicate the effect of ZrO₂ promotion on F-T activity and selectivity. While the alumina-supported Co catalysts were found to be in general more active than their silica-supported analogs, Zr promotion of both Co/SiO₂ and Co/Al₂O₃ increased significantly the overall rate of F-T synthesis, compared to the non-promoted catalysts. In addition, the promoting effect of ZrO₂ was more significant on the alumina-supported catalysts, especially the sequentially impregnated catalyst S[Co/8.5Zr]/Al₂O₃. The method of preparation and the amount of promoter used also affected the catalyst activity and selectivity. The sequentially impregnated [Co/Zr] catalysts appeared to be the most active. Addition of Zr beyond 8.5 wt% for the SiO₂-supported catalysts did not seem to have any beneficial effect. The catalysts with the highest Zr loadings (wt% Zr > 1.4) had the highest values of α compared to the non-promoted catalysts, even though the CH₄ selectivity was also slightly higher in several cases. On the other hand, small amounts of Zr promotion (wt% Zr = 0.7 or 1.4) appeared to have a slightly negative effect on the values of α .

Table 4 shows selected data obtained at 240°C, 450 psi, and H₂/CO ratio of 2, in the slurry bubble column reactor for catalysts consisting of Co supported on silica and alumina, respectively. As in the case of the fixed bed testing, the ZrO₂ promoter was found to influence the overall activity of both the silica- and alumina-supported catalysts. However, while the alumina-supported Co catalysts were also found to be in general more active than their silica-supported analogs, the promoting effect of ZrO₂ was not as significant on the

alumina-supported catalysts. Diffusion limitations in the liquid medium in the slurry bubble column reactor may be invoked to explain the discrepancies in the results obtained in the two reaction systems. The overall rate observed for the catalyst S[Co/8.5Zr]/Al₂O₃ was high, but most probably diffusion limited.

In summary, ZrO₂ appears to be an excellent rate promoter for SiO₂- and Al₂O₃-supported Co catalysts. Addition of Zr in both catalysts, probably hinders the formation of Co aluminates and Co silicates, either during the preparation and pretreatment or during the F-T synthesis reaction itself. In addition, high levels of promotion act to increase the selectivity for higher hydrocarbons.

ACKNOWLEDGMENTS

The authors gratefully acknowledge the funding of this project by DOE and the contribution of the following personnel involved in this study: S. Ali, L. Balawejder, P. Brim, B. Chen, W. Gall, and S. Renaldi.

REFERENCES

1. Withers, H. P., Jr., and Eliezer, K. F., and Mitchell, J. W., *Ind. Eng. Chem. Res.* **29**, 1807 (1990).
2. Brady, R. C., and Pettit, R., *J. Am. Chem. Soc.* **103**, 1287 (1981).
3. Reuel, R. C., and Bartholomew, C. H., *J. Catal.* **85**, 78 (1984).
4. Reuel, R. C., and Bartholomew, C. H., *J. Catal.* **85**, 63 (1984).
5. Foley, H. C., and Hong, A. J., *Appl. Catal.* **61**, 351 (1990).
6. Rathousky, J., Zukal, A., Lapidus A., and Krylova, A., *Appl. Catal.* **79**, 167 (1991).
7. Iglesia, E., Soled, S. L., and Fiato, R. A., *J. Catal.* **137**, 212 (1992).
8. Iglesia, E., Soled, S. L., Fiato, R. A., and Grayson, H., *J. Catal.* **143**, 345 (1993).
9. Bruce, L. A., Hope, G. J., and Mathews, J. F., *Appl. Catal.* **8**, 349 (1983).
10. Alekseev, O. S., Zaikovskii, V. I., and Ryndin, Yu. I., *Appl. Catal.* **63**, 37 (1990).
11. Hoek, A., Joustra, A. H., Minderhoud, J. K., and Post, M. F., *UK Pat. Appl. GB 2 125 062 A* (1983).
12. Hoek, A., Minderhoud, J. K., and Post, M. F. M., *Lednor, P. W. Eur. Pat. Appl. EP 110 449 A1* (1984).
13. Post, M. F. M. B., and Sie, S. T. B., *Eur. Pat. Appl. 0 167 215 A2* (1985).

Table 1: Catalyst Preparation Methods Used

Catalyst ^a	Step # 1 ^b		Step # 2 ^b	
	Method	Solution	Method ^a	Solution
[Co]/SiO ₂	Kneading	aqueous(Co)	N/A	N/A
S[0.7Zr/Co]/SiO ₂	Kneading	aqueous(Co)	Inc. Wet.	aqueous(Zr)
S[1.4Zr/Co]/SiO ₂	Kneading	aqueous(Co)	Inc. Wet.	aqueous(Zr)
S[8.5Zr/Co]/SiO ₂	Kneading	aqueous(Co)	Inc. Wet.	aqueous(Zr)
S[Co/4.0Zr]/SiO ₂	Inc. Wet.	aqueous(Zr)	Inc. Wet.	aqueous(Co)
S[Co/8.5Zr(O)]/SiO ₂	Inc. Wet.	organic(Zr)	Inc. Wet.	aqueous(Co)
S[Co/8.5Zr]/SiO ₂	Inc. Wet.	aqueous(Zr)	Inc. Wet.	aqueous(Co)
S[Co/15.0Zr]/SiO ₂	Inc. Wet.	aqueous(Zr)	Inc. Wet.	aqueous(Co)
CI[0.7Zr + Co]/SiO ₂	Kneading	aqueous(Co + Zr)	N/A	N/A
CI[8.5Zr + Co]/SiO ₂	Kneading	aqueous(Co + Zr)	N/A	N/A
[Co]/Al ₂ O ₃	Inc. Wet.	aqueous(Co)	N/A	N/A
CI[1.4Zr + Co]/Al ₂ O ₃	Inc. Wet.	aqueous(Co + Zr)	N/A	N/A
CI[8.5Zr + Co]/Al ₂ O ₃	Inc. Wet.	aqueous(Co + Zr)	N/A	N/A
S[8.5Zr/Co]/Al ₂ O ₃	Inc. Wet.	aqueous(Co)	Inc. Wet.	aqueous(Zr)
S[Co/8.5Zr]/Al ₂ O ₃	Inc. Wet.	aqueous(Zr)	Inc. Wet.	aqueous(Co)

(a) Nomenclature: S = sequential impregnation, CI = co-impregnation; [A/xxB] = "A" impregnated after "B", [A+xxB] = co-impregnated "A" and "B"; B(O) = organic compound of B used instead nitrate (nonaqueous impregnating solution); xx = wt% Zr.

(b) Catalysts dried for 5 hrs at 115 °C and calcined for 2 hrs at 300°C after each step.

Table 2: Catalyst Characterization Results

Catalyst	H ₂ Chemisorption		TPR	XRD
	Total (μmol H ₂ /g cat)	% Co Dispersion	% Reduct. (25-900°C)	Co ₃ O ₄ d _p (nm)
[Co]/SiO ₂	82	4.8	75	27
S[0.7Zr/Co]/SiO ₂	141	8.3	80	28
S[1.4Zr/Co]/SiO ₂	149	8.8	81	27
S[8.5Zr/Co]/SiO ₂	122	7.2	81	29
S[Co/8.5Zr(O)]/SiO ₂	87	5.1	75	31
S[Co/8.5Zr]/SiO ₂	93	5.5	75	27
CI[0.7Zr + Co]/SiO ₂	67	4.0	64	20
CI[8.5Zr + Co]/SiO ₂	125	7.3	77	24
[Co]/Al ₂ O ₃	48	2.8	85	20
CI[1.4Zr + Co]/Al ₂ O ₃	71	4.2	82	19
CI[8.5Zr + Co]/Al ₂ O ₃	55	3.2	85	26
S[8.5Zr/Co]/Al ₂ O ₃	43	2.5	79	24
S[Co/8.5Zr]/Al ₂ O ₃	114	6.7	96	22

Table 3: Fixed Bed Reaction Results

Catalyst	ACTIVITY		SELECTIVITY	
	% CO Conversion	Rate (g CH ₂ /g cat/hr)	CH ₄ (wt%)	α
[Co]/SiO ₂	2.9	0.094	22.4	0.61
S[0.7Zr/Co]/SiO ₂	3.8	0.121	26.7	0.55
S[1.4Zr/Co]/SiO ₂	3.8	0.123	28.3	0.56
S[8.5Zr/Co]/SiO ₂	3.9	0.125	28.9	0.67
S[Co/4.0Zr]/SiO ₂	2.6	0.161	22.2	0.73
S[Co/8.5Zr(O)]/SiO ₂	5.7	0.182	28.7	0.62
S[Co/8.5Zr]/SiO ₂	5.0	0.160	23.5	0.63
S[Co/15.0Zr]/SiO ₂	3.1	0.179	22.7	0.73
Cl[0.7Zr + Co]/SiO ₂	3.6	0.114	28.0	0.56
Cl[8.5Zr + Co]/SiO ₂	4.6	0.147	22.0	0.69
[Co]/Al ₂ O ₃	3.3	0.077	28.4	0.62
Cl[8.5Zr + Co]/Al ₂ O ₃	3.3	0.183	22.0	0.70
S[8.5Zr/Co]/Al ₂ O ₃	1.3	0.73	24.1	0.67
S[Co/8.5Zr]/Al ₂ O ₃	5.0	0.275	24.0	0.67

P = 1 atm, T = 220°C, H₂/CO = 2, Catalyst Weight = 0.15-0.35 g, Total Flow Rate = ca. 90 cm³/min, Time-on-stream = ca. 25 hrs

Table 4: Slurry Bubble Column Reaction Results

Catalyst	ACTIVITY		SELECTIVITY	
	% CO Conversion	Rate (g CH ₂ /g cat/hr)	CH ₄ (wt%)	α
[Co]/SiO ₂	14.3	0.67	7.6	0.83
S[Co/8.5Zr(O)]/SiO ₂	25.5	1.21	8.6	0.84
S[Co/8.5Zr]/SiO ₂	26.6	1.24	10.7	0.82
S[Co/15.0Zr]/SiO ₂	20.9	0.93	6.7	0.83
Cl[0.7Zr + Co]/SiO ₂	23.2	1.08	9.4	0.82
Cl[8.5Zr + Co]/SiO ₂	24.8	1.18	8.5	0.84
[Co]/Al ₂ O ₃	27.1	1.34	7.9	0.82
Cl[1.4Zr + Co]/Al ₂ O ₃	30.9	1.41	12.1	0.83
S[Co/8.5Zr]/Al ₂ O ₃	27.5	1.54	10.4	0.84

Catalyst weight: 13-17g, T = 240°C, P = 450 psi, H₂/CO ratio = 2, Total flow rate = ca. 15 L/min, or 3 cm/sec linear velocity, Diluent: N₂: ca. 60%.

A NOVEL APPROACH FOR THE ASSESSMENT OF THE RATE LIMITING STEP IN THE FISCHER-TROPSCH SLURRY PROCESS

J. R. Inga and B. I. Morsi
Chemical and Petroleum Engineering, University of Pittsburgh,
1249 Benedum Engineering Hall
Pittsburgh, PA 15261, U.S.A.

Keywords: Fischer Tropsch, mass transfer, bubble column

ABSTRACT

The rate limiting step in the Fischer-Tropsch (F-T) slurry process was assessed using a simple computer model. This model, unlike others, takes into account the water gas shift (WGS) reaction in the calculation of the importance of the gas-liquid mass transfer and makes use of the "Singular Kinetic Path" concept proposed by Espinoza in 1993. The predictions from the model showed that for the available catalysts the Fischer-Tropsch synthesis could be considered a kinetically-controlled process. CO has mass transfer coefficients lower than H₂, is consumed by both F-T and WGS reactions, and is likely to be the limiting reactant in the process. The reactor performance could be improved by increasing the catalyst activity and operating in the mass-controlled regime. Also, an increase of the catalyst concentration up to a maximum of 37 - 40 wt.% could improve the reactor performance, although the reactor would be operating in a mass transfer-controlled regime due to the relatively high catalyst concentration.

INTRODUCTION

Numerous studies were dedicated to the improvement of the catalyst activity using reaction temperature for Fischer-Tropsch (F-T) synthesis and currently, a number of catalysts with high activity and better selectivity are available [5 - 7]. Several studies [12, 13] also pointed out that the kinetics of the reaction and the gas-liquid mass transfer were the only significant resistances in the slurry phase F-T process. These studies, however, failed to define whether such a process is kinetically- or mass transfer-controlled. In addition, these studies only focused on hydrogen and considered the F-T reaction expression without taking into account the Water Gas Shift (WGS) reaction. As a matter of fact, carbon monoxide is consumed by both F-T and WGS reactions and subsequently it could become a limiting reactant in the overall process.

Recently, a considerable attention has been given to the F-T synthesis in a slurry phase and several contributions covering the hydrodynamics, modeling, bubble size distribution and heat transfer have been published [1 - 4]. A detailed review on modeling of the F-T synthesis was carried out by Saxena et al. [6] and other models including complex ones such as that used in the scaleup of the Sasol I Slurry Bed Process (SSBP) [7] have been used. Most of these computer models were based on second order differential equations for both the gas and liquid phases as shown in Equation (1) for the gas phase and some include a solid mass balance to account for the catalyst concentration profiles which become an important variable when using low gas velocities.

$$D_g \epsilon_g \frac{d^2}{dz^2} (C_{g,i}) - \frac{d}{dz} (u_g C_{g,i}) - k_{L,i} a (C_{L,i}^* - C_{L,i}) = 0 \quad (1)$$

Other models such as that by Deckwer et al. [5] includes a heat balance in order to consider the temperature difference in the slurry reactor. These complex computer models include a large number of parameters concerning the hydrodynamics, kinetics, and mass as well as heat transfer. These parameters, however, are seldom available under the operating conditions of the F-T synthesis and the only resort is to estimate them using other literature data available for air/water systems, liquid hydrocarbons [8] or wax [3]. Unfortunately, the majority of these available data were obtained under atmospheric conditions which raises a serious doubt about their applicability under actual process conditions [9]. In addition, most of these data were obtained for gas-liquid systems without the presence of catalyst particles which alter the slurry density and viscosity as well as gas bubbles coalescence tendency. A thorough review concerning the effect of solid particles on mass transfer has been recently published by Beenackers and van Swaaij [10]. Other factors such as column internals are usually overseen despite the fact that their importance on the hydrodynamic behavior of the slurry reactor was reported to be significant [11]. Thus, using these complex computer models in order to predict the reactor performance as well as the rate limiting step in the F-T slurry process could be cumbersome, expensive, and the predictions are strongly dependent on the accuracy of the literature data used in these models.

This paper presents a novel approach to assess the rate-limiting step in the slurry phase F-T process. A simple computer model which takes into account the WGS reaction and uses the "singular Kinetic Path" concept proposed by Espinoza in 1993 is presented.

Development of the simple model

The two assumptions used in this model were: (1) the gas phase is a plug flow; and (2) the liquid phase is a series of CSTRs. Several simplifications were also made in: (1) phase mixing; (2) kinetics equation; and (3) calculation of mass transfer coefficients.

(1) Phase mixing:

The mixing in the liquid phase was simulated by a number of CSTRs arranged in series based on the studies of the "La Porte Pilot Plant" [14]. This eliminated the need for the second order differential term in the mass balance equations for the liquid phase. Also, the dispersion or backmixing in the liquid phase was expressed in terms of a series of CSTRs [15] as given in Equation (2).

$$\frac{1}{n} = \frac{2}{Pe} - \frac{2}{Pe^2} * (1 - e^{-Pe}) \quad (2)$$

(2) Kinetic equation:

The use of various catalysts with different respective kinetic equations was overcome using the "Singular Kinetic Path" concept developed by Espinoza at Sasol [16]. His concept suggested that a single kinetic equation can be employed for any catalyst as long as the behavior of this catalyst resembles the shape of the F-T synthesis kinetic path when using iron catalyst. In the present model, the Anderson-Dry's equation given below (Equation (3)) was employed where the constant 3.5 was taken from Espinoza's work [16]. The Water Gas shift reaction rate was obtained by simplifying the one proposed by several authors [23,24].

$$r_{F-T} = A.e^{\frac{E}{RT}} \frac{P_{H_2} P_{CO}}{P_{CO} + 3.5 P_{H_2O}} \quad (3)$$

$$r_{WGS} = k_{WGS} (P_{CO} - \frac{P_{H_2} P_{CO_2}}{K_{eq} P_{H_2O}}) \quad (4)$$

(3) Mass transfer parameters:

The correlation proposed by Akita and Yoshida [17] for aqueous systems is often used for predicting mass transfer coefficients in the F-T synthesis. In the present model, the correlation by Godbole et al. [8] for predicting mass transfer coefficients for oxygen in light hydrocarbon mixtures in a bubble column operating at a superficial gas velocity up to 0.2 m/s was used. This correlation is given by Equation (5).

$$k_{L,O_2} a = 0.31 U_g^{0.603} \quad (5)$$

The prediction of the mass transfer coefficients for hydrogen and carbon monoxide was carried out using the ratio of the diffusivities to the power (2/3) as in the Calderbank and Moo Young's correlation [18]. The presence of solids was also accounted for using the data presented in Figure 2 in the review by Beenackers and van Swaaij [10].

Determination of the rate limiting step using sensitivity analysis

Equation (6) was used to calculate the relative importance of the gas-liquid mass transfer resistance (α). This equation is similar to that presented by Deckwer et al. [5, 12], however, since the water gas shift activity of the catalyst is significant, it was incorporated in the equation through $\Phi(C_i)$ [19].

$$\alpha = \frac{\frac{1}{k_L a}}{\frac{1}{k_L a} + \frac{1}{K \cdot \Phi(C_i) \cdot \epsilon_L}} \quad (6)$$

$$\Phi_{H_2} = m V_T \epsilon_L (2Ae^{-\frac{E_{FT}}{RT}} \frac{m_{H_2} C_{CO} RT m_{CO}}{C_{CO} m_{CO} + 3.5 C_{H_2O} m_{H_2O}} - Be^{-\frac{E}{RT}} (\frac{C_{CO}}{C_{H_2}} - \frac{C_{CO_2}}{C_{H_2O} K_{eq}})) \quad (7)$$

$$\Phi_{CO} = w V_T \epsilon_L (2Ae^{-\frac{E_{FT}}{RT}} \frac{m_{H_2} C_{H_2} RT m_{CO}}{C_{CO} m_{CO} + 3.5 C_{H_2O} m_{H_2O}} + Be^{-\frac{E_{WC}}{RT}} (1 - \frac{C_{CO_2} C_{H_2}}{C_{H_2O} C_{CO} K_{eq}})) \quad (8)$$

RESULTS AND DISCUSSION

Several scenarios including the Sasol I Slurry Bed Process (SSBP) were considered using the present simple model. Although the model did not consider the effect of pressure or temperature on mass transfer, the predictions from the model were comparable with those

predicted with a much more complex model used by Sasol [7]. To illustrate here the procedure, the operating conditions listed in Table 1 reported by Fox and Degen [19] were used. Different catalyst activities were also considered based on the work by Srivastava et al. [20].

The effects of the catalyst activity and concentration on the relative importance of gas-liquid mass transfer (α), relative liquid concentration ($C_{L,i}/C_{L,i}^*$), and $(CO + H_2)$ conversion were studied.

Figure 1 shows the effect of the catalyst activity on (α) and as can be seen hydrogen appears to differently behave than carbon monoxide, since the resistance to hydrogen reaches only 20% of the total resistance whereas that of carbon monoxide becomes significantly large. This difference can also be observed in the corresponding liquid concentrations. The sudden drop of the CO concentration with increasing catalyst activity could be attributed to the water gas shift reaction which also increases the H_2/CO ratio in the liquid phase. Based on this behavior, one can conclude that the reactor performance can be improved by enhancing the catalyst activity although the reactor can be operating in a mass transfer-controlled regime. It should be mentioned, however, that the improvement of the reactor performance from 0.41 to 0.44 kg(HC)/kg(Fe)/hr would require an increase of about 60% in the intrinsic catalyst activity.

The effects of catalyst concentration on (α) as well as the $(CO + H_2)$ conversion is illustrated in Figure 3 and as can be noticed the hydrogen and carbon monoxide resistances appear to increase with increasing catalyst concentration. Also, the increase of catalyst concentration almost produces a proportional improvement of $(CO + H_2)$ conversion, particularly, at low levels. The effect of high solid loading on the mass transfer rate, however, drove the process into a mass transfer-controlled regime and subsequently, the $(CO + H_2)$ conversion appeared to decrease. The maximum conversion could be achieved with a catalyst concentration between 35 and 40 wt%. Thus, the other approach to increase the reactor performance is by increasing the catalyst concentration and subsequently the catalyst becomes slightly under utilized and the mass transfer becomes the controlling rate. Nevertheless, one drawback of this approach is that at high catalyst concentrations, the separation of the catalyst from the wax becomes a critical step in the synthesis process. According to our knowledge, only two companies have successfully solved this separation step: Sasol and Exxon with their iron and cobalt catalysts, respectively.

CONCLUDING REMARKS

Based on the operating conditions and catalysts used in the simple model developed in this study, the following concluding remarks can be made:

1. The slurry phase Fischer-Tropsch synthesis with the present catalysts can be considered a kinetically-controlled process and it would require a substantial improvement of the catalyst intrinsic activity in order to change this situation.
2. The slurry reactor performance for F-T synthesis can be improved by increasing the catalyst activity and/or catalyst concentration, although, the increase of catalyst concentration up to 40 wt%, will drive the process into a mass transfer controlled-regime.
3. Since CO has a lower mass transfer coefficients than those of H_2 [22] and is consumed by Fischer-Tropsch and water gas shift reactions, it is likely to be the limiting reactant.
4. The mass transfer coefficients for H_2 and CO were predicted in this study and therefore they should be measured under the actual Fischer-Tropsch operating conditions in the presence of typical catalyst concentrations. Experimental data are also needed in the presence of high catalyst loading.

Nomenclature

A	Fischer Tropsch intrinsic catalyst activity, kmol of C to HC/kg.Fe.bar.s
B	Water Gas Shift intrinsic catalyst activity, kmol of C to HC/kg.Fe.bar.s
a	gas-liquid interfacial area relative to the expanded fluid volume, m^{-1}
C	concentration, $kmol/m^3$
C*	Concentration at saturation, $kmol/m^3$
D	Dispersion coefficient, m^2/s
E	Apparent activation energy, J/mol
K	Overall kinetic constant, s^{-1}
k_{eq}	Water gas shift equilibrium constant, $k_p = \exp(4577.8/T-4.33)$
k	mass transfer coefficient, m/s
m	solubility
n	number of CSTRs in series
Pe	Peclet number, $u_s L/\epsilon_s D_s$
P	Partial pressure, bar
R	Gas constant, J/mol.K

u	velocity, m/s
V_T	Fluidized bed volume m^3
w	catalyst concentration (kg/m^3)
z	axial position, m
<u>Subscript</u>	
i	component i
g	gas phase
L	liquid phase
<u>Greek symbols</u>	
ϵ	holdup
α	relative extent of the mass transfer resistance

References

- Deckwer W.D., Serpermen Y, Ralek M. and Schmidt B., Modeling the Fischer-Tropsch synthesis in the Slurry Phase, *Ind. Eng. Chem. Proc. Des. Dev.*, 21, (1982) 231-241.
- Saxena S.C., Rosen M., Smith D. N., and Ruether J.A., Mathematical Modeling of Fischer Tropsch slurry bubble column reactors, *Chem. Eng. Comm.*, 40, (1986) 97-151.
- Inga J.R. and Steynberg A.P., Modelling a three phase slurry reactor, Annual Meeting of the Catalyst Society of South Africa, Cape Town, South Africa, 1990.
- Deckwer W.D., Serpermen Y, Ralek M. and Schmidt B., On the relevance of mass transfer limitations in the Fischer Tropsch slurry process, *Chem. Eng. Sci.*, 36, 1981.
- Satterfield C.N. and Huff G.A., Effects of mass transfer on Fischer Tropsch synthesis in slurry reactors, *Chem. Eng. Sci.*, 35, (1980), 195.
- Inga J.R., Hydrodynamic studies and reactor modelling of a three phase slurry reactor in Fisher Tropsch application, M.Eng. Thesis, Potchefstroom University, Potchefstroom, 1993.
- Inga J.R., Hydrodynamic studies for three phase fluidized Bed reactors: A critical literature review, Annual meeting of the catalyst Society of South Africa, Golden Gate, South Africa, 1991.
- Patel S.A., Daly J.G., Bukur D.B., Bubble size distribution in Fischer Tropsch derived waxes in a bubble column, *AIChE J.*, 36 (1), (1990) 93-105.
- Saxena C.N., Heat transfer Investigation in a slurry bubble column, Final Report to DOE, University of Illinois, 1991.
- Godbole S.P., Joseph S., Shah Y.T. and Carr N.L., Hydrodynamics and mass transfer in a bubble column with an organic liquid, *Can. J. of Chem. Eng.*, 45 (12), (1984) 440-445
- Wilkinson P.M., Physical aspects and scaleup of high pressure bubble columns, Ph.D. thesis, Rijksuniversiteit, Groningen Holland, 1991.
- Beenackers A.A.C.M., and Van Swaaij W.P.M., Mass transfer in gas-liquid slurry reactors, *Chem. Eng. Sci.*, 48 (18), (1993) 3109-3139.
- Bernermann K., Steiff A., Weinspach P.M., Zum Einfluss von landsamgestromten Rohrbudeln auf die grosraumige flussigkeitsstromun in Blasensaulen, *Chem. Ing. Tech.* 63 (1), (1991) 76-77.
- Air Products and Chemicals Inc., Liquid Phase Methanol LaPorte Process Development Unit: Modification; US. DOE DE 91-005732. Topical report Task 2.3 Tracer studies in the LaPorte LPMEOH PDU, August 31, (1990).
- Levenspiel, *Chemical Reaction Engineering*, John Willey and Sons Inc., 1272.
- Espinoza R.L., Singular Kinetic Path, Presented at the Catalyst Society of South Africa, Cape Town, South Africa, (1993), 391-402.
- Akita K. and Yoshida F., Gas holdup and volumetric mass transfer coefficient in bubble columns, *Ind. Eng. Chem. Proc. Des. Dev.*, 12 (1), (1973) 76-80.
- Calderbank P.H. and Moo Young M.B., The continuous phase heat and mass transfer properties of dispersions, *Chem. Eng. Sci.*, 16, (1961), 36-54.
- Inga J.R. and Morsi B.I., Rate Limiting step in Fischer Tropsch Slurry Reactors, submitted for publication, *Chem. Eng. Sci.*
- Fox J.M., and Degen B.D., Topical report slurry reactor design studies, DOE contract No. DE-AC22-89PC 89867, (1990)
- Srivastava R.D., Rao V.U.S., Cinquegrane G. and Stiegel G.J., Catalyst for Fischer Tropsch, *Hydroc. Process.*, Feb. (1990), 59-68.
- Karandikar B. M., Morsi B.I., and Shah Y.T., Effect of Water on solubilities and mass transfer coefficients of gases in heavy fraction of Fischer-Tropsch products, *The Can. J. of Chem. Eng.*, 65, (1987), 973-981
- Kuo J.C.W. "Slurry Fischer Tropsch/ Mobil Two-Stage Process of Converting Syngas to high octane gasoline", U.S. DOE Final Rep. No DOE/PC/30022-10, Dec. 1993
- Zimmerman W.H. and Bukur D.B. "Reaction Kinetics over iron catalysts used for the Fischer Tropsch synthesis", *Can. J. of Chem. Eng.* 68, 292-301 (1990)

TABLE 1

Fischer Tropsch slurry bed design basis: From Fox and Degen [19]

Diameter	4.8	m
Length	12.0	m
Cross Sectional Area	15.2	m ²
Reactor Volume	211	m ³
Temperature	257	°C
Pressure	28.3	atm
Slurry Concentration	35.0	wt. %
Gas Velocity	0.14	m/s
Catalyst Performance	0.41	Kg/Kg.hr

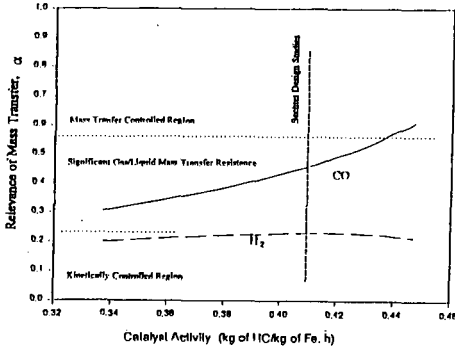


Figure 1: Effect of catalyst activity on the relative mass transfer resistance (α).

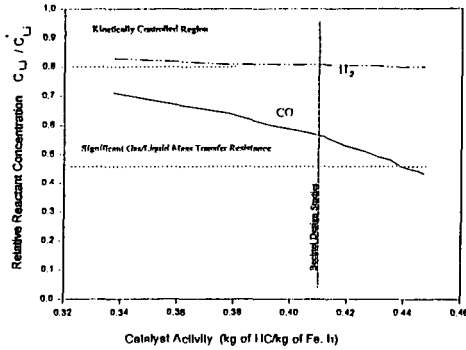


Figure 2: Effect of catalyst activity on the reactants liquid concentration.

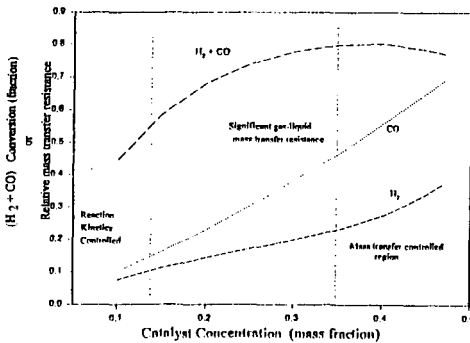


Figure 3. Effect of catalyst concentration on H₂+CO conversion and on the relative mass transfer resistance (α).

SULFATED ZIRCONIA
AS A CO-CATALYST IN FISCHER-TROPSCH SYNTHESIS

Xuemin Song and Abdelhamid Sayari*
Department of Chemical Engineering, Université Laval
Ste-Foy, Québec, Canada G1K 7P4

Keywords: Fischer-Tropsch synthesis, sulfated zirconia, synthesis gas, branched hydrocarbons.

INTRODUCTION

During the last decade, the average composition of gasoline underwent dramatic changes to make up for the gradual removal of lead compounds, and to meet a strong market demand for premium high octane gasoline. From 1980 to 1988, the average aromatic content in gasoline increased from 22 to 32% and consequently the average octane number increased from 83 to 88.4 [1,2]. Modest increases in olefin and light paraffin (butane) contents also took place. The same tendency was observed in Western Europe [3].

At present, most of the compounds whose concentrations have increased are considered to be directly or indirectly as a threat to the environment and/or human health [2,4]. The challenge is to bring down aromatics, olefins and light hydrocarbons in gasoline to more acceptable levels without adverse effects on the gasoline performance [4]. The most common approach to address this problem is the addition of oxygenated compounds such as MTBE, TAME or ethanol into gasoline. Another approach is to increase the concentration of branched hydrocarbons in gasoline. Indeed, such hydrocarbons have high octane numbers and no major environmental drawbacks. However, according to Unzelman [5], within the limits of existing technologies, isoparaffins cannot be made via isomerization and alkylation in sufficient amounts to replace aromatics below 30%. The objective of the present work is to synthesize branched hydrocarbons from carbon sources other than petroleum. The most obvious choice is synthesis gas (CO/H₂).

The approach we have taken is to use a hybrid catalyst comprised of a Fischer-Tropsch synthesis (FTS) catalyst and a hydroisomerization acid catalyst. The purpose is that the mainly linear hydrocarbons generated on the FTS catalyst would isomerize on the acid catalyst before leaving the reactor. Solid superacid catalysts such as sulfated zirconia (SO₄²⁻/ZrO₂) exhibit excellent hydroisomerization properties with the formation of significant amounts of branched hydrocarbons [6]. Therefore, we chose to combine Ru loaded on Y zeolite as the FTS catalyst and SO₄²⁻/ZrO₂ as the isomerization catalyst. In a previous paper [7], we reported data obtained using the hydrogen bracketing technique at atmospheric pressure. In the present communication, we deal with reaction studies in a continuous flow reactor at elevated pressures (mostly at 10 atm).

EXPERIMENTAL

SO₄²⁻/ZrO₂ and Pt/SO₄²⁻/ZrO₂ catalysts were prepared as described earlier [7]. Surface area and sulfur content of the two catalysts were ca. 90 m²/g and 1.5 wt%. Pt content in Pt/SO₄²⁻/ZrO₂ was 1 wt%. The FTS catalyst used in this work was 2 wt% Ru loaded on KY zeolite prepared by ion exchange using Ru(NH₃)₆Cl₃. Procedures for the preparation of RuKY, the decomposition of the ruthenium complex, and the prereduction of RuKY are the same as those described in [7] for RuNaY. The catalyst thus formed was exchanged again with a dilute solution of K₂CO₃ (0.006 M) to neutralize the protons formed during the decomposition of the Ru complex, and eliminate their possible contribution to the formation of branched hydrocarbons. This catalyst, designated as RuKY-K, was then reduced at 420 °C in flowing H₂ for 4 h.

FTS reaction was carried out in a CDS-804 Micro-Pilot Plant coupled with an on-line gas chromatograph (HP 5890 Series II). The reactor part was described in [7]. Product analysis was carried out using flame ionization (FID) and thermoconductivity (TCD) detectors operating in a parallel mode. A capillary column (PONA from HP, 50m x 0.2mm x 0.5µm) and a stainless-steel column (1/8 in. O.D. x 12 ft. long) packed with Porapak Q (80/100 mesh) were linked to FID and TCD respectively, and used for product separation. All valves and transfer lines between the reactor and the GC were heated to prevent the products from condensation. In a typical experiment, the same amount (0.3 g, unless specified otherwise) of prereduced

RuKY-K and $\text{SO}_4^{2-}/\text{ZrO}_2$ or $\text{Pt}/\text{SO}_4^{2-}/\text{ZrO}_2$ were loaded in two separate layers in the reactor, with the FTS catalyst being upstream. They were first reduced at 300 °C for 1 h under a H_2 flow of 40 ml/min and then cooled to reaction temperature (250 °C) under flowing helium. The reactor was pressurized to 10 atm with He, before switching to synthesis gas ($\text{CO}/\text{H}_2 = 1:2$, 20 ml/min).

RESULTS AND DISCUSSION

Under the experimental conditions used in the present work, the superacid catalyst did not contribute to CO transformation. CO conversion was due to RuKY-Y catalyst only, and was kept below 10% to minimize the effects of heat and mass transfer. The composition of the C_7 hydrocarbon fraction was used to monitor the effect of $\text{SO}_4^{2-}/\text{ZrO}_2$ on product selectivity. Fig. 1 shows $i\text{C}_7\%$ and $\text{C}_7\%$ vs. time-on-stream over different catalysts, where $i\text{C}_7\%$ and $\text{C}_7\%$ designate the content of branched C_7 paraffins and of C_7 olefins in the C_7 hydrocarbon fraction, respectively. Over RuKY-Y catalyst, at 10 atm and 250 °C, $i\text{C}_7\%$ was below 10 wt%, while the amount of C_7 olefins was very high ($\text{C}_7\% \approx 67$ wt%). When $\text{SO}_4^{2-}/\text{ZrO}_2$ was loaded downstream of the RuKY-K catalyst, $i\text{C}_7\%$ increased significantly, while only negligible amounts of C_7 olefins were produced in the early stages of the reaction. However, a deactivation of $\text{SO}_4^{2-}/\text{ZrO}_2$ catalyst was subsequently observed, as shown by the gradual decrease in $i\text{C}_7\%$ and the increase in $\text{C}_7\%$. Addition of small amounts (1 wt%) of Pt to $\text{SO}_4^{2-}/\text{ZrO}_2$ significantly improved the stability of the catalyst. Under steady state, the $i\text{C}_7\%$ and $\text{C}_7\%$ reached 60 wt% and 10 wt%, respectively.

$\text{SO}_4^{2-}/\text{ZrO}_2$ and $\text{Pt}/\text{SO}_4^{2-}/\text{ZrO}_2$ showed different degrees of deactivation during reaction. Two possible deactivation mechanisms were proposed: (i) reduction of S^{6+} to lower oxidation states [8,9]; or (ii) coke deposition on acidic sites [8]. Our TPR results [10] showed that no reduction of surface sulfur species on both $\text{SO}_4^{2-}/\text{ZrO}_2$ and $\text{Pt}/\text{SO}_4^{2-}/\text{ZrO}_2$ occurs below 350 °C. The deactivation of $\text{SO}_4^{2-}/\text{ZrO}_2$ under our experimental conditions was attributed to coke deposition [7]. On the other hand, CO is known to chemisorb on coordinatively unsaturated surface (CUS) cations which are usually considered as strong Lewis acid sites. Pinna et al. [11] reported that CO can adsorb on CUS Zr^{4+} cations, and the adsorption of CO reversibly poisons active sites for n-butane isomerization, suggesting that the presence of Lewis sites made superacidic by the inductive effect of sulfate species is essential for the occurrence of catalytic activity. Other researchers [12-14] proposed a dual-site model to represent the nature of active sites on $\text{SO}_4^{2-}/\text{ZrO}_2$. They suggested that the strongly acidic Bronsted sites are responsible for the catalysis [12, 13, 15]. But the strong acidity of the Bronsted sites requires the presence of adjacent Lewis sites [12-14]. Clearfield et al. [12] and Lunsford et al. [13] argued that through an inductive effect, electrons are withdrawn from O-H bond of surface bisulfate by CUS Zr^{4+} cations, thus yielding stronger Bronsted acid sites. Therefore, whatever the nature of the active sites is, the adsorption of CO on Lewis acid sites of $\text{SO}_4^{2-}/\text{ZrO}_2$ will adversely influence the acid strength. As a result, isomerization of hydrocarbons, an acid catalyzed reaction, will be suppressed. To further elaborate on this point, the effect of CO on isomerization of n-butane over $\text{Pt}/\text{SO}_4^{2-}/\text{ZrO}_2$ is being investigated in our laboratory.

Hydrocarbon selectivities under steady state are shown in Fig. 2. It is seen that the presence of $\text{Pt}/\text{SO}_4^{2-}/\text{ZrO}_2$ downstream of RuKY-K has two effects: (i) it alters the normal Schulz-Flory distribution by decreasing the selectivity to C_3 hydrocarbons and by increasing that to C_4 's; (ii) it shifts product distribution to lighter hydrocarbons (in particular C_1). The first effect was found to be due to an oligomerization-cracking mechanism of C_3 olefin into C_4 hydrocarbons [7]. The second effect implies the involvement of cracking or hydrogenolysis of primary FT products, which was not observed under atmospheric pressure [7]. To investigate the effect of pressure on FTS product cracking or hydrogenolysis, two reaction experiments were performed at 5 atm, with and without $\text{Pt}/\text{SO}_4^{2-}/\text{ZrO}_2$ catalyst respectively. The results are shown in Fig. 3. By comparing Fig. 2 and Fig. 3, it was found that the net increase in selectivity to C_1 due to the presence of $\text{Pt}/\text{SO}_4^{2-}/\text{ZrO}_2$ is higher at 10 atm than at 5 atm, which suggests a favorable hydrogenolysis at a higher pressure.

Table 1 depicts the effect of the amount of $\text{Pt}/\text{SO}_4^{2-}/\text{ZrO}_2$ used in the hybrid catalyst bed on the composition of C_7 hydrocarbons

under steady state. The increase in the amount of the acid component results in a decrease in olefin contents and an increase in branched C₇ paraffins. In addition, the use of a larger amount of Pt/SO₄²⁻/ZrO₂ favors the formation of di-branched C₇ paraffins which have higher octane numbers than mono-branched paraffins.

REFERENCES

- [1] R.A. Corbet, Oil & Gas J., June 18, 1990, p. 42.
- [2] G.H. Unzelman, Oil & Gas J., April 9, 1990, p. 43.
- [3] H. Hallie and P.J. Nat, Erdol Kohle, 41 (1988) 491.
- [4] R.A. Corbet, Oil & Gas J., June 18, 1990, p. 33.
- [5] G.H. Unzelman, Oil & Gas J., April 23, 1990, p. 91.
- [6] M.Y. Wen, I. Wender and J.W. Tierney, Energy and Fuels, 4 (1990) 372.
- [7] X. Song and A. Sayari, Appl. Catal. A: General, 110 (1994) 121.
- [8] J.C. Yori, J.C. Luy and J.M. Parera, Appl. Catal., 46 (1989) 103.
- [9] J.R. Sohn and H.W. Kim, J. Mol. Catal., 52 (1989) 361.
- [10] A. Dicko, X. Song, A. Adnot and A. Sayari, J. Catal., 150 (1994), in press.
- [11] F. Pinna, M. Signoretto, G. Strukul, G. Cerrato and C. Morterra, Catal. Lett., 26 (1994) 339.
- [12] A. Clearfield, G.P.D. Serrette and A.H. Khazi-Syed, Catal. Today, 20 (1994) 295.
- [13] J.H. Lunsford, H. Sang, S.M. Campbell, C.H. Liang and R.G. Anthony, Catal. Lett., 27 (1994) 305.
- [14] P. Nascimento, C. Akrapoulou, M. Oszagyan, G. Coudurier, C. Travers, J.F. Joly and J.C. Vedrine, Stud. Surf. Sci. Catal., 75 (1993) 1185.
- [15] F.R. Chen, G. Coudurier, J.F. Joly and J.C. Vedrine, J. Catal., 143 (1993) 616.

TABLE 1

Effect of the amount of Pt/SO₄²⁻/ZrO₂ on the composition of C₇ hydrocarbons (RuKY-K = 0.3 g, P = 10 atm)

Amount of Pt/SO ₄ ²⁻ /ZrO ₂ (g)	0	0.3	0.6	0.9
C ₇ ^o %	66.0	9.7	0	0
iC ₇ %	7.0	61.0	76.0	78.0
mono-branched C ₇	100	64.0	62.2	58.0
di-branched C ₇	0	36.0	37.8	42.0

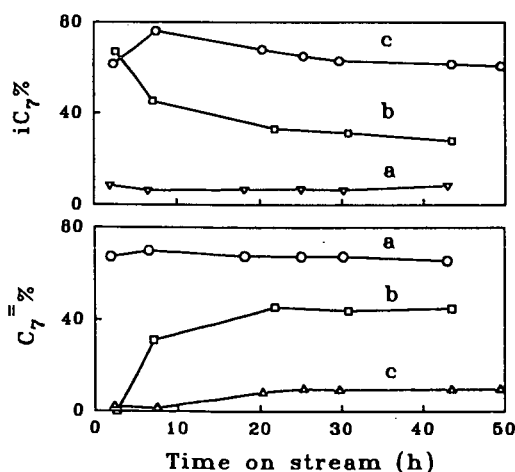


Fig. 1 The composition of C₇ hydrocarbons as a function of time on stream over (a) RuKY-K, (b) RuKY-K + SO₄²⁻/ZrO₂, and (c) RuKY-K + Pt/SO₄²⁻/ZrO₂.

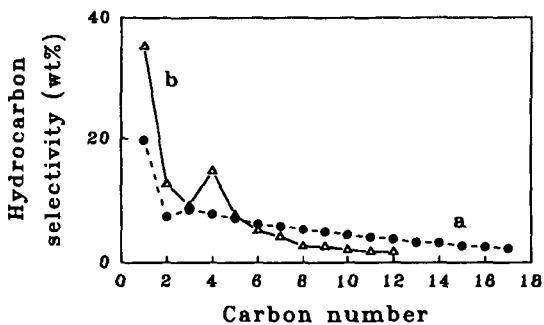


Fig. 2 Hydrocarbon selectivity under steady state at 10 atm over (a) RuKY-K, and (b) RuKY-K + Pt/SO₄²⁻/ZrO₂.

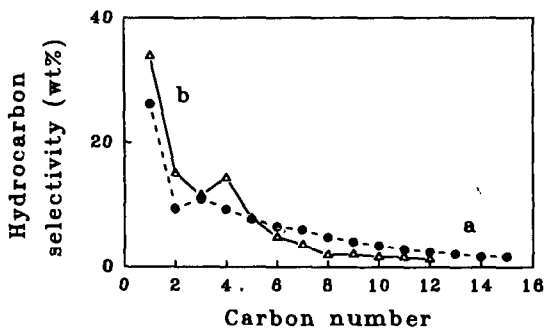


Fig. 3 Hydrocarbon selectivity under steady state at 5 atm over (a) RuKY-K, and (b) RuKY-K + Pt/SO₄²⁻/ZrO₂.

**PREPARATION OF FISCHER-TROPSCH CATALYSTS FROM
COBALT/IRON HYDROTALCITES**

B. H. Howard, J. J. Boff, M. F. Zarochak, and M. A. McDonald
U. S. Dept. of Energy-Pittsburgh Energy Technology Center
P. O. Box 10940, Pittsburgh, PA 15236

Keywords: Hydrotalcites, Fischer-Tropsch, Catalysts

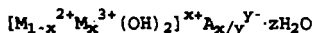
ABSTRACT

Compounds with the hydrotalcite structure ("hydrotalcites") have properties that make them attractive as precursors for Fischer-Tropsch catalysts. A series of single-phase hydrotalcites with cobalt/iron ratios ranging from 3/1 to 1/3 have been synthesized. Mixed cobalt/iron oxides have been prepared from these hydrotalcites by controlled thermal decomposition. Thermal decomposition typically results in either a single mixed metal oxide with a spinel structure or a mixture of oxides with the spinel structure. The BET surface areas of the spinel samples have been found to be as high as about 150 m²/g.

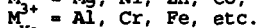
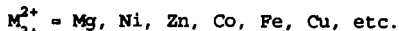
INTRODUCTION

Mixed metal oxides are important in many catalytic applications, both as catalysts and supports. The precursors used in the syntheses of mixed metal oxides are known to influence the physical and chemical characteristics of the resulting mixed metal oxides. Precursors commonly used for the preparation of these oxides include mixed metal hydroxides and carbonates coprecipitated from basic solution. Materials with a hydrotalcite-like structure, commonly referred to as hydrotalcites after one of the best known minerals of this structural group, have received much attention recently as precursors for catalytic applications. Examples include catalysts for methanol synthesis containing Cu, Zn, Cr, and Al (1,2,3) and catalysts for Fischer-Tropsch (FT) synthesis containing Co, Cu, Zn, and Cr (4).

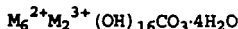
Hydrotalcites have a layered structure similar to clays. The structure consists of stacks of brucite-like metal hydroxide sheets in which substitution of trivalent metal cations for divalent metal cations within the sheets results in a net positive charge. The positive charge is balanced in the structure by hydrated anions between the sheets. A generalized formula for hydrotalcite-like compounds can be written as:



where M²⁺ and M³⁺ can be a variety of metals with appropriate ionic radii. The charge compensating anion is also variable with the ionic radius of the charge compensating anion being of only minor importance because the layer separation can adjust to accommodate size differences. Examples are:



There are many naturally occurring minerals having this structure. These minerals typically have the ideal stoichiometry:



Compounds with the hydrotalcite structure have several characteristics that make them valuable as precursors for Fischer-Tropsch catalysts. Among these is the ability of the structure to accommodate a variety of potentially useful transition metals in a single lattice and the ability to control the synthesis conditions to yield a high surface area material upon decomposition to a spinel phase. Furthermore, Co-containing and Fe-containing spinel phases have shown good activity and selectivity for FT synthesis and, when judiciously prepared and pretreated, have the potential for the physical stability required of a slurry FT catalyst.

The purpose of this research is to investigate the potential of hydrotalcites as precursors for the preparation of slurry Co/Fe Fischer-Tropsch catalysts. We report results from the initial phase of this work, the preparation of Co/Fe hydrotalcite samples and their thermal decomposition to spinel phases of intermediate-

to-high surface area. The emphasis of future publications will shift to modifications of the precipitation and decomposition procedures described here, the development of suitable pretreatment procedures, and catalytic tests of FT synthesis activity in a fixed bed micro-reactor and a slurry autoclave.

EXPERIMENTAL

The hydrotalcites in this study were prepared by a precipitation in base of the appropriate metal salts. The specific conditions used for the syntheses were varied to yield single-phase, well-crystallized hydrotalcites when possible. An aqueous solution of metal salts was prepared that contained the required ratio of metals for the target hydrotalcite, typically with a total metal concentration of about 0.5 M. The metal salt solution was added dropwise to an aqueous base which typically had an initial concentration of about 1 M. Concentrations were varied for some experiments. Potassium bases were used in most experiments. Potassium is typically used to promote iron F-T catalysts and additional potassium will be impregnated in many of these spinel samples before their use as catalysts. Thus, trace amounts of potassium retained in a hydrotalcite precursor are less likely to affect the behavior of the catalyst than are trace amounts of sodium from sodium bases. Additions were usually done at 25°C with magnetic stirring. The pH was monitored during the syntheses. Usually, at the end of the addition the temperature of the slurry was increased to about 60°C. The slurry was aged, typically for 18 hours, at elevated temperature to promote hydrotalcite formation. After the aging period the product was isolated by filtration, washed and dried at 50°C. Hydrotalcites were thermally decomposed in air at various temperatures between 125 and 1000°C, usually for 2.5 hours, to determine what mixed metal oxide(s) would be formed.

The phases resulting from the hydrotalcite syntheses and the thermal decompositions were determined by means of x-ray diffraction (XRD). Morphologies of these materials were studied with scanning electron microscopy (SEM). Surface areas of the mixed oxides were measured by application of the BET method to N₂ physisorption isotherms. The reduction characteristics of the mixed metal oxides were investigated by means of temperature programmed reduction (TPR) with 10% H₂ in argon, 10% CO in helium, or 5% H₂ / 5% CO in argon. The TPR studies were done using an Altamira Instruments AMI-1 unit with an Ametek mass spectrometer for gas analysis.

RESULTS AND DISCUSSION

A stepwise strategy was used to develop the hydrotalcite syntheses. First, the hydrotalcite compositional range attainable for Co (II) with Fe (III) was determined. Then a method for the addition of Cu (II) to the crystal lattice was tested. Finally, the use of Fe (II) to increase the iron content of the hydrotalcite lattice was investigated.

Cobalt (II) nitrate and iron (III) nitrate were used as starting materials for the first part of the synthesis study. Potassium bicarbonate solution at an initial concentration of 1.25 M was used as the base. Co (II) to Fe (III) atom ratios ranging from 4/1 to 1/3 were attempted in this series of experiments. The results are shown in Table 1. With this method well-crystallized, single-phase hydrotalcites could be prepared with Co (II) to Fe (III) atom ratios from 3/1 to 1/1. At lower cobalt contents some poorly-crystallized iron (III) hydroxide was produced along with hydrotalcite and, at higher cobalt contents, some cobalt carbonate was produced. The starting pH for a synthesis was about 8. During the addition of metal salt solution, the pH typically dropped below 7 and a pinkish-tan slurry formed. As the slurry was aged and heated to 60°C, the pH rose to around 9 accompanied by a change in color to a darker reddish-brown, usually indicating formation of the hydrotalcite.

Copper (II) addition to the hydrotalcite lattice was initially attempted by substituting copper (II) nitrate for part of the cobalt (II) nitrate still using the same synthesis method. (Copper is frequently added to precipitated iron catalysts to facilitate reduction.) The ratio used was 1 Cu (II) / 2 Co (II) / 2 Fe (III). The copper loading used was much higher than typical for Fischer-Tropsch promotion. This high copper concentration was used so that

any undesired phases produced during the synthesis could be detected and identified by XRD. The initial synthesis attempt resulted in primarily hydrotalcite with a trace of malachite, $\text{Cu}_2\text{CO}_3(\text{OH})_2$. Lowering the base concentration to 1.0 M avoided the malachite contamination resulting in single phase hydrotalcite. This result showed that Cu (II) could be introduced into the Co/Fe hydrotalcite lattice.

A number of experiments were conducted in an attempt to increase the iron content of the hydrotalcite lattice. Table 2 outlines several of the more successful experiments and the resulting compounds. In all experiments in this series metal chloride salts were used. Several of the syntheses were based on the work reported by Uzunova et al. (5). The M^{3+} required for a stable hydrotalcite lattice was provided by the oxidation of some of the Fe (II) to Fe (III) through contact with atmospheric oxygen during the synthesis. The result of this set of experiments was the extension of the hydrotalcite cobalt to iron ratio to 1/3. Work is continuing to increase the iron content to higher levels.

The thermal decomposition behavior of several Co/Fe hydrotalcites were examined. The most extensive studies of decomposition behavior was done for an intermediate composition hydrotalcite, an atom ratio of 2Co to 1Fe, which was decomposed in air at temperatures between 125 and 1000°C. The samples were heated quickly by placing them in a muffle furnace that was already at the desired decomposition temperature and holding them at temperature for 2.5 hours. The results are shown in Table 3. It was found that a spinel phase, referred to as spinel A, was the only crystalline compound present following decomposition at temperatures of 200 to 600°C. Decomposition at 700°C produced a second spinel, spinel B, which was the dominant phase after decomposition at 800°C. Decomposition at 900°C yielded only spinel B, and decomposition above 1000°C began to decompose spinel B to cobalt oxides in addition. The surface areas for these samples were found to drop from 153 to 18 m^2/g . This loss of surface area was probably due primarily to a loss of internal particle porosity because no evidence for sintering was apparent in SEM. Hydrotalcites with other Co to Fe ratios were found to show similar behavior. However, for some high iron hydrotalcites two spinels were always present after decomposition. It was also found that the rate of decomposition at a given temperature influenced the spinels formed.

Preliminary TPR studies were done on a 2Co/1Fe sample decomposed at 600°C. In 10% CO/He, reduction proceeded rapidly above 300°C as reflected by the large mass spectrum peaks at $m/z=28$ and 44. The consumption of CO continued to the end-point of the temperature scan, 450°C. Much of the CO consumption at higher temperatures is likely due to carbon deposition from the Boudouard reaction. In contrast, reduction in H_2 , the typical reductant for Co-rich samples, was less favorable. A TPR in 10% H_2/Ar showed less reduction at 300°C, with reduction rates peaking at about 400°C. In both experiments, the samples were cooled to room temperature in inert gas flow after reaching the 450°C end point of the TPR. In both cases, the predominant solid phase detected by XRD was a cubic phase isostructural with $\alpha\text{-Fe}$. In the case of the CO-reduced sample, a small amount of an additional unidentified phase was also present.

ACKNOWLEDGEMENTS

The authors gratefully acknowledge N. E. Johnson for helpful discussions during this project. B. H. Howard gratefully acknowledges support for this research provided under Contract # DE-AC05-76OR00033 between the U. S. Department of Energy and the Oak Ridge Institute for Science and Education.

DISCLAIMER

Reference in this report to any specific commercial product, process, or service is to facilitate understanding and does not necessarily imply its endorsement or favoring by the United States Department of Energy.

REFERENCES

1. Fornasari, G.; D' Huysser, H.; Mintchev, L.; Trifirò, F.; Vaccari, A., *J. Catal.* **1992**, *135*, 386.
2. Riva, A.; Trifirò, F.; Vaccari, A.; Mintchev, L.; Busca, G., *J. Chem. Soc., Faraday Trans. 1* **1988**, *84(5)*, 1423.
3. Busetto, C.; Del Piero, G.; Manara, G.; Trifirò, F.; Vaccari, A., *J. Catal.* **1984**, *85*, 260.
4. Fornasari, G.; Gusi, S.; Trifirò, F.; Vaccari, A., *Ind. Eng. Chem. Res.* **1987**, *26*, 1500.
5. Uzunova, E.; Klissurski, D.; Mitov, I.; Stefanov, P., *Chem. Mater.* **1993**, *5*, 576.

Table 1. Results of Co (II)/Fe (III) hydrotalcite preparations using metal nitrates.

<u>Co (II) to Fe (III)</u>	<u>Resulting Phases</u>
4/1.	HTC + trace CoCO_3 + trace unidentified
3/1	HTC + trace CoCO_3
2/1	HTC
1/1	HTC
1/2	HTC + minor Fe(OH)_3
1/3	HTC + Fe(OH)_3

HTC = hydrotalcite

Table 2. Use of Fe (II) to increase iron content of hydrotalcite prepared using metal chlorides.

<u>Co (II)</u>	<u>Fe (II)</u>	<u>Base</u>	<u>Start pH</u>	<u>Result</u>
1	3	KHCO_3	8.0	HTC + trace Fe(OH)_3
1	3	$\text{KHCO}_3 + \text{K}_2\text{CO}_3$	8.9	Goethite + CoCO_3
1	2	$\text{KOH} + \text{K}_2\text{CO}_3$	12.8	HTC
1	3	$\text{KOH} + \text{K}_2\text{CO}_3$	12.8	HTC

HTC = hydrotalcite

Table 3. Thermal decomposition of 2Co/1Fe hydrotalcite.

<u>Temperature °C</u>	<u>Phase</u>	<u>Surface area m^2/g</u>
50	HTC	-
125	HTC + amorph.	-
200	Spinel A	-
300	Spinel A	153
400	Spinel A	95
500	Spinel A	57
600	Spinel A	29
700	Spinel A + B	18
800	Spinel A + B	-
900	Spinel B	-
1000	Spinel B + $\text{CoO} + \text{Co}_3\text{O}_4$	-

SEPARATION OF FISCHER-TROPSCH CATALYST/WAX MIXTURES USING DENSE GAS EXTRACTION. Marc W. Eyring, Paul C. Rohar, Richard F. Hickey, and Curt M. White, U.S. Dept. of Energy, PETC, P.O. Box 10940, Pittsburgh, PA 15236-0940 and Michael S. Quiring, Kerr-McGee Corp., Kerr-McGee Technical Center, P.O. Box 25861, Oklahoma City, OK, 73125

The separation of a Fischer-Tropsch catalyst from wax products is an important issue when the synthesis is conducted in a slurry bubble column reactor. This paper describes a new technique based on dense gas extraction of the soluble hydrocarbon components from the insoluble catalyst particles using light hydrocarbons as propane, butane, and pentane as the solvent. The extractions were conducted in a continuous unit operated near the critical point of the extraction gas on a catalyst/wax mixture containing about 4.91 wt% catalyst. The catalyst-free wax was collected in the second stage collector while the catalyst and some insoluble wax components were collected in the first stage collector. The yield of catalyst-free wax was about 60 wt% of the feed mixture. The catalyst content of the catalyst/wax mixture in the first stage was about 14.8 wt%. The catalyst content in the second stage collector was less than 1 part in 100,000.

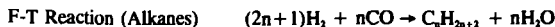
DATA ANALYSIS PROCEDURES IN FISCHER-TROPSCH SYNTHESIS

Charles B. Benham ^{CSB}
 Rentech, Inc.
 1331 17th Street, Suite 720
 Denver, CO 80202

Keywords: Fischer-Tropsch, Schultz-Flory, Synthesis

In performing tests on Fischer-Tropsch (F-T) catalysts, it is useful to be able to assess immediately the approximate activity and selectivity of the catalyst with a minimum of information. The procedure described in this paper requires only gas chromatographic data on the gases to and from the reactor. Further, the only gases which need be analyzed are hydrogen, carbon monoxide, methane and carbon dioxide. No flowrate data is needed.

Consider the following reactions:



Assume the following:

- 1) The F-T product carbon number distribution can be characterized using a single chain-growth parameter; and
- 2) The feed gas is comprised of only hydrogen, carbon monoxide and inert gases; and
- 3) The hydrogen to carbon monoxide ratio in the feed gas, M_f , is known.
- 4) The relative amounts of hydrogen, carbon monoxide, methane, and carbon dioxide in the tail gas are known.

From assumption 1, the number of moles of hydrocarbon having n carbon atoms can be expressed in the usual manner as:

$$N_n = \alpha^{n-1} N_{CH_4}$$

Where N_n and N_{CH_4} denote the number of moles of hydrocarbons produced having n and 1 carbon atoms respectively.

Let superscripts f and t denote feed and tail gases. Therefore, from the stoichiometry of the above reactions, the following relationships are apparent:

$$N_{H_2}^t = N_{H_2}^f - \sum_{n=1}^{\infty} (2n+1) N_n + N_{CO_2}^t$$

$$= N_{H_2}^f - \frac{(3-\alpha)}{(1-\alpha)^2} N_{CH_4} + N_{CO_2}^t \quad (1)$$

$$N_{CO}^t = N_{CO}^f - \sum_{n=1}^{\infty} n N_n - N_{CO_2}^t$$

$$= N_{CO}^f - \frac{1}{(1-\alpha)^2} N_{CH_4} - N_{CO_2}^t \quad (2)$$

Let ϵ represent the overall carbon monoxide conversion:

$$N_{CO}^t = (1-\epsilon)N_{CO}^f \quad (3)$$

The subscript i represents any component. By dividing equations (1) and (2) by N_{CO}^t , invoking equation (3), and letting the normalized composition be denoted by R 's, ($R_i = N_i^t / N_{CO}^t$) the following equations are obtained:

$$R_{H_2} = \frac{M_f}{(1-\epsilon)} - \frac{(3-\alpha)}{(1-\alpha)^2} R_{CH_4} + R_{CO_2} \quad (4)$$

$$1 = \frac{1}{(1-\epsilon)} - \frac{1}{(1-\alpha)^2} R_{CH_4} - R_{CO_2} \quad (5)$$

Let $Z = 1/(1-\alpha)$. Then equations (4) and (5) can be written as:

$$R_{H_2} = \frac{M_f}{(1-\epsilon)} - (2Z^2 + Z)R_{CH_4} + R_{CO_2} \quad (6)$$

$$\frac{\epsilon}{(1-\epsilon)} = Z^2 R_{CH_4} + R_{CO_2} \quad (7)$$

Equations (6) and (7) can be solved simultaneously for ϵ and Z :

$$\text{For } M_f = 2, Z = \frac{3R_{CO_2} + 2 - R_{H_2}}{R_{CH_4}}$$

$$\text{For } M_f = 2, Z = 1 + \sqrt{1 - \frac{4(M_f - 2)}{R_{CH_4} [1(M_f - 2)(1 + R_{CO_2}) + 3R_{CO_2} + 2 - R_{H_2}]}} \frac{1(M_f - 2)(1 + R_{CO_2}) + 3R_{CO_2} + 2 - R_{H_2}}{2(M_f - 2)}$$

$$\text{and } \epsilon = \frac{Z^2 R_{CH_4} + R_{CO_2}}{(Z^2 R_{CH_4} + R_{CO_2} + 1)}$$